



**Flanders**  
State of  
the Art

15\_068\_5  
FHR reports

# Modelling Belgian Coastal zone and Scheldt mouth area

Sub report 5  
Progress report  
Scenarios Vlaamse Baaien and model developments

DEPARTMENT  
MOBILITY &  
PUBLIC  
WORKS

[www.flandershydraulicsresearch.be](http://www.flandershydraulicsresearch.be)

# Modelling Belgian Coastal zone and Scheldt mouth area

## Sub report 5: Progress report - Scenarios Vlaamse Baaien and model developments

Kolokythas, G.; De Maerschallck, B.; Vanlede, J.; Mostaert, F.

Legal notice

Flanders Hydraulics Research is of the opinion that the information and positions in this report are substantiated by the available data and knowledge at the time of writing.  
 The positions taken in this report are those of Flanders Hydraulics Research and do not reflect necessarily the opinion of the Government of Flanders or any of its institutions.  
 Flanders Hydraulics Research nor any person or company acting on behalf of Flanders Hydraulics Research is responsible for any loss or damage arising from the use of the information in this report.

Copyright and citation

© The Government of Flanders, Department of Mobility and Public Works, Flanders Hydraulics Research 2017  
 D/2017/3241/276

This publication should be cited as follows:

**Kolokythas, G.; De Maerschalck, B.; Vanlede, J.; Mostaert, F.** (2017). Modelling Belgian Coastal zone and Scheldt mouth area: Sub report 5: Progress report - Scenarios Vlaamse Baaien and model developments. Version 5.0. FHR Reports, 15\_068\_5. Flanders Hydraulics Research: Antwerp.



Until the date of release reproduction of and reference to this publication is prohibited except in case explicit and written permission is given by the customer or by Flanders Hydraulics Research. Acknowledging the source correctly is always mandatory.

Document identification

Customer:	Vlaams Nederlands Scheldecommissie (VNSC)	Ref.:	WL2017R15_068_5
Keywords (3-5):	Vlaamse Baaien, Belgische Kust, morfologie		
Text (p.):	45	Appendices (p.):	25
Confidentiality:	<input checked="" type="checkbox"/> Yes	Released as from:	01/01/2025
		Exception:	<input checked="" type="checkbox"/> The Government of Flanders

Author(s):	Kolokythas, G.; De Maerschalck, B.
------------	------------------------------------

Control

	Name	Signature
Reviser(s):	Vanlede, J.	
Project leader:	De Maerschalck, B.	

Approval

Head of Division:	Mostaert, F.	
-------------------	--------------	--

## Abstract

In the present report, the work that has been done in the framework of 'Vlaamse Baaien' Masterplan in the first six months of the three-year contract of the position '**Modelleur in het kader van project 15\_068: Modelling getij, sedimenttransport en morfologie voor de Belgische kustzone volgens gekend projectplan**', is presented. Part of the work has been reported to Maritime Access before as individual FHR memos. The present report is an extended compilation of these memos. Additionally to the memos the progress regarding to the implementation of an advanced mesh generation toolbox is added to the report. The report is internally revised according to the FHR Document Quality system.

First, results from Telemac3D hydrodynamic simulations for the case of a seaward coastal defense line spanning along the entire Belgian coast, are presented. To this end, two three-dimensional unstructured Telemac models are utilized, namely the Zeebrugge (ZB) model, and the Scaldis model, for comparison of the numerical results. In addition, the perspectives of a new finite element mesh generator, named GMSH, are investigated through a successful testing in the construction of a qualitative grid for one of the investigated scenarios.

Next, the sea level rise effect on the hydrodynamic flow at the Belgian coast and especially on the Zeebrugge port accessibility is investigated again by means of the Zeebrugge Telemac3D model. Three different scenarios of future sea level rise are considered, i.e. a moderate sea level rise of 60 cm by the year 2100, a warm scenario with sea level rise of 90 cm and a worst case scenario of sea level rise scenario of 200 cm. The main conclusion is that the impact of sea level rise on the port accessibility is limited. Only in the worst case scenario a significant impact on the LNG carriers access (with respect to the maximum allowed cross currents 1.5 kn) is observed.



# Contents

Abstract .....	III
Contents .....	V
List of tables.....	VII
List of figures .....	VIII
1 Introduction.....	1
2 ‘Vlaamse Baaien’ dunebelt scenarios.....	4
2.1 Scenarios overview.....	4
2.2 Zeebrugge (ZB) model: Set-up.....	5
2.2.1 Computational grid.....	6
2.2.2 Offshore boundary conditions.....	8
2.2.3 Simulation period .....	8
2.3 ZB model: Results .....	8
2.3.1 Effects on the flow velocity field .....	8
2.3.2 Port accessibility .....	9
2.4 Scaldis model: Set-up .....	11
2.5 Scaldis model: Results .....	12
2.5.1 Effects on the flow velocity field .....	12
2.6 GMSH grid testing.....	14
2.6.1 General .....	14
2.6.2 Quality metrics .....	15
2.6.3 Results .....	16
3 Impact of Sea level rise on the Zeebrugge port accessibility .....	18
3.1 Model set-up .....	18
3.1.1 Computational grid.....	18
3.1.2 Offshore boundary conditions.....	18
3.1.3 Simulation period .....	18
3.1.4 SLR scenarios .....	19
3.2 SLR results.....	20
3.2.1 Tidal analysis.....	20
3.2.2 Sea level rise impact on coastal and estuarine hydrodynamics.....	31
3.2.3 Sea level rise impact on port accessibility .....	35

Summary.....	44
References.....	45
Appendix A: Summary of model settings .....	A1
Appendix B: Maximum flow velocities during ebb and flood – scenarios I3 and I4.....	A2
Appendix C: Dunebelt scenarios I1 and I2.....	A3
Appendix D: Maximum flow velocities during ebb and flood – SLR scenarios.....	A5
Appendix E: Memo: CSM and ZUNO run of 2009 including 60, 90 and 200 cm sea level rise.....	A10
1 Introduction.....	A10
2 Model settings.....	A10
2.1 Modelling software .....	A10
2.2 CSM MODEL.....	A10
2.3 ZUNO MODEL .....	A12
3 Validation.....	A14
4 Scenarios.....	A17
5 List of References .....	A24
6 Annex 1: Definition of Statistics .....	A25

## List of tables

Table 1: List of delivered FHR reports and memos within project 15_068.....	3
Table 2: Main settings of Scaldis and ZB models.....	11
Table 3: Description of investigated scenarios.....	19
Table 4: Maximum depth-averaged transverse velocities along the Pas van het Zand trajectory during spring tide and total duration of the time barriers per 24 hr on the basis of the maximum allowed velocities (1.5 and 2 kn) for all the investigated scenarios.....	43
Table 2-1: Model parameters of CSM model. ....	A11
Table 2-2: Model parameters of ZUNO model. ....	A13
Table 3-1: Statistical parameters for the water level time series (CSM vs. measurements) .....	A16
Table 3-2: Statistical parameters for the water level time series (ZUNO vs. measurements). ....	A17
Table 4-1: Description of scenarios. ....	A18
Table 4-2: Comparison of harmonic component M2, S2 and M4 with and without SLR.....	A23
Table 4-3: Statistical analysis on velocities.....	A23



## List of figures

Figure 1: Bathymetry and topography of the ‘closed dunebelt’ scenario I3.....	4
Figure 2: Bathymetry and topography of the ‘open dunebelt’ scenario I4.....	5
Figure 3: Bathymetry and topography of the Reference (current state) scenario I3.....	5
Figure 4: Computational grid and bathymetry of ‘Vlaamse Baaien’ dunebelt scenario I3. ....	6
Figure 5: Detail of the computational grid, focusing at the coastal are between Newport (West boundary) and Ostend (East boundary).....	7
Figure 6: Dune cross-section at the location indicated in Figure 5. ....	7
Figure 7: Maximum depth-averaged flow velocity (magnitude [m/s]) for dunebelt scenario I3 (left) and I4 (right) during spring tide [25-Apr-2009 03:20 → 26-Apr-2009 03:50]. ....	8
Figure 8: Difference in maximum depth-averaged flow velocity [m/s] between dunebelt scenario I3 and Reference scenario (left) and I4 and Reference scenario (right) during spring tide [25-Apr-2009 03:20 → 26-Apr-2009 03:50].....	9
Figure 9: Window barriers for the, transverse to the Pas van Zand trajectory, depth-averaged velocities greater than 2kn (above) and 1.5kn (below) calculated for scenario I4 during spring tide.....	10
Figure 10: Spatiotemporal variation of the depth-averaged, transverse to the Pas van Zand trajectory, flow velocities during spring tide for scenario I4 (left). Difference plot versus Reference scenario (right). ....	10
Figure 11: Computational grid and bathymetry of ‘Vlaamse Baaien’ dunebelt scenario I4 incorporated in Scaldis model.....	11
Figure 12: Water level variation in time at Paardenmarkt.....	12
Figure 13: Difference in maximum depth-averaged flow velocity [m/s] between dunebelt scenario I4 and Reference scenario during spring tide [21-Sep-2013 04:30 → 22-Sep-2013 05:00] for <b>Scaldis model</b> .....	13
Figure 14: Difference in maximum depth-averaged flow velocity [m/s] between dunebelt scenario I4 and Reference scenario during spring tide [25-Apr-2009 03:20 → 26-Apr-2009 03:50] for the <b>ZB model</b> .....	13
Figure 15: Difference in maximum depth-averaged flow velocity [m/s] between dunebelt scenario I4 and Reference scenario during flood phase [21-Sep-2013 12:10 → 16:10] (left) and ebb phase [21-Sep-2013 17:10 → 20:10] (right) for the <b>Scaldis model</b> .....	14
Figure 16: Difference in maximum depth-averaged flow velocity [m/s] between dunebelt scenario I4 and Reference scenario during flood phase [25-Apr-2009 11:00 → 15:00] (left) and ebb phase [25-Apr-2009 16:00 → 19:00] (right) for the <b>ZB model</b> .....	14
Figure 17: Part of the ZB computational grid in the area of interest made by use of GMSH, where regions of varied resolution are indicated. ....	15
Figure 18: Quality metrics for the computational grid of scenario I4. ....	16
Figure 19: Maximum depth-averaged flow velocity (magnitude [m/s]) for dunebelt scenario I4 during spring tide [25-Apr-2009 03:20 → 26-Apr-2009 03:50] – GMSH grid. ....	17
Figure 20: Difference in maximum depth-averaged flow velocity [m/s] between dunebelt scenario I4 and Reference scenario during spring tide [25-Apr-2009 03:20 → 26-Apr-2009 03:50] – GMSH grid.....	17
Figure 21: Computational grid and bathymetry of the utilized T3D hydrodynamic model for the SLR simulations. ....	19

Figure 22: Locations used in the basic tidal analysis.....	20
Figure 23: Bias in the complete water level time-series between the sea level rise scenarios and the Reference scenario.....	21
Figure 24: Water level time-series (16/04/2009 – 01/05/2009) at port of Zeebrugge for all the investigated scenarios.....	21
Figure 25: Bias in the time of high water levels between the sea level rise scenarios and the Reference scenario.....	22
Figure 26: Bias in the time of low water levels between the sea level rise scenarios and the Reference scenario.....	23
Figure 27: Averaged HW and LW time shifts versus sea level rise.....	23
Figure 28: Bias in the high water levels between the sea level rise scenarios and the Reference scenario. .	24
Figure 29: Bias in the low water levels between the sea level rise scenarios and the Reference scenario....	25
Figure 30: Averaged HW and LW bias versus sea level rise. ....	25
Figure 31: Amplitude of the M2 tidal constituent at the considered locations for all the investigated scenarios.....	26
Figure 32: Amplitude of the S2 tidal constituent at the considered locations for all the investigated scenarios.....	27
Figure 33: Amplitude of the M4 tidal constituent at the considered locations for all the investigated scenarios.....	27
Figure 34: Averaged M2, S2, and M4 amplitude differences between each of the sea level rise scenarios and the Reference scenario versus sea level rise.....	28
Figure 35: Phase of the M2 tidal constituent at the considered locations for all the investigated scenarios.	29
Figure 36: Phase of the S2 tidal constituent at the considered locations for all the investigated scenarios.	29
Figure 37: Phase of the M4 tidal constituent at the considered locations for all the investigated scenarios.	30
Figure 38: Averaged M2, S2, and M4 phase differences between each of the sea level rise scenarios and the Reference scenario versus sea level rise.....	30
Figure 39: Maximum depth-averaged flow velocity (magnitude, m/s) during spring tide for the Reference and the sea level rise scenarios.....	31
Figure 40: Difference in maximum depth-averaged flow velocity (magnitude, m/s) during spring tide between the sea level rise scenarios and the Reference scenario.....	32
Figure 41: Difference in maximum depth-averaged flow velocity (magnitude, m/s) during spring tide between the sea level rise scenarios and the Reference scenario at the area around Zeebrugge port. ....	33
Figure 42: Difference in maximum depth-averaged flow velocity (magnitude) during <b>flood phase</b> of the spring tide between the sea level rise scenarios and the Reference scenario at the area around Zeebrugge port.....	33
Figure 43: Difference in maximum depth-averaged flow velocity (magnitude) during <b>ebb phase</b> of the spring tide between the sea level rise scenarios and the Reference scenario at the area around Zeebrugge port.	33
Figure 44: Maximum depth-averaged flow velocity (magnitude, m/s) during spring tide for the Reference and the sea level rise scenarios at the area of Western Scheldt.....	34
Figure 45: Difference in maximum depth-averaged flow velocity (magnitude, m/s) during spring tide between the sea level rise scenarios and the Reference scenario at the area of Western Scheldt.....	35

Figure 46: Bathymetry with respect to the mean sea level (MSL) at the area of Western Scheldt for the Reference (left) and the Worst-case sea level rise scenario (right). ..... 35

Figure 47: Spatiotemporal evolution of the depth-averaged transverse current along the Pas van het Zand trajectory during the spring tide for the Reference scenario..... 36

Figure 48: Time barriers for the transverse to the Pas van het Zand trajectory, depth-averaged current greater than 2kn (above) and 1.5kn (below) calculated for the Reference scenario during spring tide. .... 37

Figure 49: Depth-averaged transverse current at the Pas van het Zand trajectory (close to the port entrance, Aa) and in CDNB (Ad) during spring tide for the Reference scenario. .... 37

Figure 50: Spatiotemporal evolution of the depth-averaged transverse current along the Pas van het Zand trajectory during the spring tide for the Moderate SLR scenario (left). Difference plot versus Reference scenario (right). ..... 38

Figure 51: Time barriers for the transverse to the Pas van Zand trajectory, depth-averaged current greater than 2kn (above) and 1.5kn (below) calculated for the Moderate scenario (SLR060) during spring tide. .... 38

Figure 52: Depth-averaged transverse current at the Pas van het Zand trajectory (close to the port entrance, Aa) and in CDNB (Ad) during spring tide for the Moderate scenario (SLR060). .... 39

Figure 53: Spatiotemporal evolution of the depth-averaged transverse current along the Pas van het Zand trajectory during the spring tide for the Warm sea level rise scenario (left). Difference plot versus Reference scenario (right). ..... 40

Figure 54: Time barriers for the transverse to the Pas van Zand trajectory, depth-averaged current greater than 2kn (above) and 1.5kn (below) calculated for the Warm scenario (SLR090) during spring tide. .... 40

Figure 55: Depth-averaged transverse current at the Pas van het Zand trajectory (close to the port entrance, Aa) and in CDNB (Ad) during spring tide for the Warm scenario (SLR090). .... 41

Figure 56: Spatiotemporal evolution of the depth-averaged transverse current along the Pas van het Zand trajectory during the spring tide for the Worst-case sea level rise scenario (left). Difference plot versus Reference scenario (right). ..... 42

Figure 57: Time barriers for the transverse to the Pas van Zand trajectory, depth-averaged current greater than 2kn (above) and 1.5kn (below) calculated for the Worst-case scenario (SLR200) during spring tide.... 42

Figure 58: Depth-averaged transverse current at the Pas van het Zand trajectory (close to the port entrance, Aa) and in CDNB (Ad) during spring tide for the Worst-case scenario (SLR200). .... 43

Figure 59: Maximum depth-averaged flow velocity (magnitude [m/s]) during flood phase [25-Apr-2009 11:00 → 15:00] (left) and ebb phase [25-Apr-2009 16:00 → 19:00] (right) for dunebelt scenario I3. .... A2

Figure 60: Maximum depth-averaged flow velocity (magnitude [m/s]) during flood phase [25-Apr-2009 11:00 → 15:00] (left) and ebb phase [25-Apr-2009 16:00 → 19:00] (right) for dunebelt scenario I4. .... A2

Figure 61: Bathymetry of the dunebelt scenarios I1 and I2. .... A3

Figure 62: Maximum depth-averaged flow velocity (magnitude) for dunebelt scenario I1 (left) and I2 (right) during spring tide. .... A3

Figure 63: Difference in maximum depth-averaged flow velocity between dunebelt scenario I1 and Reference scenario (left) and I2 and Reference scenario (right) during spring tide. .... A4

Figure 64: Window barriers for the, transverse to the Pas van Zand trajectory, depth-averaged velocities greater than 2kn (above) and 1.5kn (below) calculated for scenario I1 during spring tide..... A4

Figure 65: Maximum depth-averaged flow velocity (magnitude) during flood phase of the spring tide for the Reference and the sea level rise scenarios. .... A5

Figure 66: Maximum depth-averaged flow velocity (magnitude) during ebb phase of the spring tide for the Reference and the sea level rise scenarios. .... A6

Figure 67: Difference in maximum depth-averaged flow velocity (magnitude) during flood phase of the spring tide between the sea level rise scenarios and the Reference scenario. .... A7

Figure 68: Difference in maximum depth-averaged flow velocity (magnitude) during ebb phase of the spring tide between the sea level rise scenarios and the Reference scenario. .... A7

Figure 69: Maximum depth-averaged flow velocity (magnitude) during flood phase of the spring tide for the Reference and the sea level rise scenarios at the area of Western Scheldt. .... A8

Figure 70: Maximum depth-averaged flow velocity (magnitude) during ebb phase of the spring tide for the Reference and the sea level rise scenarios at the area of Western Scheldt. .... A8

Figure 71: Difference in maximum depth-averaged flow velocity (magnitude) during flood phase of the spring tide between the sea level rise scenarios and the Reference scenario at the area of Western Scheldt. .... A9

Figure 72: Difference in maximum depth-averaged flow velocity (magnitude) during ebb phase of the spring tide between the sea level rise scenarios and the Reference scenario at the area of Western Scheldt. .... A9



## Samenvatting

Dit rapport geeft de voortgang van het eerste halve jaar binnen het project 15\_068 *Modellering Belgische Kustzone en Scheldemonding*. Het project wordt uitgevoerd binnen het kader van het eerdere *Vlaamse Baaien*, tegenwoordig *Complex Project Kustvisie*. Delen van de uitvoering van het project zijn eerder opgeleverd in de vorm van WL-memo's, voornamelijk in de vorm van rekennota's per set van scenario's. Het voorliggende rapport is een compilatie van deze memo's, uitgebreid met de beschrijving van de modelontwikkelingen binnen het eerste half jaar van het project. Binnen deze ontwikkelingen is er vooral gewerkt aan de implementatie van een geavanceerde flexibele mesh-generatie toolbox.

Het eerste deel van het rapport beschrijft de TELEMAC3D simulaties voor de scenario's betreffende een zeewaartse kustverdediging bestaande uit een gesloten duinengordel voor de volledige Belgische kust. Twee verschillende beschikbare TELEMAC modellen werden gebruikt: het door IMDC ontwikkelde Zeebrugge model en het door het Waterbouwkundig Laboratorium ontwikkelde Scaldis model. Voor de implementatie van een zeewaartse duinengordel werden de modellen ter plaatse van de duinengordel lokaal verfijnd. Teneinde automatische en flexibele gridverfijningen te kunnen toepassen en kwalitatieve grids te kunnen genereren, werd de eindige elementen gridgenerator GMSH, ontwikkeld door de universiteit van Louvain-La-Neuve, getest.

Het tweede deel van het rapport beschrijft de studie naar de gevolgen van zeespiegelstijging voor de stromingen in de Belgische kustzone en mondingsgebied en in het bijzonder de nautische toegankelijkheid van de haven van Zeebrugge. Drie scenario's werden geanalyseerd: een mild scenario van 60 cm zeespiegelstijging tegen 2100, een warm scenario van 90 cm en een worst case scenario van 200 cm. Op basis van de TELEMAC3D simulaties kan men constateren dat de impact op de toegankelijkheid zeer beperkt is. Enkel in het worst case scenario geval werd een significante impact op de toegankelijkheid voor LNG tankers bij springtij vastgesteld.

# 1 Introduction

The Masterplan 'Vlaamse Baaien', which was proposed by the Flemish Government in May 2014, outlines the need to develop an integrated vision for the Belgian coast in a long term period, i.e. up to year 2100. The main objective of this Masterplan is to investigate possible coastal interventions, that could ensure that the Belgian coast is able to withstand the climatic change impacts, storms and floods, as well as it will remain attractive in economic terms providing also opportunities for renewable energy production. One of the goals is to achieve a win-win situation between coastal protection and the improvement of the maritime access to the port of Zeebrugge for inland vessels by creating a sheltered estuarine connection to the Scheldt. Currently only a limited number of certified inland vessels are conditionally, depending on the wave climate, allowed to make use of the maritime trajectory between Zeebrugge and the mouth of the Western Scheldt to connect the port with the inland waterway network. For the protection of this maritime waterway and the coast, the idea of a broad protection belt, which could be made and maintained in a natural and sustainable way, is adopted.

A first set of possible scenarios has been analyzed for currents, waves and morphodynamic response in previous reports (De Maerschalck *et al.*, 2016, 2017; Hassan *et al.*, 2016; Suzuki *et al.*, 2016). In the present report, the work that has been done by the authors in the first six months of the three-year contract of the position '**Modelleur in het kader van project 15\_068: Modelling getij, sedimenttransport en morfologie voor de Belgische kustzone volgens gekend projectplan**', is presented. A list of the preceding reports and memos delivered so far within project 15\_068 given in Table 1.

First, results from Telemac3D hydrodynamic simulations for the case of a seaward coastal defense line, hereafter called dunebelt, spanning along the entire Belgian coast, are presented. The simulations include cases of a dunebelt with fixed outline which is either completely closed or has an opening at the entrance of the Zeebrugge port. To this end, two three-dimensional unstructured Telemac models are utilized, namely the Zeebrugge (ZB) model (IMDC 2013, 2015), and the Scaldis model (Smolders *et al.* 2016), for comparison of the numerical results. In addition, the perspectives of a new finite element mesh generator, named GMSH (Geuzaine and Remacle, 2009), are investigated through a successful testing in the construction of a qualitative grid for one of the dunebelt scenarios.

Next, the effect of sea level rise on the hydrodynamic flow in the vicinity of the Belgian coast in general and on the Zeebrugge port accessibility particularly, is investigated. In order to achieve this goal, numerical simulations by means of the Zeebrugge Telemac3D model are performed considering three different scenarios of future sea level rise, i.e. a moderate sea level rise of 60 cm by the year 2100, a warm scenario with sea level rise of 90 cm and a worst case scenario of sea level rise scenario of 200 cm.

Table 1: List of delivered FHR reports and memos within project 15\_068.

Title	ID
Modelling Vlaamse Baaien, Deelrapport 1: Hydrodynamische Modelling Scenario's Oostkust	WL2016R15_068_1
Modelling Belgische Kustzone en Scheldemonding, Deelrapport 2: Morfologische analyse scenario's Vlaamse Baaien	WL2017R15_068_2
Modelling Belgische Kustzone en Scheldemonding, Deelrapport 3: Modelling van de morfologische effecten na aanleg nieuwe Geul van de Walvischstaart	WL2017R15_068_3
Modelling Belgische Kustzone en Scheldemonding, Rekennota: Berekening golfklimaat Vlaamse Baaien scenario's E4 en F1	WL2017R15_068_4
Memo: Modelling of bed morphology evolution at Knokke for a beach nourishment scenario (G2) by XBeach	WL2016M15_068_5
Memo: Morfologische analyse scenario's Vlaamse Baaien	WL2016M15_068_7
Memo: Morfodynamische effecten aanleg nieuwe geul van de Walvischstaart	WL2016M15_068_11
Memo: Geul van de Walvischstaart: samenvatting morfologisch onderzoek stabiliteit en baggerbeslag	WL2016M15_068_13
Memo: Hydrodynamic modelling of 'Vlaamse Baaien' dunebelt scenarios I3 and I4	WL2016M15_068_16
Memo: Sea level rise impact on Zeebrugge port accessibility - Telemac3D hydrodynamic modelling	WL2016M15_068_20



## 2 ‘Vlaamse Baaien’ dunebelt scenarios

In this chapter results from the hydrodynamic Telemac3D simulations considering two scenarios of a dunebelt spanning along the entire Belgian coast from Dunkirk to Cadzand, are presented. The presented scenarios are nearly identical except the scenario I3 is considered completely closed, whereas scenario I4 considers an opening at the entrance of Zeebrugge harbor. The results of these simulations are also compared to the current situation. Note that prior to scenarios I3 and I4, two other layouts of a closed seaward defense line (scenarios I1 and I2) have been investigated in De Maerschack *et al.* (2016). Scenarios I3 and I4 are considered as an optimization of I1 and I2 with respect to their impact on the coastal currents.

The aforementioned simulations were firstly performed by use of the Zeebrugge (ZB) model (IMDC 2013, 2015). An extra simulation for scenario I4 was performed by use of Scaldis (Smolders *et al.* 2016), which extends about 30 km further to the southwest direction compared to the ZB one, mainly in order to ensure that the flow results at the area close to the southwestern end of the dunebelt (French borders) are not, or minimally affected by the boundary of the (ZB model) domain.

Finally, a new unstructured computational grid is constructed and tested for scenario I4 using a new finite element mesh generator, named GMSH (Geuzaine and Remacle, 2009). Then the results are compared to the corresponding ones of the initial grid.

### 2.1 Scenarios overview

The bathymetry and topography of the two dunebelt scenarios I3 and I4, as well as the one of the Reference scenario, are shown respectively in Figure 1 to Figure 3. As mentioned before, the only difference between these two scenarios is that in scenario I3 the dunebelt is considered completely closed, while scenario I4 considers an opening at the entrance of Zeebrugge harbor. The maximum distance of the dunebelt from the current coastline is about 3000 m (at the West Coast). The topography of the dunebelt was provided by Maritime Access Division (aMT). More details about the bathymetry of the Reference scenario, in which the dunebelt topography was added, can be found in De Maerschack *et al.* (2016).

Figure 1: Bathymetry and topography of the ‘closed dunebelt’ scenario I3.

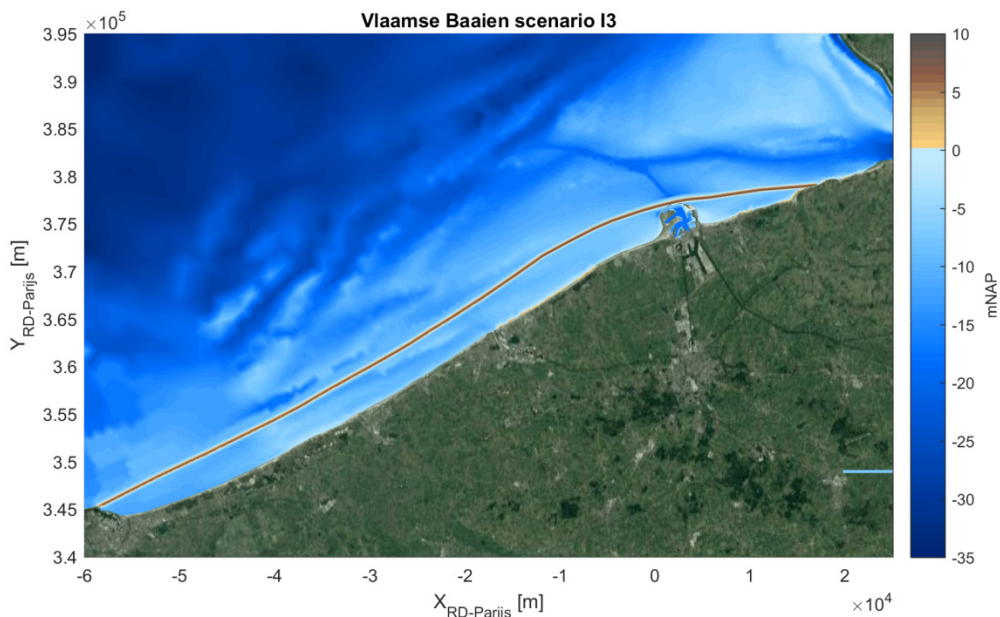


Figure 2: Bathymetry and topography of the 'open dunebelt' scenario I4.

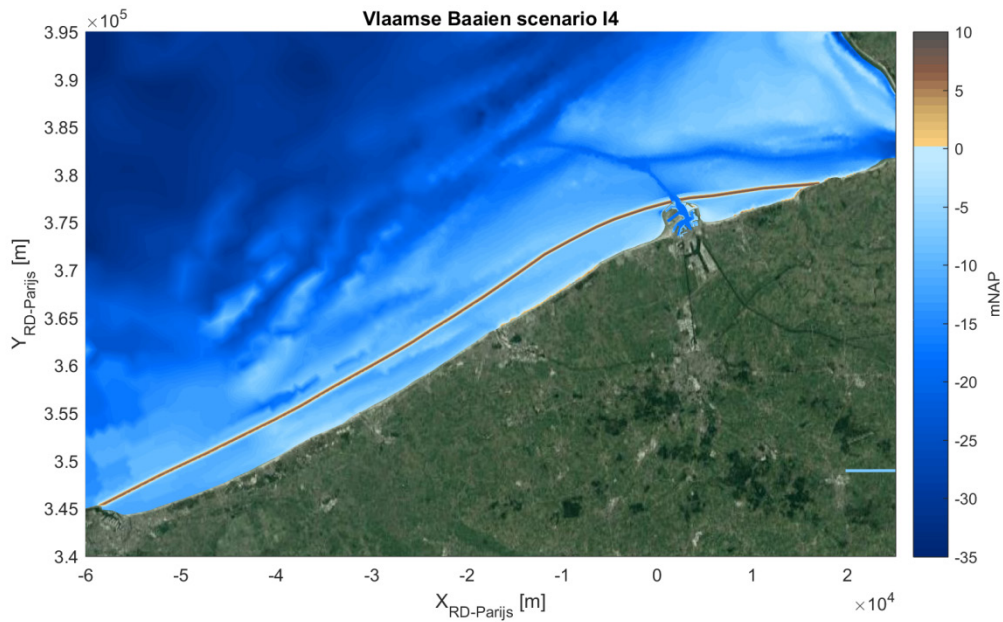
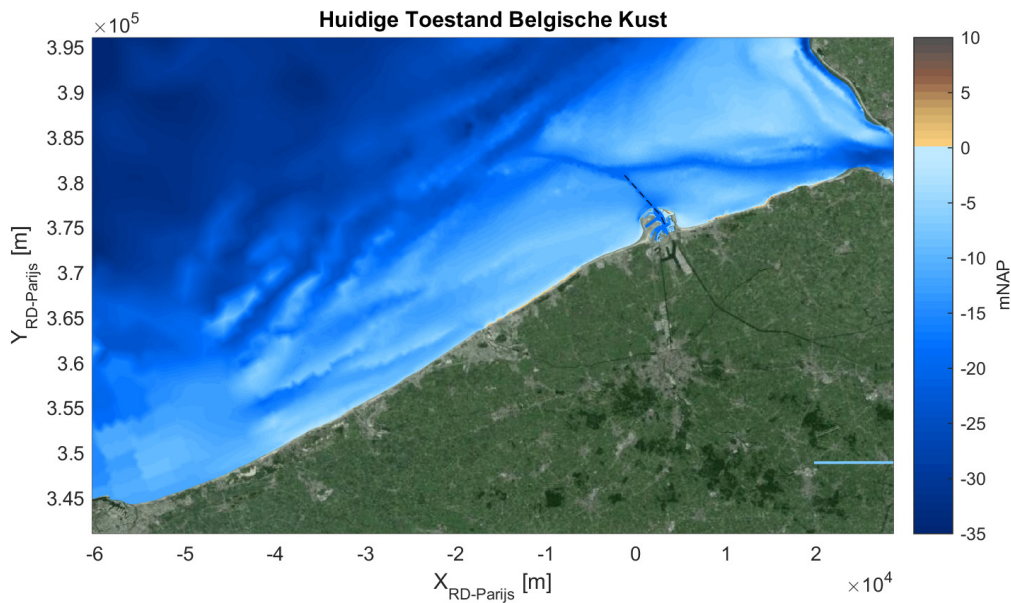


Figure 3: Bathymetry and topography of the Reference (current state) scenario I3.



## 2.2 Zeebrugge (ZB) model: Set-up

As mentioned before, a 3D unstructured TELEMAC model, also known as Zeebrugge (ZB) model, has been used for the simulations. The model is originally developed by IMDC (IMDC 2013, 2015) by order of Maritime Access Division. It has been used before for designing and analyzing the impact of a number of scenarios within the framework of the Vlaamse Baaien project (De Maerschalck *et al.*, 2016). For the scenarios discussed in this memo, the grid is locally adapted to the bathymetry of the dunebelt, see section 2.2.1.

For a comprehensive reading of the model setup and calibration, the reader is referred to the above mentioned reports. Appendix A contains a short summary of the model settings.

### 2.2.1 Computational grid

An unstructured computational grid consisting of 312 874 calculation points was established on a domain that covers the Southern North Sea from Dunkirk to Stellendam, including the Eastern Scheldt, the Western Scheldt and the Lower Sea Scheldt (Beneden-Zeeschelde), see Figure 4. The resolution of the grid varies from 5 to 10 m in the Zeebrugge harbor, becomes 20 m within a radius of about 4.5 km around the harbor and reaches a size up to 3 to 4 km at the semi-circular offshore boundary of the model. It has to be noted that the computational grid presented in De Maerschalck *et al.* (2016) was utilized as a basis for the construction of the present grid. In fact, the existing grid is for these scenarios locally refined along a narrow zone that covers the dunebelt area from the height of De Haan to the west boundary of the model, i.e. the shaded area in Figure 4.

In Figure 5, a detail of the grid at the refined area at the coastal area between Newport and Ostend is shown. The refinement of the grid was done by use of BlueKenue pre/post processing tool considering a hardline along the dune crest and imposing a size of 100 m for the neighboring elements at each side of the crestline as a refinement criterion. In this way, an adequate representation of the dune profile was achieved, Figure 6, without any manual intervention at the bathymetry values and so the dunebelt topography was successfully incorporated in the roughest part of the existing grid. The 2267 calculation points added after the local refinement affected only slightly the computational time. In the vertical direction, ten layers in a non-uniform sigma-coordinate system are used. The resolution is higher near the bed and the free surface. More details about the construction of the computational grid can be found in IMDC (2013).

Figure 4: Computational grid and bathymetry of 'Vlaamse Baaien' dunebelt scenario I3. The shadow zone shows the area of local refinement of the grid used in De Maerschalck *et al.* (2016).

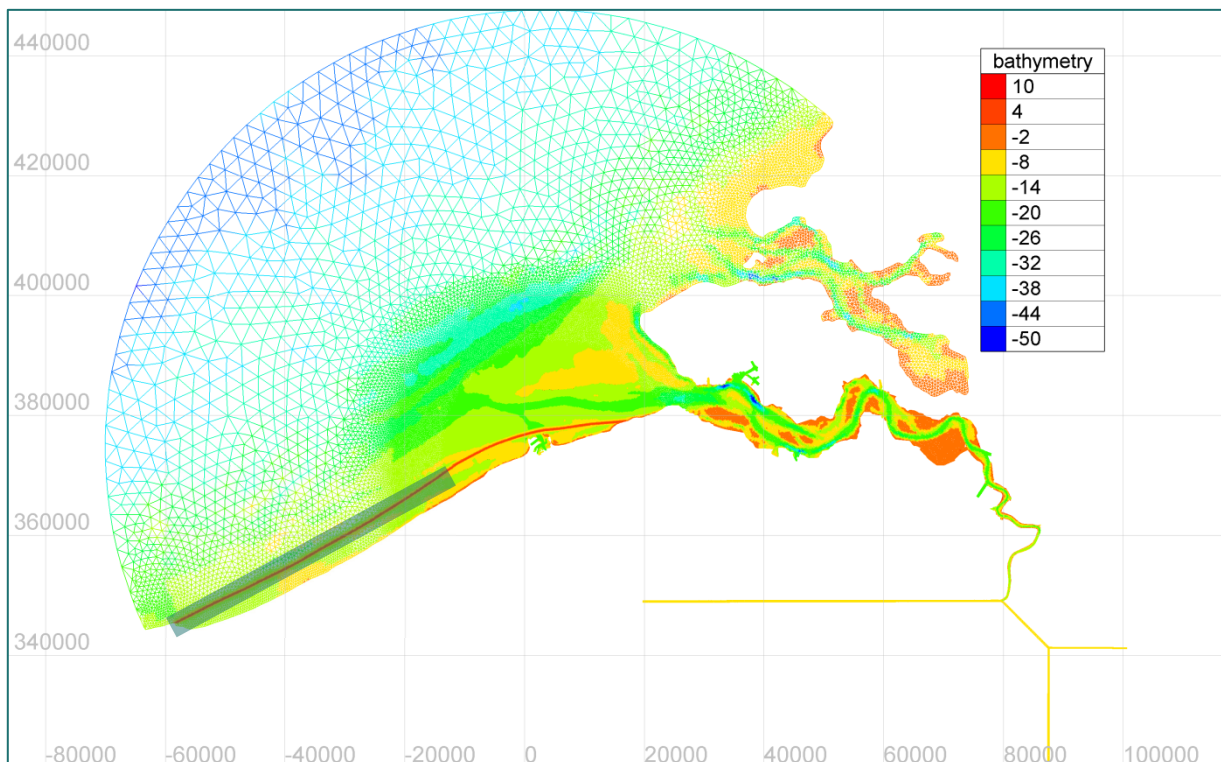


Figure 5: Detail of the computational grid, focusing at the coastal are between Newport (West boundary) and Ostend (East boundary).  
The black solid line corresponds to the topography cross-section presented in Figure 6.

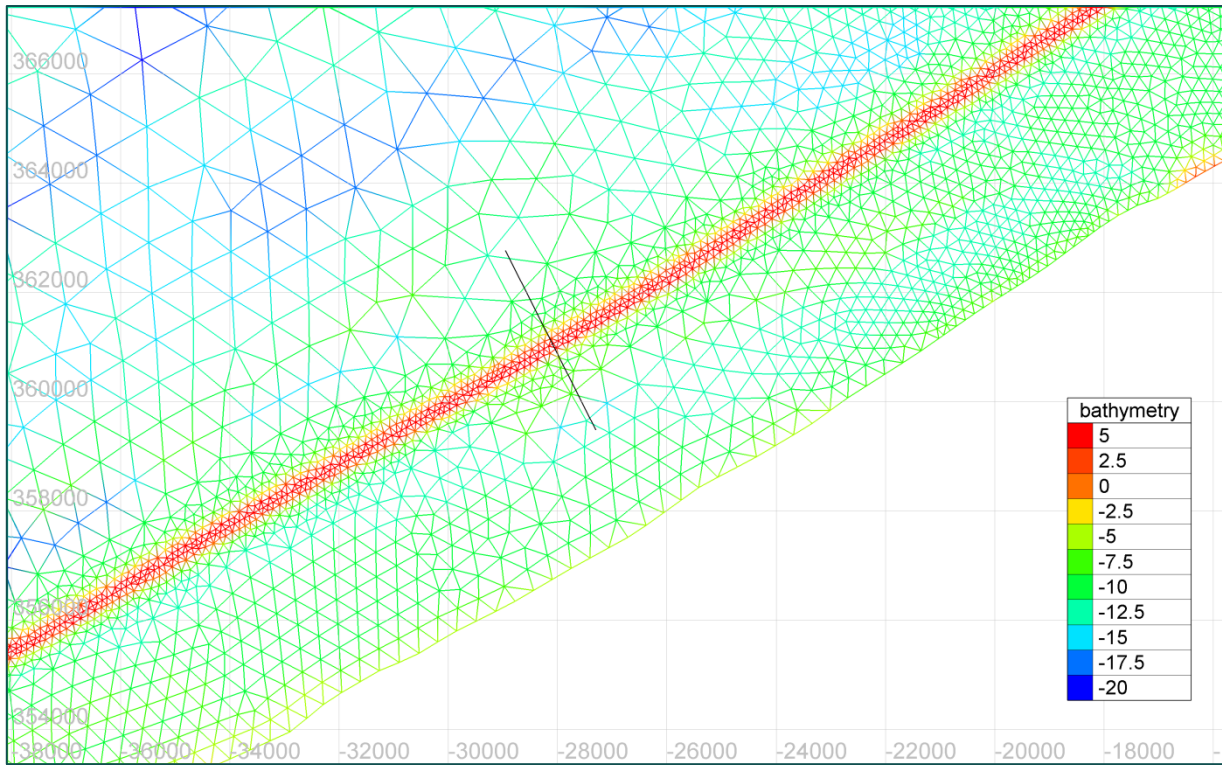
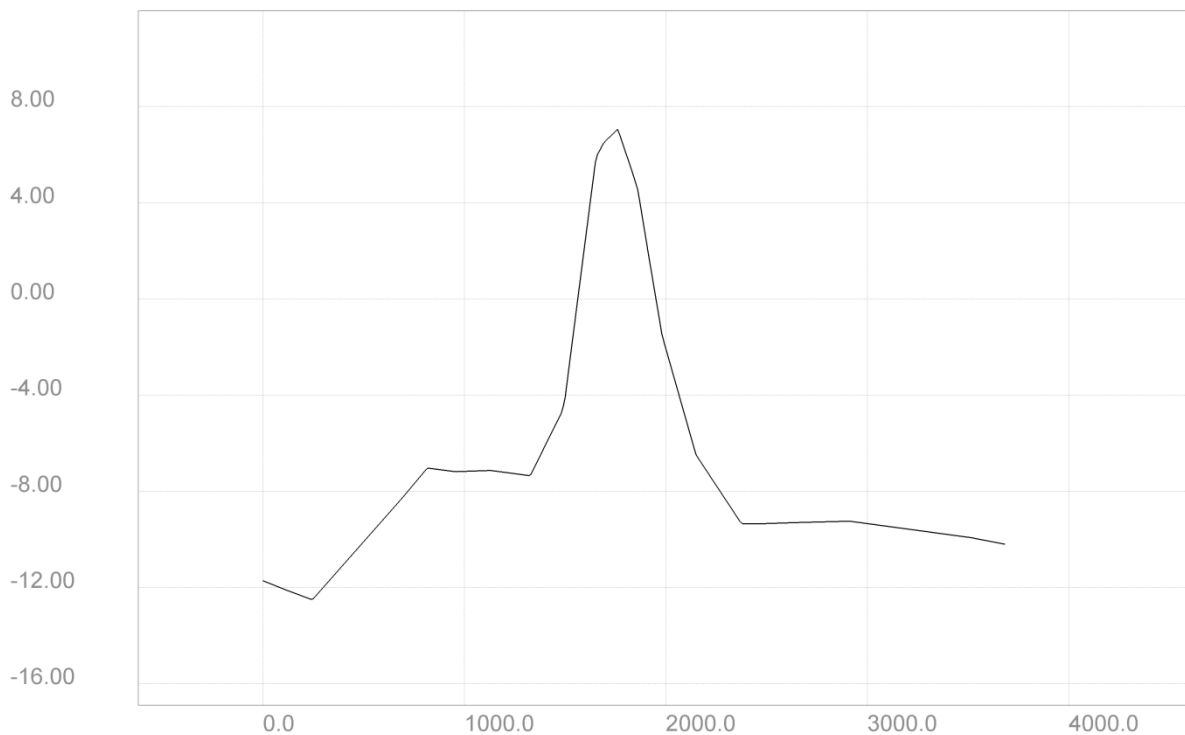


Figure 6: Dune cross-section at the location indicated in Figure 5.  
In the horizontal axis the distance from the landward boundary of the cross-section is shown. Vertical axis is in m NAP.



### 2.2.2 Offshore boundary conditions

The offshore (or sea) boundary conditions, imposed at every computational node along the semi-circular boundary, are provided by the CSM-ZUNO model train (Leysen *et al.*, 2012) through nesting. The Continental Shelf Model (CSM) and the nested ZUNO (ZUIDelijke NOordzee - Southern North Sea) model have run successively for a period of one month, i.e. April 2009. More details about the ZUNO model set-up can be found in IMDC (2015).

### 2.2.3 Simulation period

The model calculates water levels and currents for a period from 17/04/2009 to 27/04/2009. The analysis of currents and port accessibility is based on the period of a spring tide from 25/4/2009 3:20 to 26/04/2009 3:50.

## 2.3 ZB model: Results

### 2.3.1 Effects on the flow velocity field

The maximum depth-averaged flow during spring tide for scenarios I3 and I4, and the difference of each of them with the Reference scenario, are shown in Figure 7 and Figure 8, respectively. As expected, the differences in the flow field between scenarios I3 and I4 are restricted in the area of the harbor entrance and are hardly noticeable in Figure 7, as well as in Figure 8. In Figure 53 and Figure 54 of Appendix B, the maximum depth-averaged flow during the flood phase and the ebb phase of the simulated spring tide for scenarios I3 and I4, are shown respectively.

It is found that the construction of a seawall at a distance of about 3000 m from the West coastline leads to a general increase of the maximum flow magnitude of order 10 to 20 cm/s, along the western part of the Belgian coast up to 20 km offshore (Figure 8), which is significantly larger than in case of the former scenarios I1 and I2 (dunebelt located at 300 and 1800 m offshore). Two peaks are observed at the West Coast: one at the French borders and another one at the height of De Haan. Northeast of Zeebrugge, near Wielingen gully, an increase of 10-20 cm/s in the maximum flow rate is also observed, which is lower than in the scenario I2, see Appendix C. On the contrary, reduction (20-30 cm/s) of the flow strength is observed in the area around the Pas van het Zand gully and a milder one (10-15 cm/s) at the mouth of Scheldt estuary.

Figure 7: Maximum depth-averaged flow velocity (magnitude [m/s]) for dunebelt scenario I3 (left) and I4 (right) during spring tide [25-Apr-2009 03:20 → 26-Apr-2009 03:50].

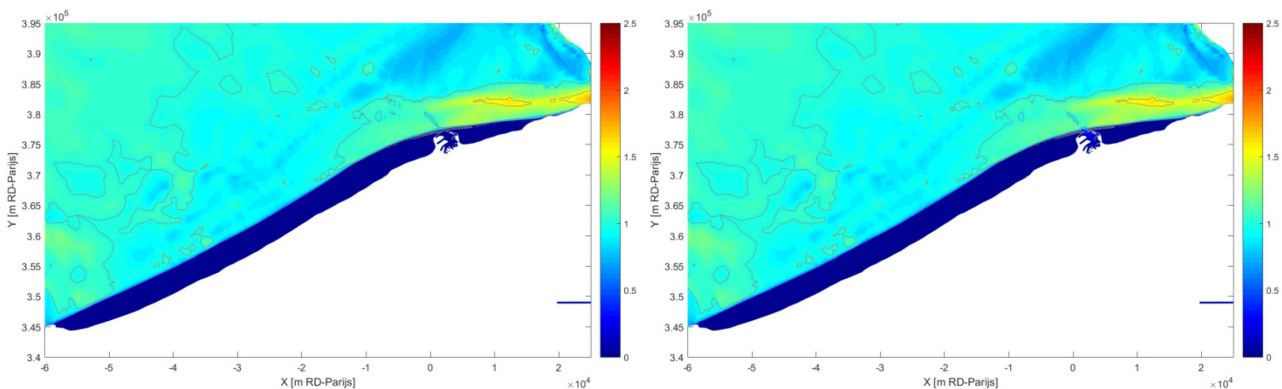
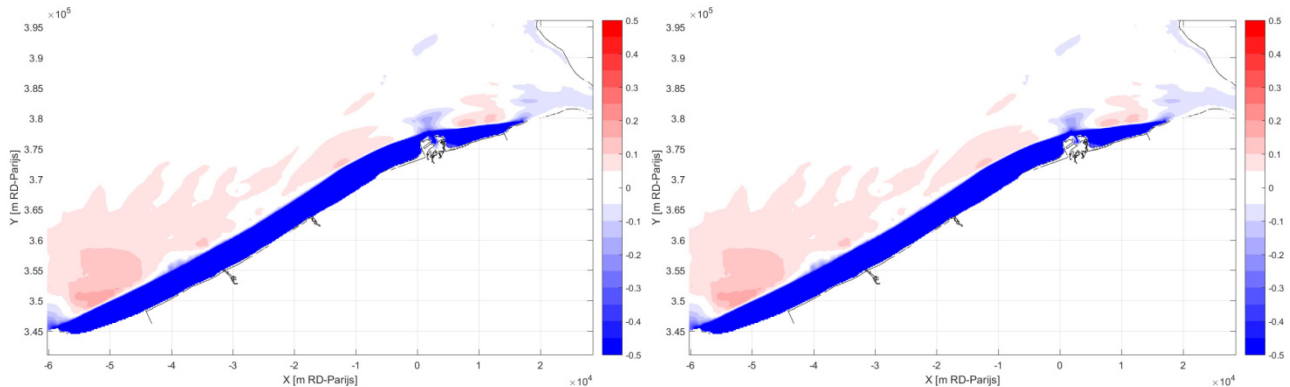


Figure 8: Difference in maximum depth-averaged flow velocity [m/s] between dunebelt scenario I3 and Reference scenario (left) and I4 and Reference scenario (right) during spring tide [25-Apr-2009 03:20 → 26-Apr-2009 03:50].



### 2.3.2 Port accessibility

The shape of the dunebelt has a positive effect on the accessibility (under the assumption that the seawall provides a passage to the sea, i.e. scenario I4). This is indicated in Figure 9, where the time-windows of transverse, to the Pas van Zand trajectory, velocities greater than 1.5kn and 2kn during spring tide, are shown. Specifically, it is indicated that transverse velocities along the trajectory are always less than 2kn, while they exceed 1.5kn only for one hour during flood phase (spring tide). The corresponding figure for the Reference scenario (figure 11 in De Maerschack et al., 2016) showed that there exist 2-hour time windows of velocities greater than 2kn during flood phase, while 3-hour windows during flood and 1-hour windows during ebb of velocities greater than 1.5kn<sup>1</sup> were observed.

The spatiotemporal variation of the depth-averaged flow velocity along the Pas van Zand trajectory is shown in Figure 10, where the parts of increased velocities are located on the trajectory. There is also given a difference plot of the velocity variation versus the Reference scenario, in which the positive effect of the dunebelt it is clearly indicated, as reduction of the velocity magnitude is greater than 1m/s at the entrance of the harbor.

<sup>1</sup> Note that in this report and in (De Maerschack et al., 2016) cross velocities along the navigation track are averaged over the entire water depth. In (Dujardin et al., 2011) the velocities are averaged over the top 10 m of the water column resulting in slightly higher cross velocities and longer time windows of exceeding cross velocities.

Figure 9: Window barriers for the, transverse to the Pas van Zand trajectory, depth-averaged velocities greater than 2kn (above) and 1.5kn (below) calculated for scenario I4 during spring tide.

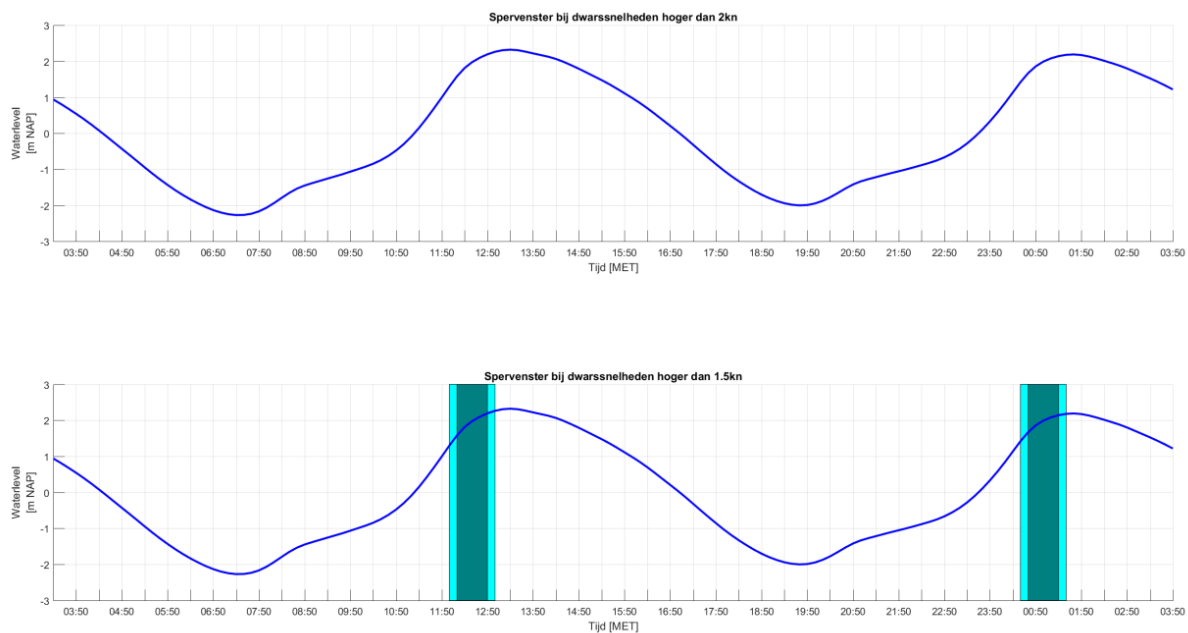
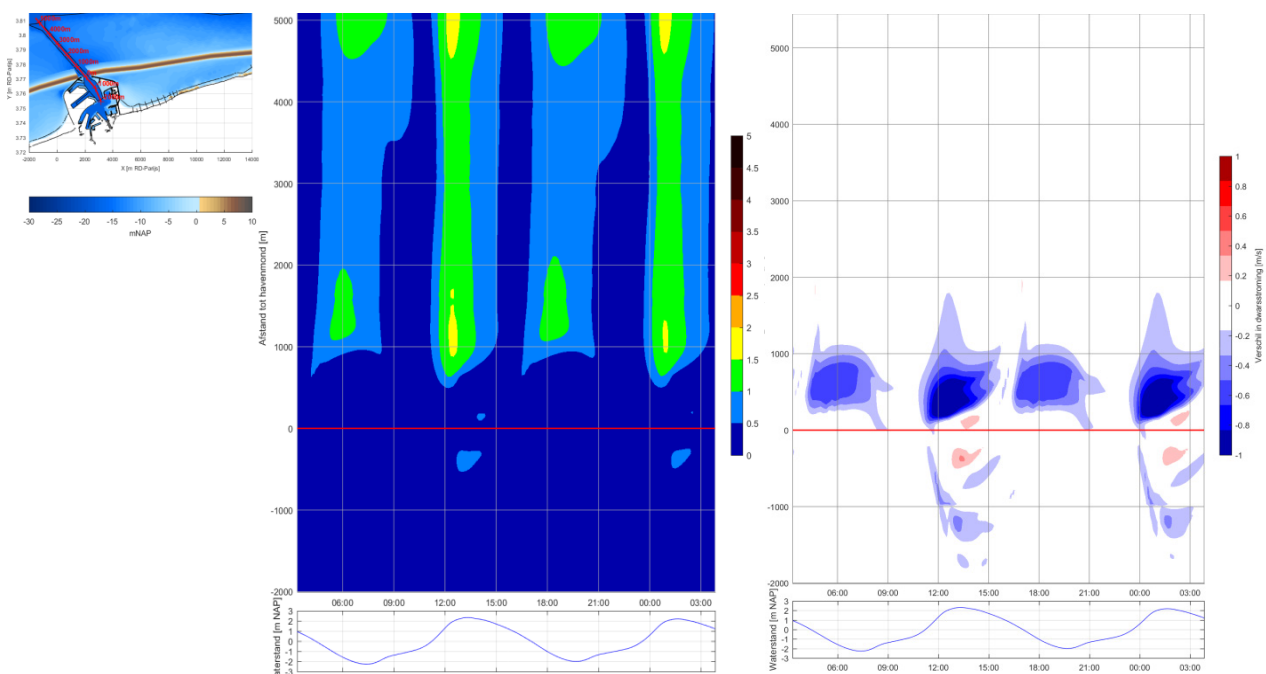


Figure 10: Spatiotemporal variation of the depth-averaged, transverse to the Pas van Zand trajectory, flow velocities during spring tide for scenario I4 (left). Difference plot versus Reference scenario (right).



## 2.4 Scaldis model: Set-up

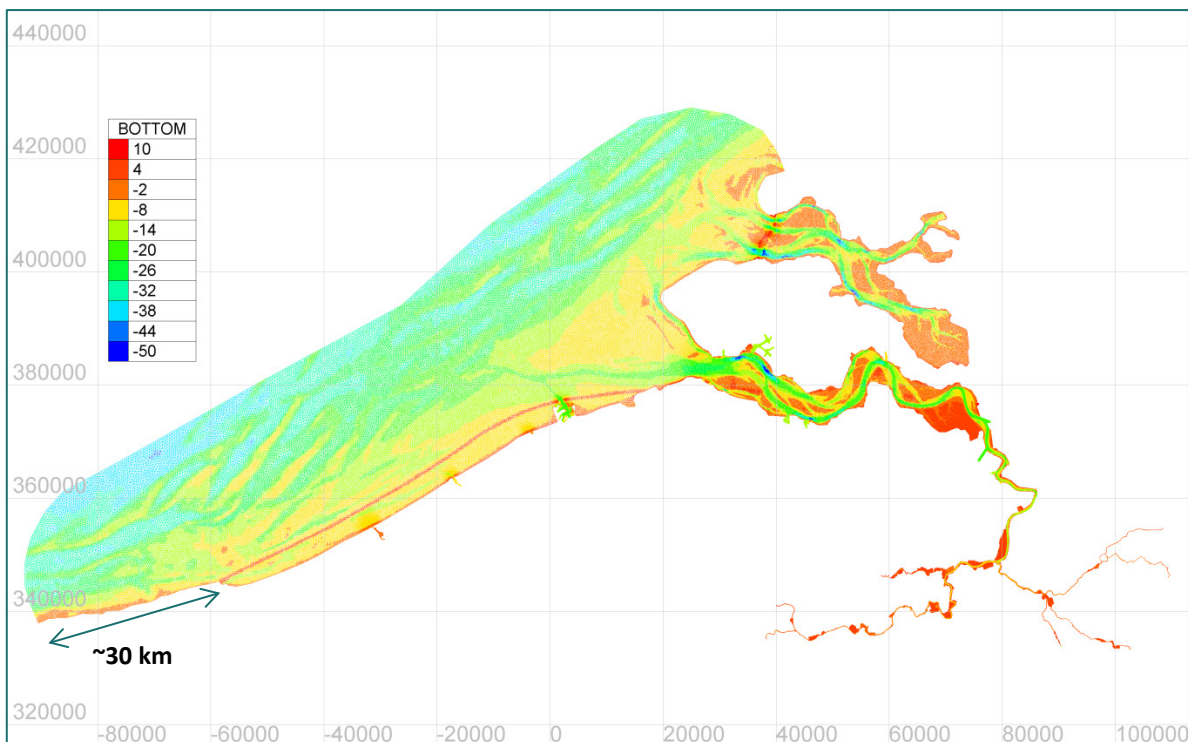
As mentioned in the beginning of this Chapter, the 3D unstructured TELEMAC model named ‘Scaldis’ (Smolders *et al.* 2016) has been used in order to ensure that the southwestern boundary of the ZB model domain has a negligible impact on the currents near the French border. The original grid, which consists of 459 692 nodes and 873 419 elements (per layer), was used without any refinement. The grid and the bathymetry of the model after the incorporation of the dunebelt (scenario I4) is shown in Figure 11. In the coastal area the resolution varies from 500 to 200 m depending on the depth. The resolution in the Eastern Scheldt is 200 m, while in the Western Scheldt the resolution is 120 m. The most important model settings are described in the second column following table:

Table 2: Main settings of Scaldis and ZB models.

Parameter	Scaldis	ZB
Time step	4 s	20 s
Number of layers (vertical)	5	10
Version TELEMAC	TELEMAC V7P2R0	TELEMAC V7P0R1
Salt transport	On	Off
Wind	Off	Off
Bed roughness	Manning (0.022 in the coastal area)	Manning (0.02 in the coastal area)
Simulation period	13/09/2013 00:00 -23/09/2013 00:00	17/04/2009 00:00 -27/04/2009 00:00

Note that although the simulated periods are different for both models, the time periods for the model comparison were properly selected so that the tidal conditions of the two models were comparable. For a comprehensive reading of the model setup and calibration, the reader is referred to the above mentioned reports.

Figure 11: Computational grid and bathymetry of ‘Vlaamse Baaien’ dunebelt scenario I4 incorporated in Scaldis model.



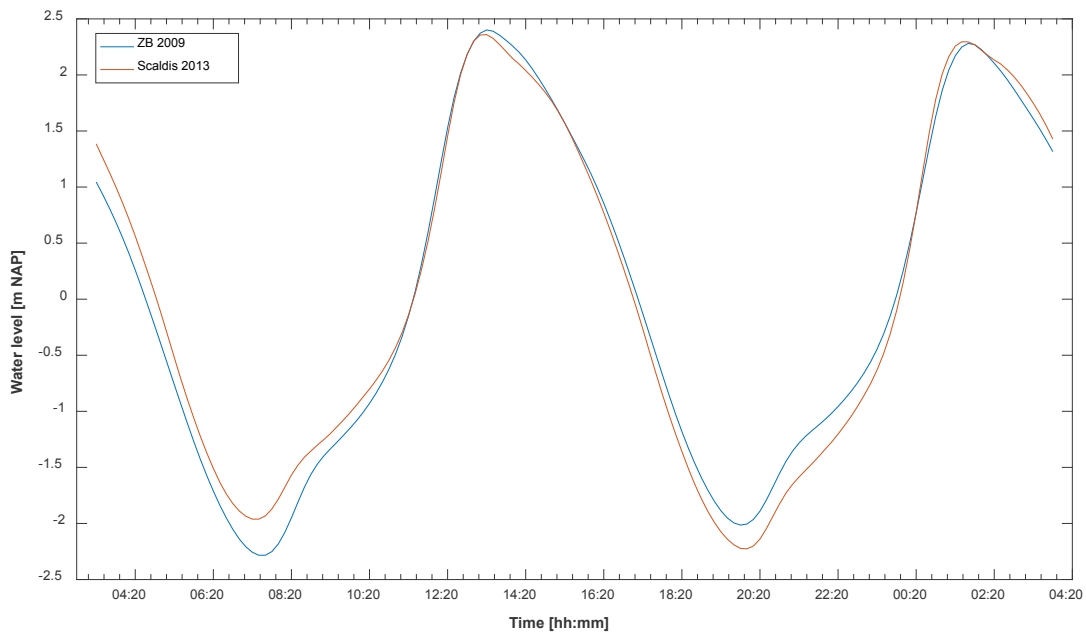


## 2.5 Scaldis model: Results

Two different scenarios were simulated by Scaldis: The Reference scenario (current situation) and the dunebelt scenario I4 of 'Vlaamse Baaien'. The objective was to create difference plots of the flow velocity field between the two scenarios and compare them with the corresponding ones of the ZB model.

In order to be sure that the selected hydrodynamic forcing is similar in both models (as the offshore boundary conditions refer to different simulation periods – see Table 2), the water level variation in time at a random coastal position (Paardenmarkt) was compared between the two models (Figure 12).

Figure 12: Water level variation in time at Paardenmarkt.



### 2.5.1 Effects on the flow velocity field

The difference plots of the maximum depth-averaged flow during spring tide between scenario I4 and the Reference scenario, are shown in Figure 13 and Figure 14, respectively for the Scaldis and the ZB model. In general, the difference patterns (both increase and decrease patterns) are quite similar in both plots, especially East of Oostende and in the vicinity of Zeebrugge harbor ( $x_{RD} > -2 \times 10^4$ ), although the grid resolution, the simulation period and a quite a few of the models' settings are not the same. The most important finding is that the disturbance of the flow due to the presence of the dunebelt at the southwestern boundary of the model is restricted to the vicinity of Dunkerke (up to  $x_{RD} \approx -6.5 \times 10^4$ , close to the end of dune) as shown in Figure 13, which agrees well with the results of the ZB model (Figure 14). The increase of maximum velocity in the area between the French border and Oostende ( $-6 \times 10^4 < x_{RD} < -2 \times 10^4$ ), presents differences between the two models, which can be attributed to the difference in the local grid resolution (the ZB grid is quite rough at this region, this will be refined in the future model developments, see also section 2.6). In Figure 15 and Figure 16, the difference plots of the maximum depth-averaged flow during the flood phase and the ebb phase of the simulated spring tide, are shown respectively for the two models.

Figure 13: Difference in maximum depth-averaged flow velocity [m/s] between dunebelt scenario I4 and Reference scenario during spring tide [21-Sep-2013 04:30 → 22-Sep-2013 05:00] for **Scaldis model**.

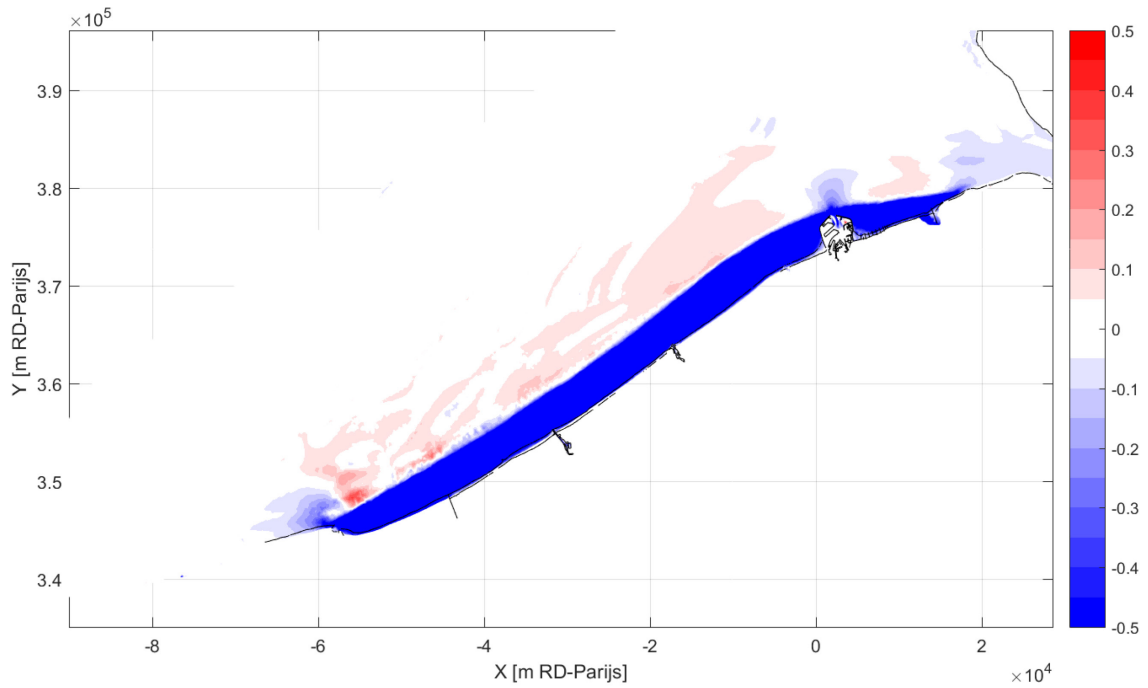


Figure 14: Difference in maximum depth-averaged flow velocity [m/s] between dunebelt scenario I4 and Reference scenario during spring tide [25-Apr-2009 03:20 → 26-Apr-2009 03:50] for the **ZB model**.

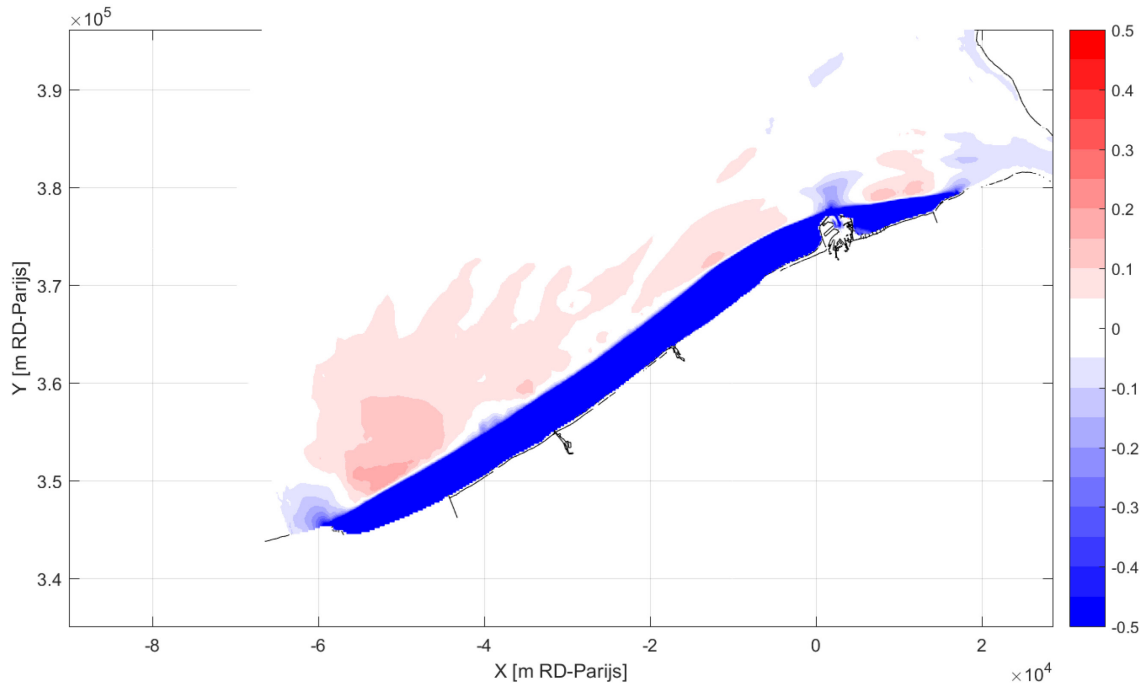


Figure 15: Difference in maximum depth-averaged flow velocity [m/s] between dunebelt scenario I4 and Reference scenario during flood phase [21-Sep-2013 12:10 → 16:10] (left) and ebb phase [21-Sep-2013 17:10 → 20:10] (right) for the **Scaldis model**.

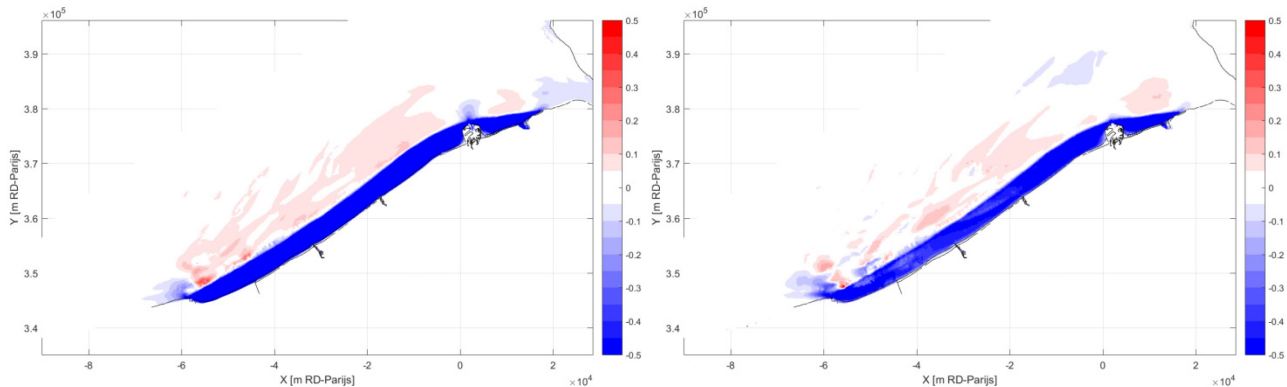
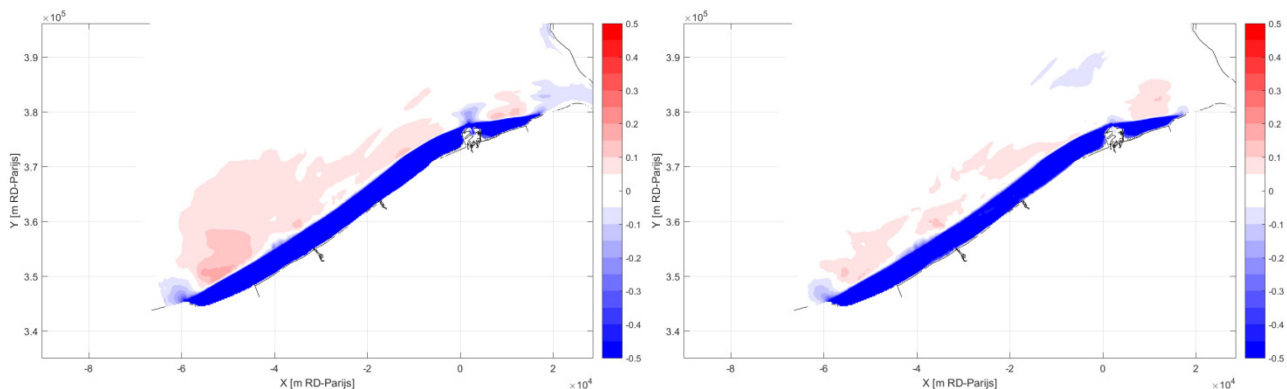


Figure 16: Difference in maximum depth-averaged flow velocity [m/s] between dunebelt scenario I4 and Reference scenario during flood phase [25-Apr-2009 11:00 → 15:00] (left) and ebb phase [25-Apr-2009 16:00 → 19:00] (right) for the **ZB model**.



## 2.6 GMSH grid testing

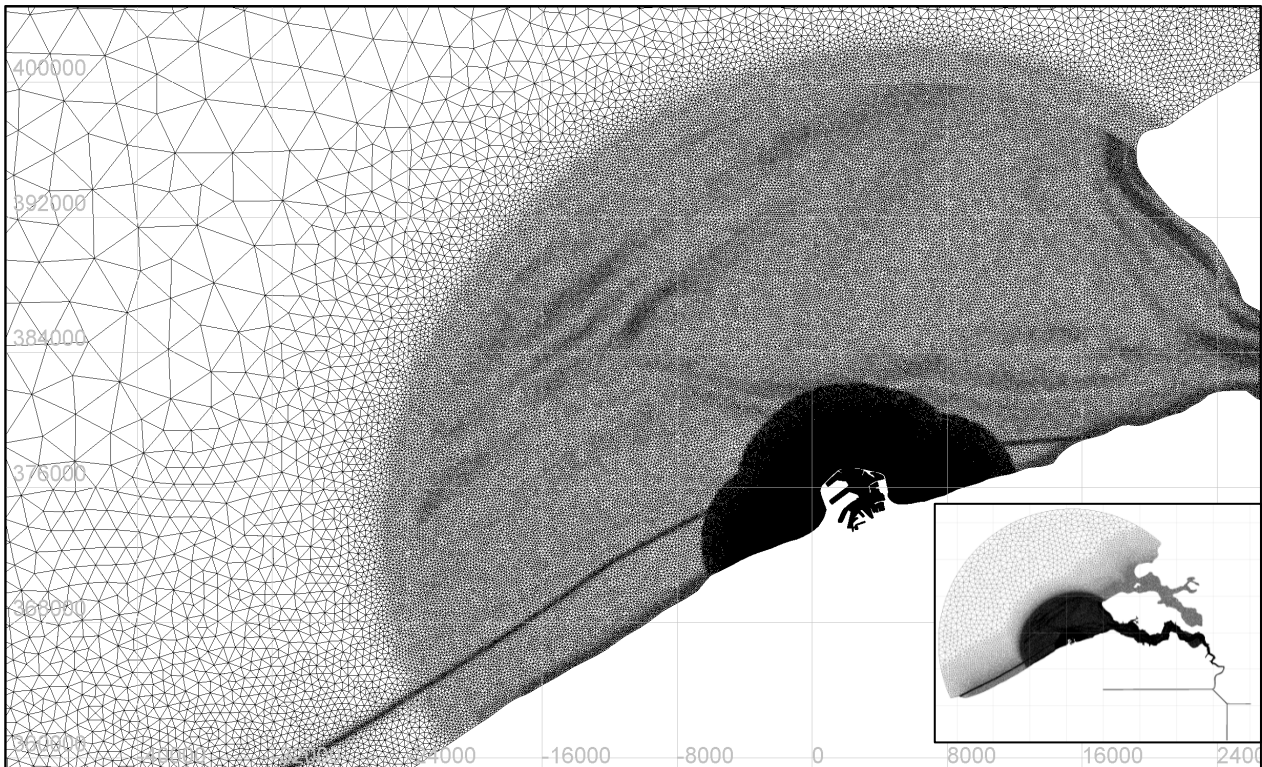
### 2.6.1 General

A new unstructured computational grid to be used in Telemac3D hydrodynamic simulations is constructed and tested for scenario I4 using the finite element mesh generator GMSH (Geuzaine and Remacle, 2009). One of the main advantages of this meshing tool is the accurate specification of the target element size based on different conditions such as the local bathymetry, the bathymetry gradient, the distance from specified boundary lines, etc.. Moreover, this grid generator allows for efficient generating adapted grid for new scenarios with a limited number of manual interventions.

The computational grid consists of 325 940 nodes (643 422 triangular elements) with the maximum resolution of 10 m being in the Zeebrugge harbor and in a distance of 1500 m around it and then the grid size becomes 50 m within a radius of about 9 km around the harbor (see Figure 17). The resolution of the grid restricted by the fictitious elliptic arc which intersects Westkapelle (east end) and Ostend (west end) varies from 100 m to 200 m based on the bathymetry gradient. The gradient of the bathymetry is selected as a target value to ensure higher resolution in the vicinity of steep bathymetries like channel slopes. A higher resolution is here justified since it is expected that at locations with steep bathymetry gradients, also flow velocity gradients will occur. The same holds for non-smooth geometries, like harbor breakwaters. The resolution at the Western Scheldt estuary is defined in exactly the same manner, while a constant

resolution of 400 m is chosen for the Eastern Scheldt. Moving further from the coast to the offshore direction, the resolution reduces and reaches a size up to 3 km at the semi-circular offshore boundary of the model. Lastly, the grid size along the dunebelt varies from 70 m at the crest to 250 m at the tow based on the local bathymetry-topography.

Figure 17: Part of the ZB computational grid in the area of interest made by use of GMSH, where regions of varied resolution are indicated.



### 2.6.2 Quality metrics

The mesh quality control is based on the calculation of the following three basic metrics:

- Skewness: determines how close to an ideal shape, i.e. equiangular triangle, a grid cell is. It is defined as:

$$Sk = \max\left[\frac{(\vartheta_{max} - \vartheta_e)}{(180 - \vartheta_e)}, \frac{(\vartheta_e - \vartheta_{min})}{\vartheta_e}\right]$$

where  $\vartheta_{max}$  and  $\vartheta_{min}$  are the maximum and the minimum angles of a cell, respectively, and  $\vartheta_e = 60$  is the angle of an equiangular cell. Skewness varies between 0 and 1. According to the definition of skewness, a value of 0 indicates an equilateral cell (best) and a value of 1 indicates a completely degenerated cell (worst). Degenerate cells (slivers) are characterized by nodes that are nearly co-linear. Note that  $Sk$  values up to 0.95 are considered acceptable (ANSYS, 2015).

- Aspect ratio: The aspect ratio of a triangular cell is defined as:

$$AR = 2R_i/R_o$$

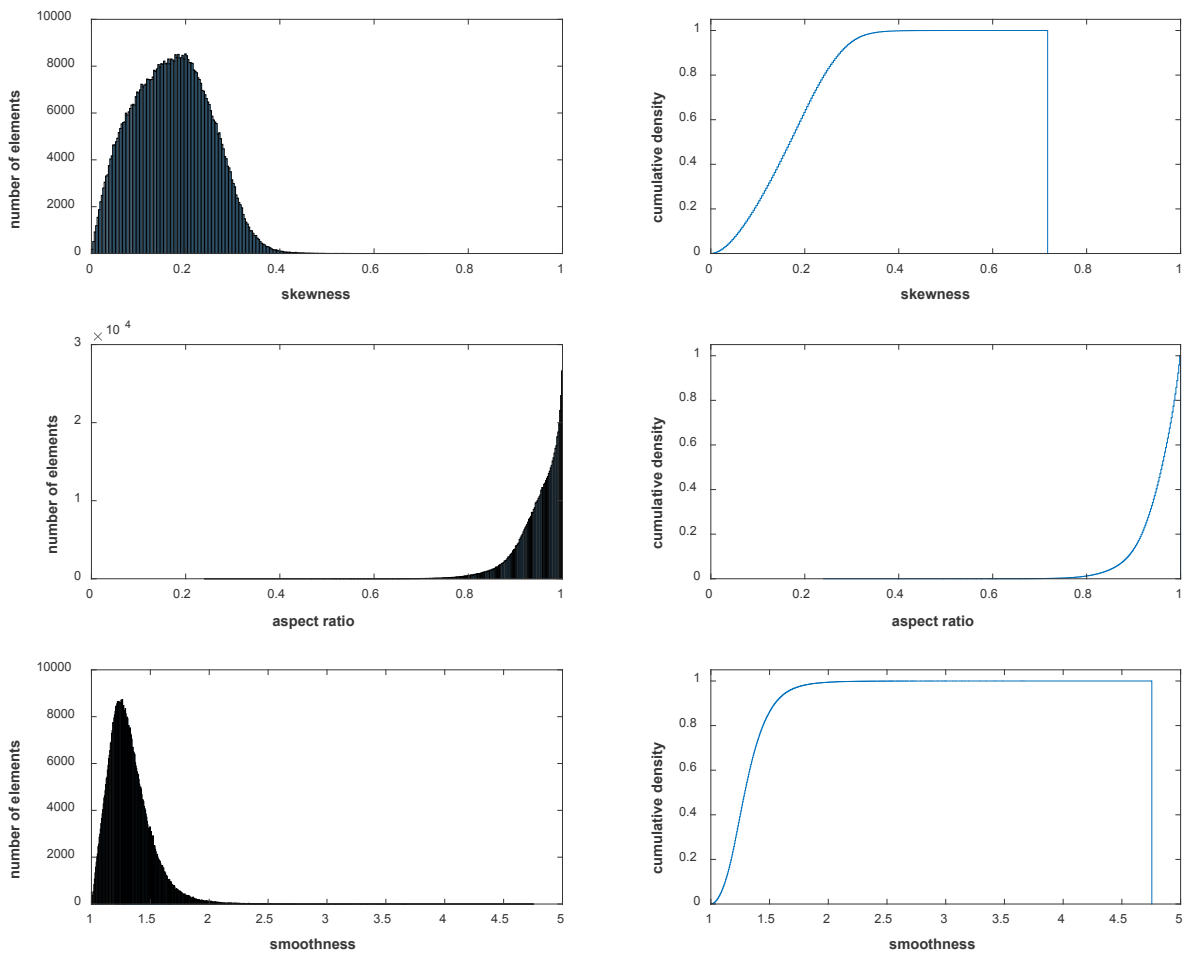
where  $R_i$  is the radius of the circle inscribed in a triangle and  $R_o$  is the radius of the circle circumscribed around the triangle. The aspect ratio varies between 0 and 1. The larger aspect ratio implies the better quality of the triangle and so the aspect ratio of the equilateral triangle is 1.

- Smoothness: is defined as the area ratio of two adjacent cells (same inner face). According to ANSYS (2015) it is recommended that the smoothness remains lower than 2.5 (area of larger cell over the one of the smaller cell). Meshes with smoothness values greater than 5 are of poor quality.

Note that the GMSH software is designed to optimize for these quality parameters taking into account the geometric complexity and the user defined targets without the need for manual interventions.

In Figure 18, the aforementioned quality metrics for the mesh constructed for scenario I4, are presented. On the subfigures of the left column the quality metrics are plotted versus the number of elements, while in the right column versus the cumulative density or else the cumulative percentage (divided by 100) of the elements. The constructed mesh is generally of very good quality as indicated by the skewness distribution ( $Sk < 0.42$  for 99.9% of the elements), the aspect ratio distribution ( $AR > 0.7$  for 99.9% of the elements), and the smoothness distribution since 99.9% of the elements presented values lower than 2.35.

Figure 18: Quality metrics for the computational grid of scenario I4.



### 2.6.3 Results

The maximum depth-averaged flow during spring tide for scenario I4, and the difference of the maximum velocity with respect to the Reference scenario, are shown in Figure 19 and Figure 20, respectively. Comparing Figure 19 to the corresponding one of Figure 7 (right subfigure) and Figure 20 to the corresponding one of Figure 8 (right subfigure), it appears that the numerical predictions of the new (GMSH) grid are almost identical to the ones of the original ZB model. Very slight differences are observed close the western boundary (see Figure 20) due to larger difference of the local grid size between the two utilized meshes. We have to remark that although grid is refined in this area, still the quality of the underlying bathymetric data source us rather poor is this area. This will be refined later on.

Figure 19: Maximum depth-averaged flow velocity (magnitude [m/s]) for dunebelt scenario I4 during spring tide [25-Apr-2009 03:20 → 26-Apr-2009 03:50] – GMSH grid.

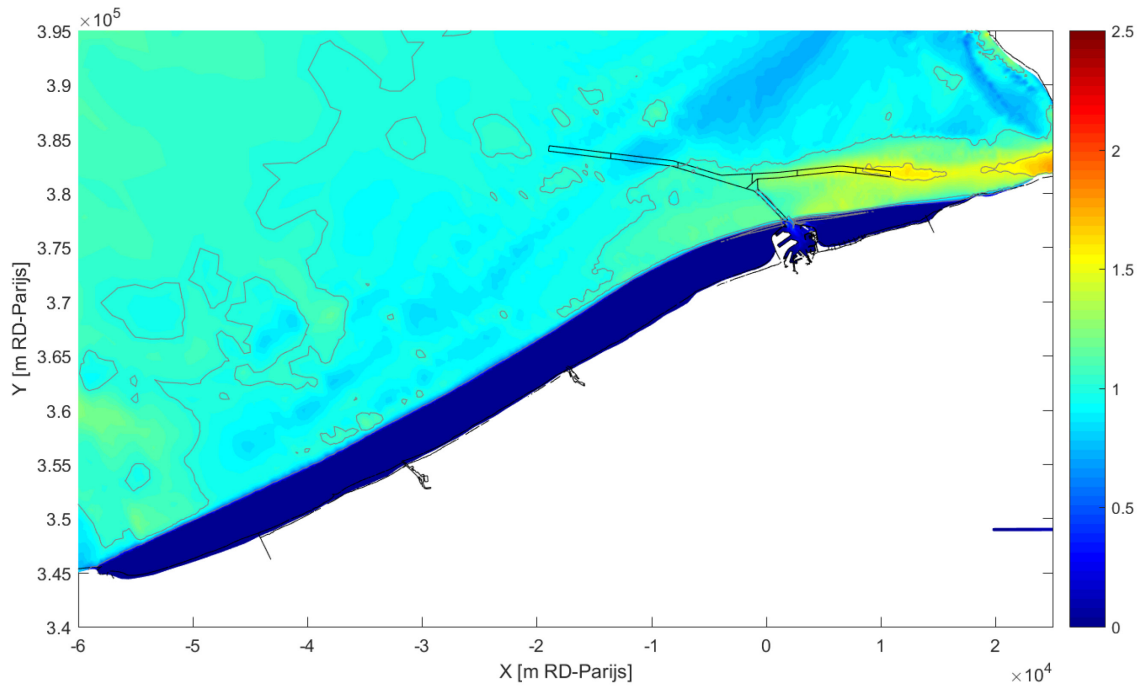
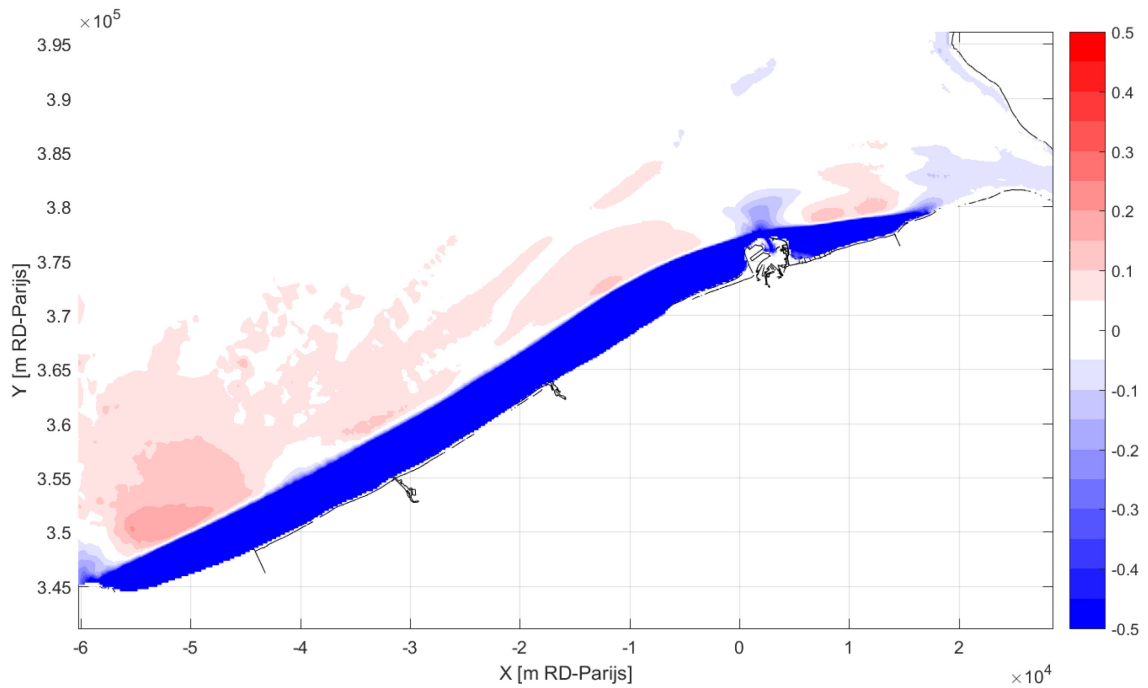


Figure 20: Difference in maximum depth-averaged flow velocity [m/s] between dunebelt scenario I4 and Reference scenario during spring tide [25-Apr-2009 03:20 → 26-Apr-2009 03:50] – GMSH grid.



## 3 Impact of Sea level rise on the Zeebrugge port accessibility

The impact of sea level rise on the currents near the Belgian coast and especially at the Zeebrugge port access, is investigated in this Chapter through Telemac3D hydrodynamic simulations. Three different scenarios of future sea level rise along with the Reference scenario (current situation). The selected scenarios for the sea level rise are identical to those determined in the framework of the CLIMAR project for the evaluation of climate change impacts, (Van den Eynde *et al.*, 2009), i.e. a moderate sea level rise of 60 cm by the year 2100, a warm scenario with sea level rise of 90 cm and a worst case scenario of sea level rise scenario of 200 cm. The boundary conditions for the Telemac3D model are derived from a CSM-ZUNO model run with the increased water levels superimposed on the CSM continental shelf boundaries.

In the following section the basic elements of the model set-up are given. Then the results of a tidal analysis for possible changes in the amplitude and the tidal phase, the hydrodynamic flow results focusing at the coastal area and the Western Scheldt mouth, and the investigation of the port accessibility for the considered scenarios, are presented.

### 3.1 Model set-up

#### 3.1.1 Computational grid

The numerical simulations of the sea level rise (SLR) scenarios are performed by use of the Zeebrugge (ZB) model which was utilized for the simulation of the dunebelt scenarios (see Section 2.2). It has to be noted though that the local refinement of the grid along the narrow zone that covers the dunebelt no longer exists, meaning that the computational grid for the SLR simulations is identical to the one presented in De Maerschalck *et al.* (2016) consisting of 310607 calculation points (see Figure 21).

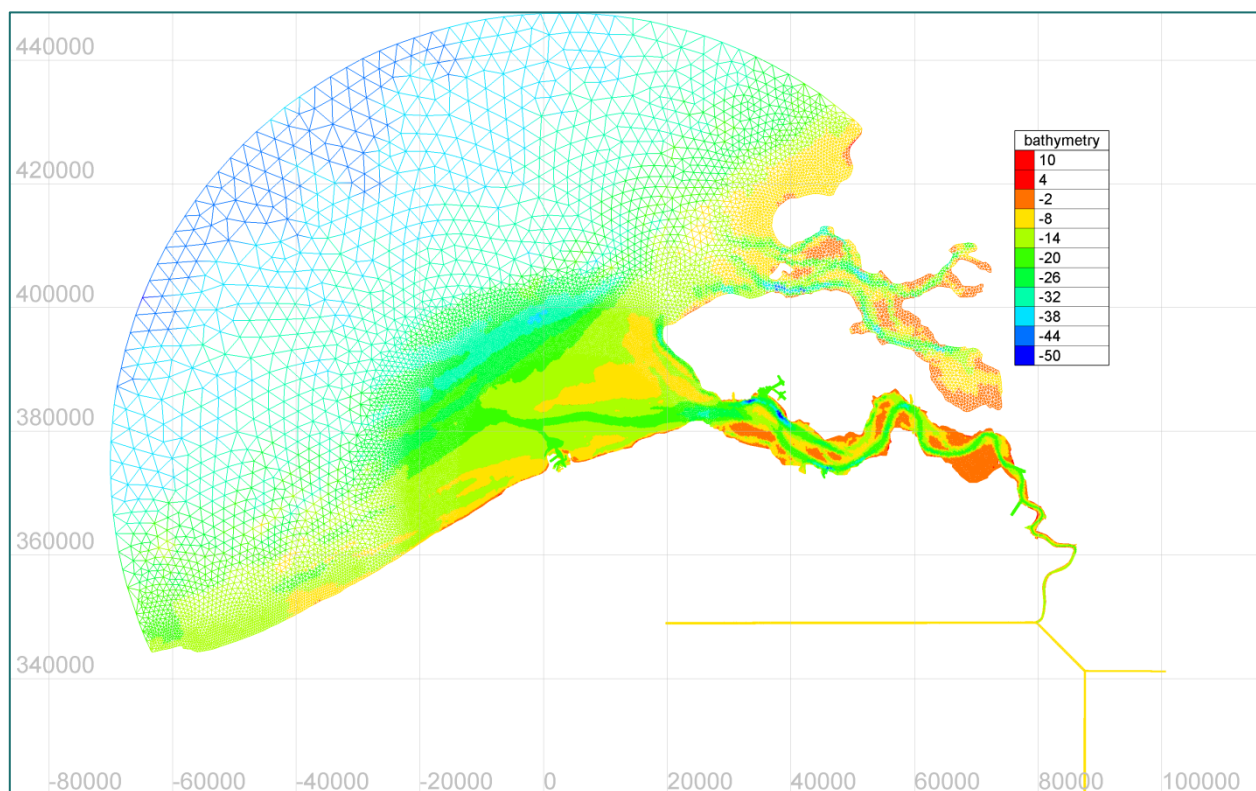
#### 3.1.2 Offshore boundary conditions

The offshore (or sea) boundary conditions, imposed at every computational node along the semi-circular boundary, are provided by the CSM-ZUNO models (Leyssen *et al.*, 2012) through nesting. The Continental Shelf Model (CSM) and the nested ZUNO v3 model have run successively for the period from 01/04/2009 to 01/05/2009, considering absence of wind (harmonic run), for the current situation as well as the considered sea level rise scenarios. Details about the setup and the results of the CSM-ZUNO simulations for the generation of the sea boundary conditions for each scenario can be found in the memo of Chu (2017) which is added in Appendix E: .

#### 3.1.3 Simulation period

The model calculates water levels and flow velocities for the period from 15/04/2009 to 01/05/2009. The basic tidal analysis is based on the period from 16/04/2009 to 01/05/2009, while the analysis of currents and port accessibility is based on the period of a spring tide and specifically from 25/04/2009 3:20 to 26/04/2009 3:50.

Figure 21: Computational grid and bathymetry of the utilized T3D hydrodynamic model for the SLR simulations.



### 3.1.4 SLR scenarios

The selected scenarios of future sea level rise (SLR) are identical to the moderate, the warm and the worst case scenario for the year 2100, according to the determination within the CLIMAR project (Van den Eynde *et al.*, 2009). This means that three scenarios, which foresee increase of the mean sea level equal to 60 cm, 90 cm and 200 cm, are considered in the present study. In the following table, the investigated cases and their identifiers are presented.

Table 3: Description of investigated scenarios.

Scenario	ID	Sea level rise [cm]
Reference	T0	0
Moderate	SLR060	60
Warm	SLR090	90
Worst-case	SLR200	200



## 3.2 SLR results

The presented results include: (a) a tidal analysis for changes in the amplitude and the tidal phase, (b) comparison of the flow velocity field between the sea level rise scenarios and the Reference scenario and (c) port accessibility investigation through comparison of the transverse currents along the Pas van het Zand navigation channel among the considered scenarios.

### 3.2.1 Tidal analysis

The basic tidal analysis is performed for the period from 16/04/2009 to 01/05/2009, which includes both neap and spring tidal cycles, in order to investigate the influence of the sea level rise on the basic tidal characteristics. The results of the analysis refer to selected locations at the coast and the Scheldt estuary, where continuous measurements are also conducted (see Figure 22).

#### Basic tidal analysis

The bias in the complete water level time-series between the sea level rise scenarios and the Reference scenario, presented in Figure 23, indicates the successful response of the model to the imposition of the offshore boundary conditions for each of the sea level rise scenarios. In other words the difference between the mean sea level of the sea level rise scenarios and the Reference scenario almost coincides with the imposed sea level rise at all locations. For a rough but clear view of how the sea level rise affects the tide, the temporal evolution of the water level at the port of Zeebrugge is shown for all the investigated scenarios in Figure 24, where the rise of the mean water level is obvious. On the contrary, effects of sea level rise on tidal amplitude and phase are not so obvious in the specific figure.

Figure 22: Locations used in the basic tidal analysis.

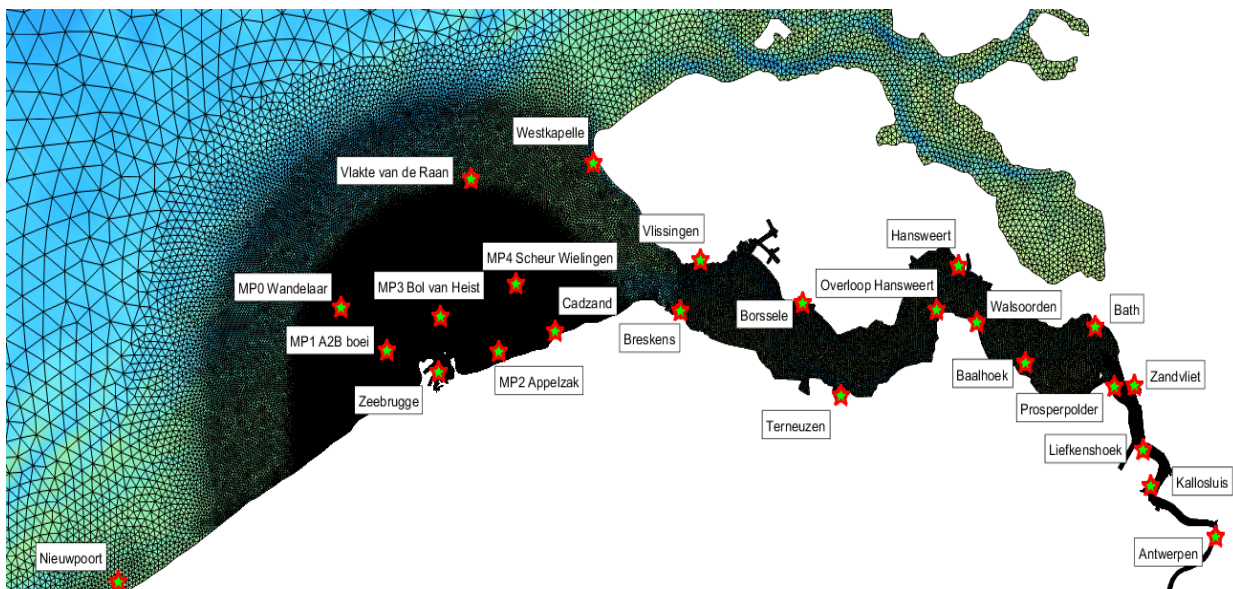


Figure 23: Bias in the complete water level time-series between the sea level rise scenarios and the Reference scenario.

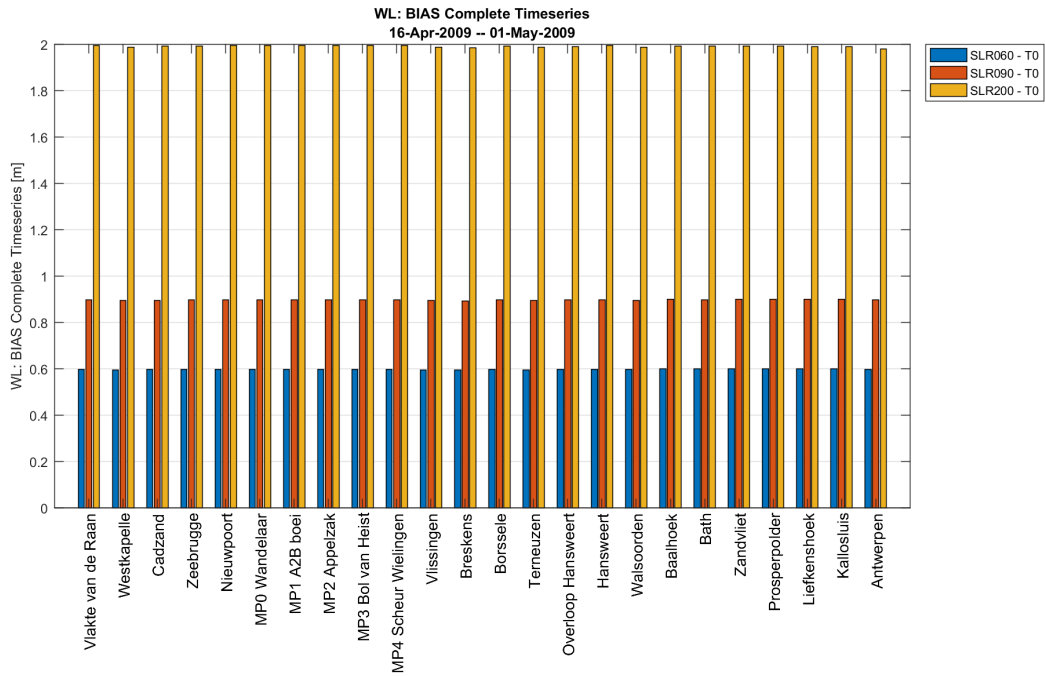
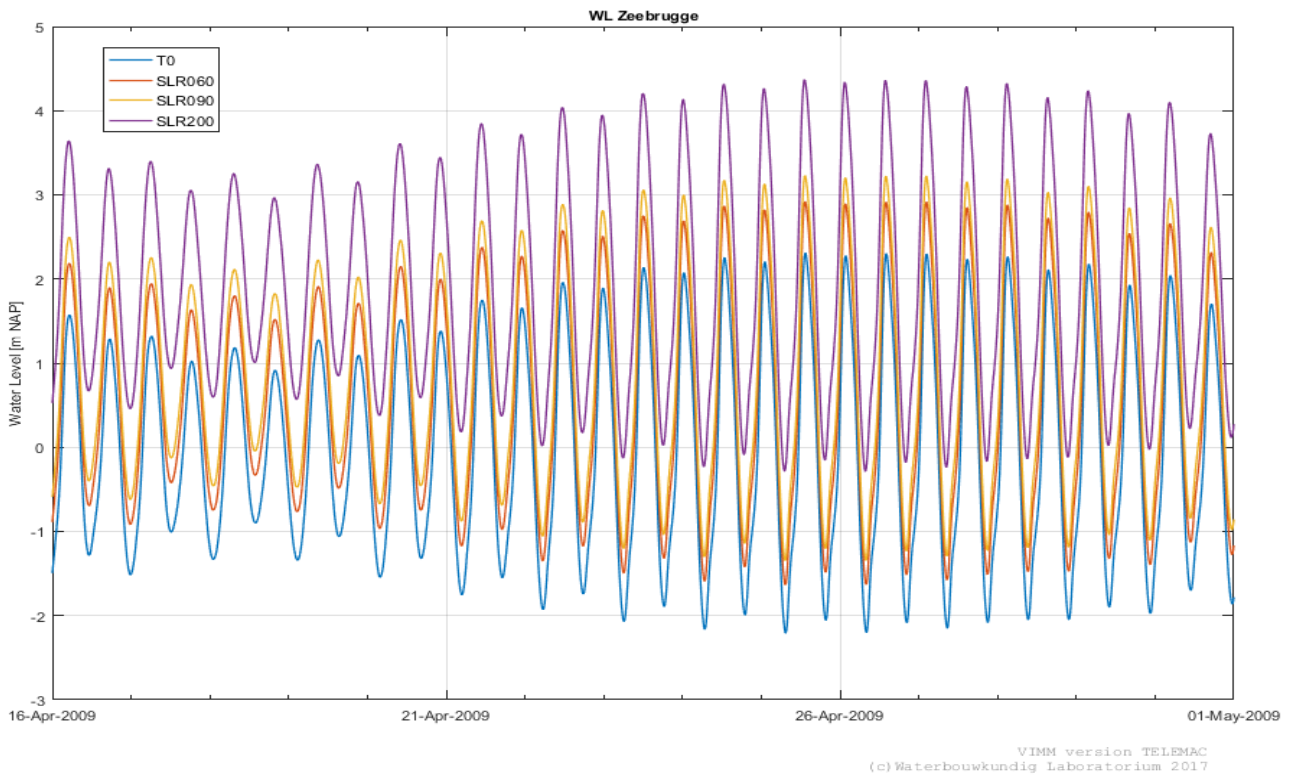


Figure 24: Water level time-series (16/04/2009 – 01/05/2009) at port of Zeebrugge for all the investigated scenarios.



In Figure 25 and Figure 26 the bias in the time of occurrence of high and low water levels between the sea level rise scenarios and the Reference scenario, are shown, respectively. The most obvious indication of the two figures is that the sea level rise leads to acceleration of the tidal wave, since both high and low water levels present a backward shift in time for all the considered scenarios and locations. The Moderate (SLR060) and the Warm (SLR090) scenarios exhibit relatively low bias in time (about 4 and 7 minutes at the coastal locations, respectively), while the backward time shift of the Worst-case scenario (SLR200) is by far larger than the other two (about 15 minutes at the coast). Furthermore, a general trend of increasing time shift as the tidal wave approaches and enters the Western Scheldt is observed, especially in Figure 26. For example, high and low water levels in Nieuwpoort, Wandelaar and A2B boei present the smaller bias values (for SLR200 from 7 to 15 min), while in the Western Scheldt ranges from about 25 to 35 min. This behavior can be roughly explained by the wave theory for shallow waters, according to which the celerity of the tidal wave, defined as  $C = (gh)^{1/2}$  -where  $g$  is the gravitational acceleration and  $h$  is the water depth- increases with increasing water depth.

Further analysis of the results of Figure 25 and Figure 26 leads to some interesting findings which however should be used with caution. In Figure 27, the average time shift of high and low water level of all locations is plotted against the considered sea level rises (y-axis is reversed). The lines of best fit for HW and LW time shifts resulting from linear regression and the corresponding R-squared values are also depicted. It is found that the absolute value of the time shift increases more or less linearly with the sea level rise for both high and low water. However, it is observed that the HW and LW time shift lines exhibit a deviation between them as the sea level rise becomes larger, i.e. the LW-line gradient is larger than the HW-line one. This behavior possibly indicates influence of the sea level rise on the tidal asymmetry and should be further investigated. A change in tidal asymmetry can have an impact in sediment transport and long term morphology.

Figure 25: Bias in the time of high water levels between the sea level rise scenarios and the Reference scenario.

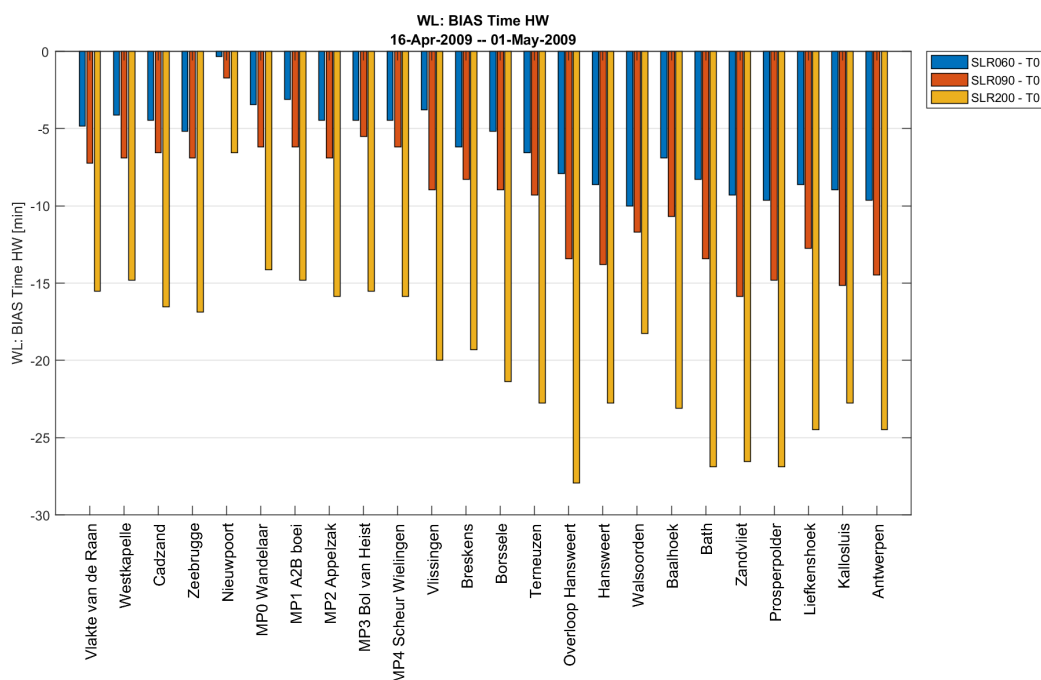


Figure 26: Bias in the time of low water levels between the sea level rise scenarios and the Reference scenario.

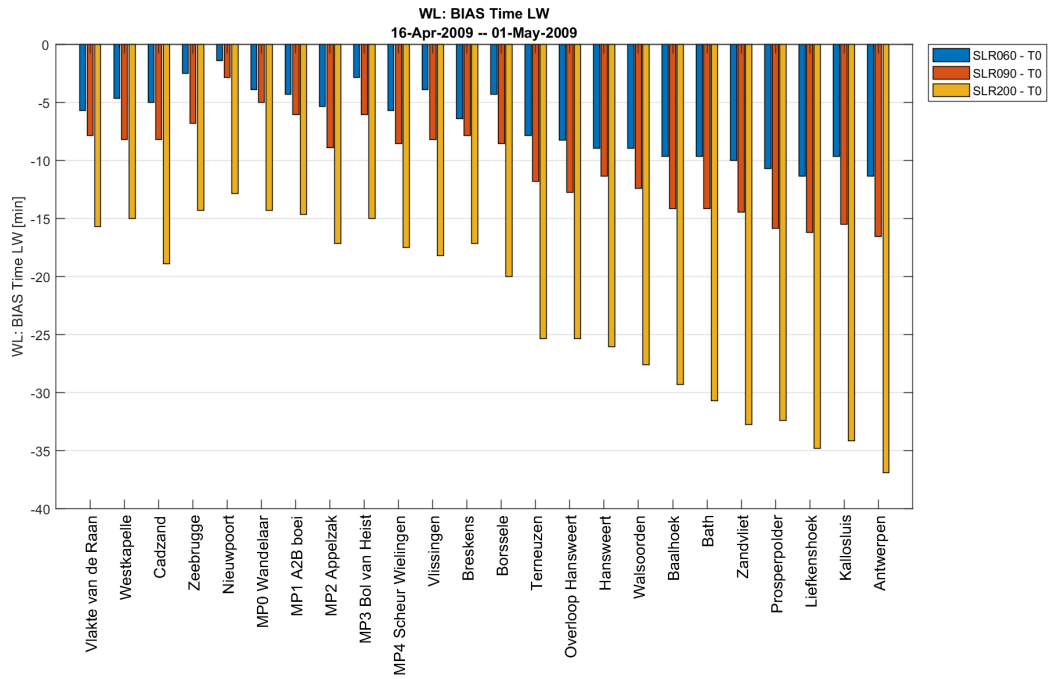
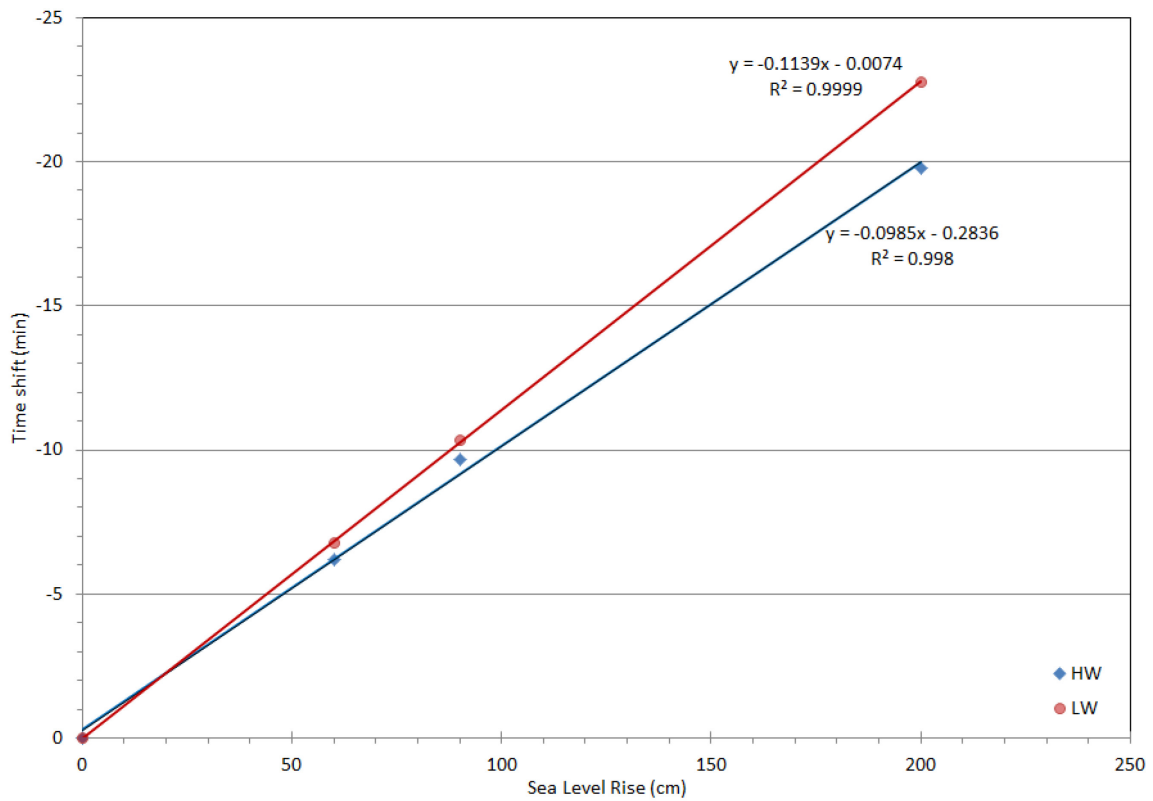


Figure 27: Averaged HW and LW time shifts versus sea level rise.



The bias in the high (HW) and low water (LW) levels between the sea level rise scenarios and the Reference scenario at the selected observation points, are shown, respectively, in Figure 28 and Figure 29. It is found that for all the scenarios, the biases in HW levels at all stations are a few centimeters higher than the mean sea level (MSL) increase, which can be considered equal to the bias in the complete water level time series (see Figure 23). On the other hand, biases in LW levels are always a few centimeters lower than the MSL increase. This is an indication that the sea level rise leads to increase of the tidal amplitude. In Figure 29, it is shown that the observations points in the Western Scheldt exhibit in general lower LW levels compared to the coastal observation points (difference  $\approx$  2-3 cm for SLR200). As for the bias in HW levels, there is no obvious difference between the coastal and the estuarine observation points (see Figure 28).

After being spatially averaged (for all the observation points), the results presented in Figure 28 and Figure 29 are represented graphically against the considered sea level rises in Figure 30. The lines of best fit for the biases in HW and LW levels resulting from linear regression and the corresponding R-squared values are also depicted. It is found that the water level biases increase linearly with the sea level rise for both high and low water. However, it is observed that the LW-line gradient with respect to the 1:1 line (dashed line) is slightly larger than the one of the HW-line indicating that the decrease of the LW level is more enhanced with increasing sea level rise compared to the increase of HW level. In other words the increase of the tidal amplitude is slightly asymmetrical. Finally the predicted increase of the mean tidal amplitude for each of the three investigated scenarios can be calculated subtracting the considered rise from the HW and the LW biases and adding the two resulting (absolute) values. The resulting amplitudes are 5.1 cm, 7.4 cm and 18.3 cm for the SLR060, SLR090 and SLR200 scenarios, respectively.

Figure 28: Bias in the high water levels between the sea level rise scenarios and the Reference scenario.

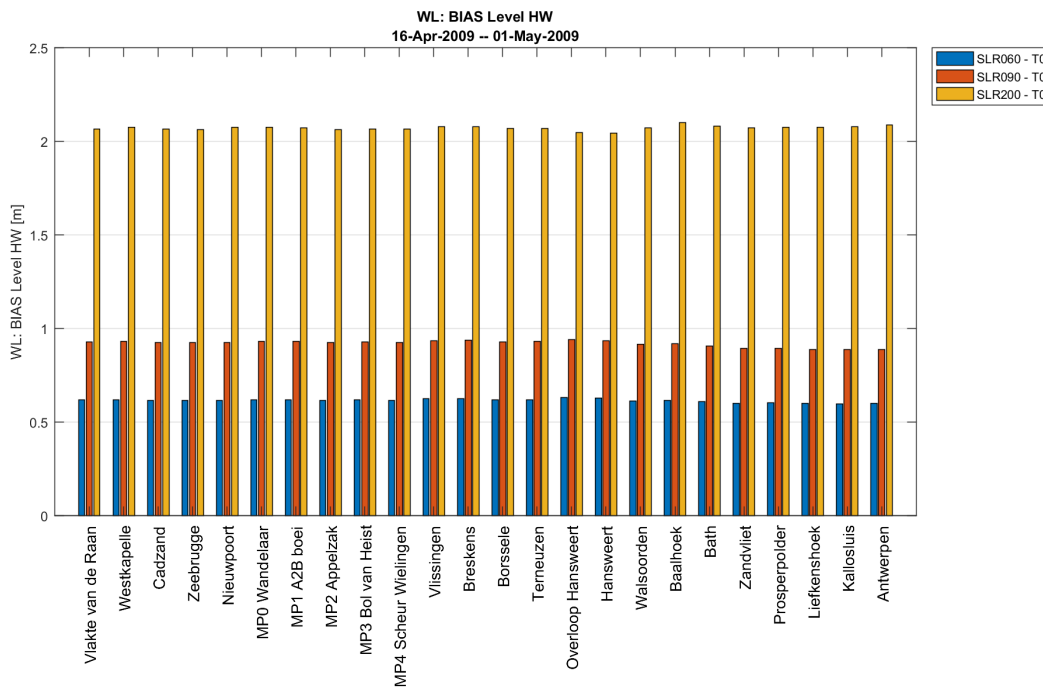


Figure 29: Bias in the low water levels between the sea level rise scenarios and the Reference scenario.

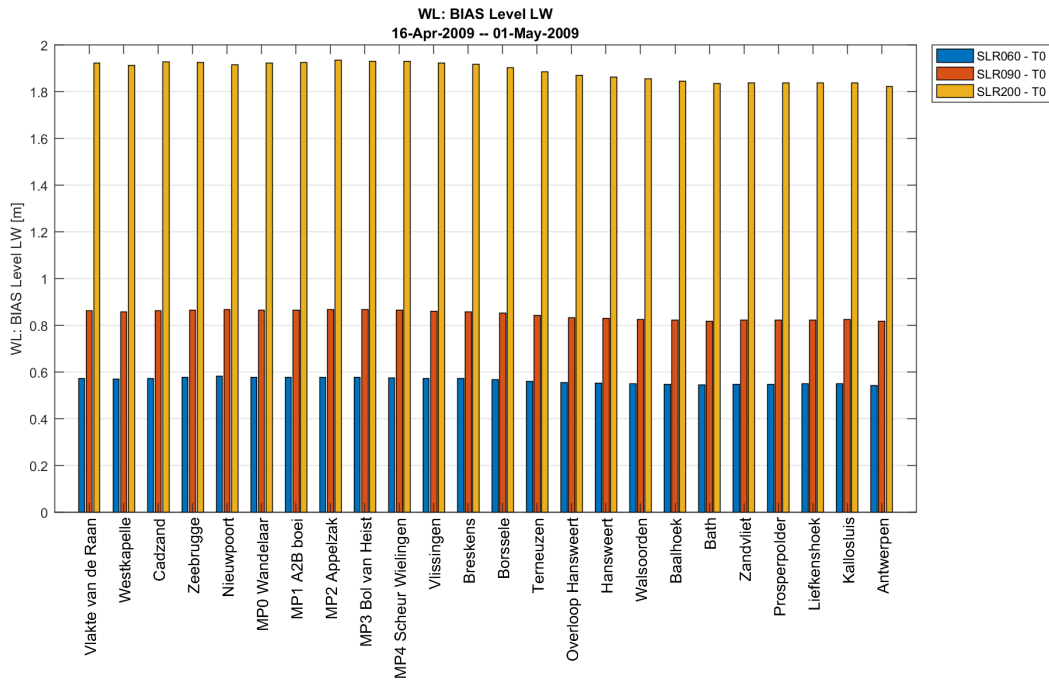
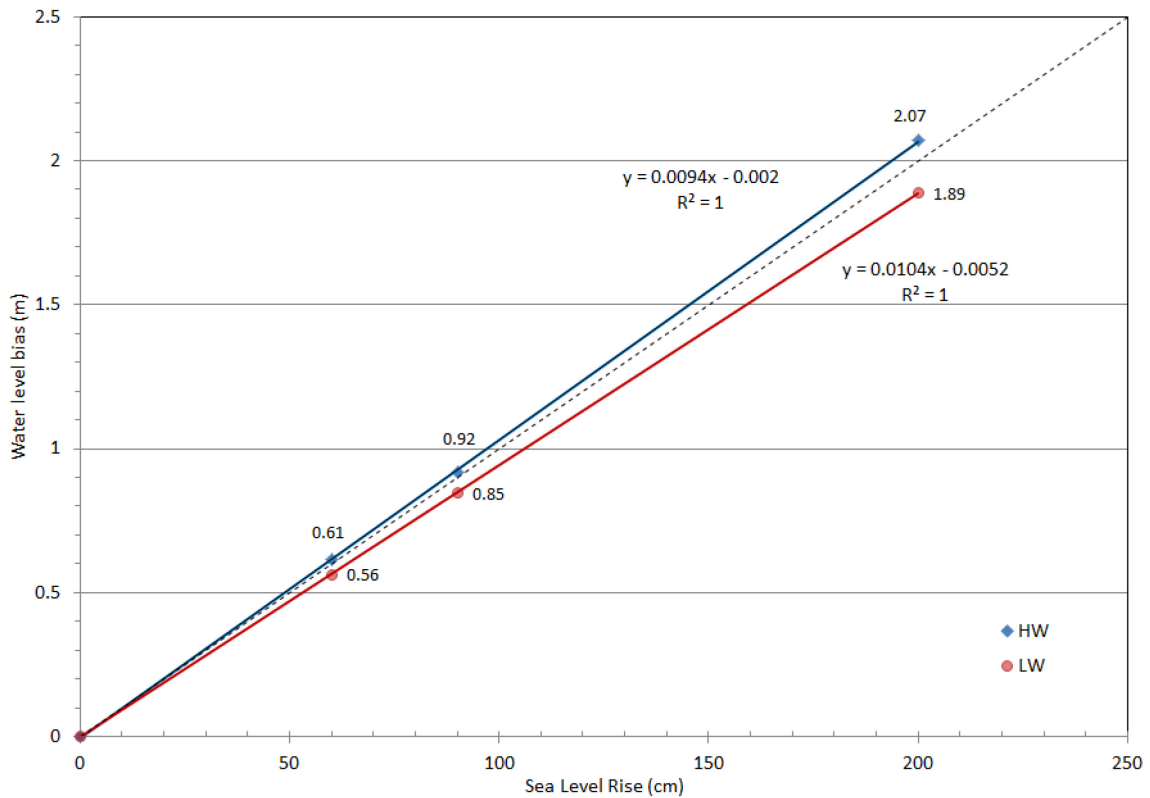


Figure 30: Averaged HW and LW bias versus sea level rise.



### Basic harmonic analysis

The amplitude of the most important harmonic constituents of the tide, i.e. the M2, S2, M4 constituents, at the considered locations for all the investigated scenarios are shown respectively in Figure 31, Figure 32 and Figure 33. As expected, the M2 and S2 amplitudes increase with increasing sea level and this increase is enhanced as the tidal wave reaches the mouth and the upstream locations of the Western Scheldt. For the Warm scenario (SLR090), for instance, the increase of M2 amplitude at Nieuwpoort is 3.5 cm, while in Antwerp is almost doubled (6.8 cm), while the corresponding S2 amplitude is increased from 1 cm at Nieuwpoort to 2.2 cm in Antwerp. On the contrary, M4 amplitude mainly decreases with increasing sea level rise, with the decrease being enhanced upstream the Scheldt estuary. Note that only at two locations (Breskens and Vlissingen) the M4 amplitude increases slightly with increasing sea level rise.

In Figure 34, the averaged (over all locations) M2, S2 and M4 amplitude differences between each of the sea level rise scenarios and the Reference scenario are plotted against the considered sea level rises. The best fit lines (linear regression) and the corresponding R-squared values are also depicted. It is also found that the average amplitudes increase (M2 and S2) or decrease (M4) almost linearly with the sea level rise.

Figure 31: Amplitude of the M2 tidal constituent at the considered locations for all the investigated scenarios.

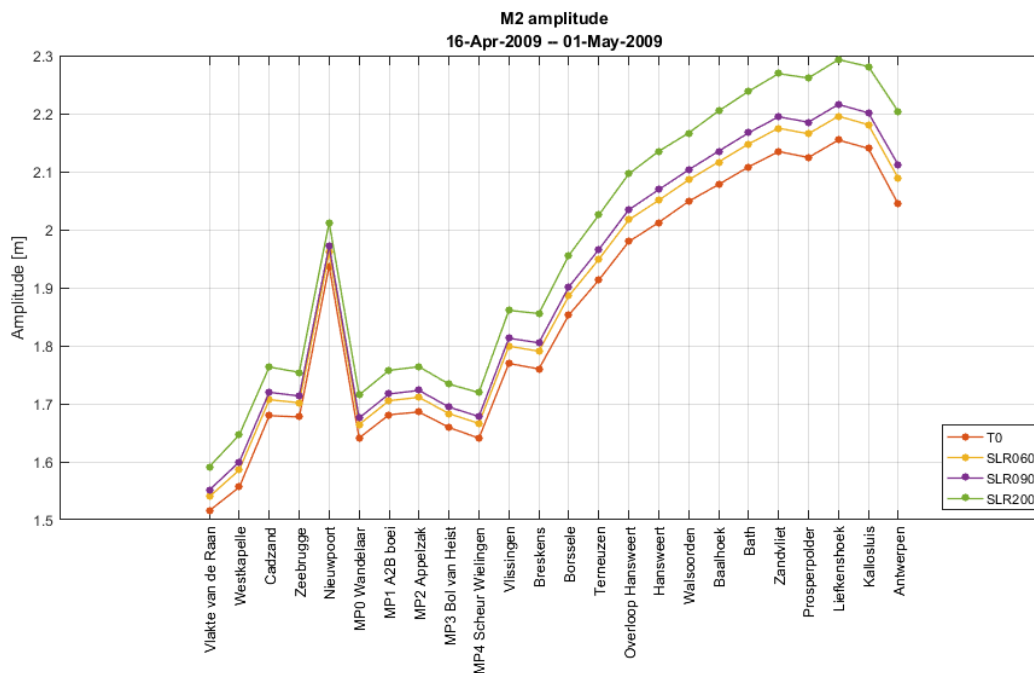


Figure 32: Amplitude of the S2 tidal constituent at the considered locations for all the investigated scenarios.

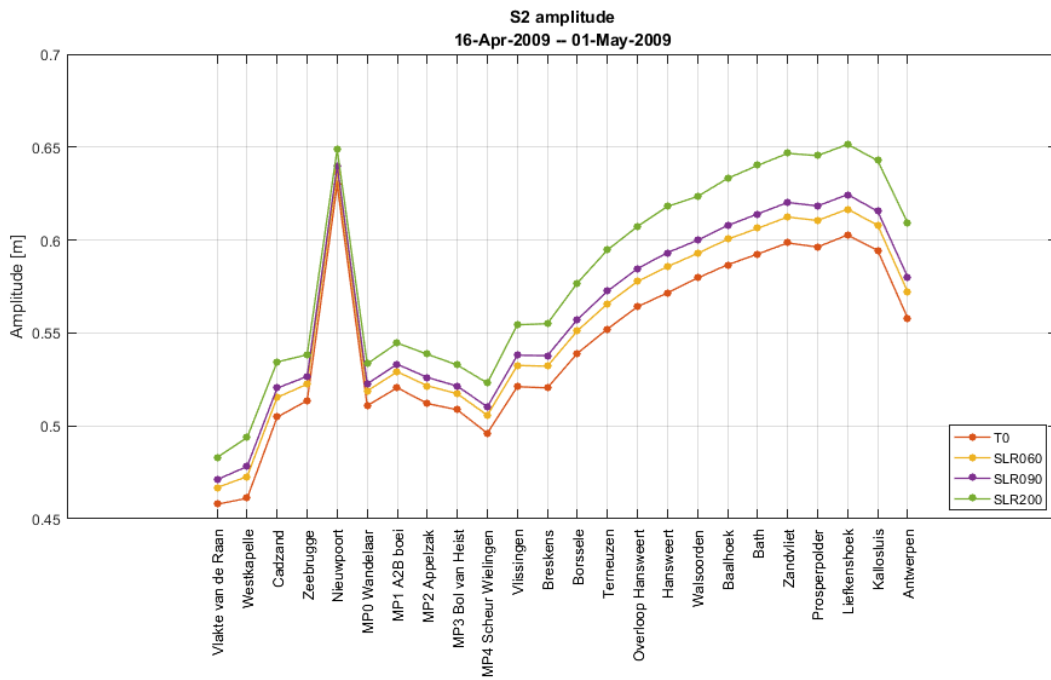


Figure 33: Amplitude of the M4 tidal constituent at the considered locations for all the investigated scenarios.

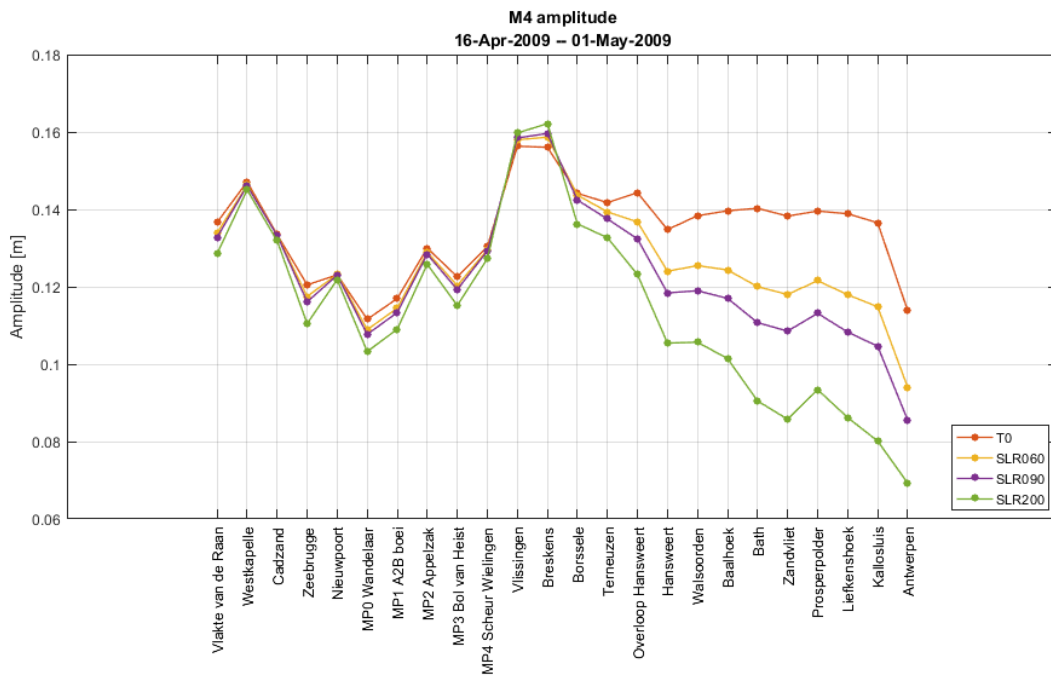
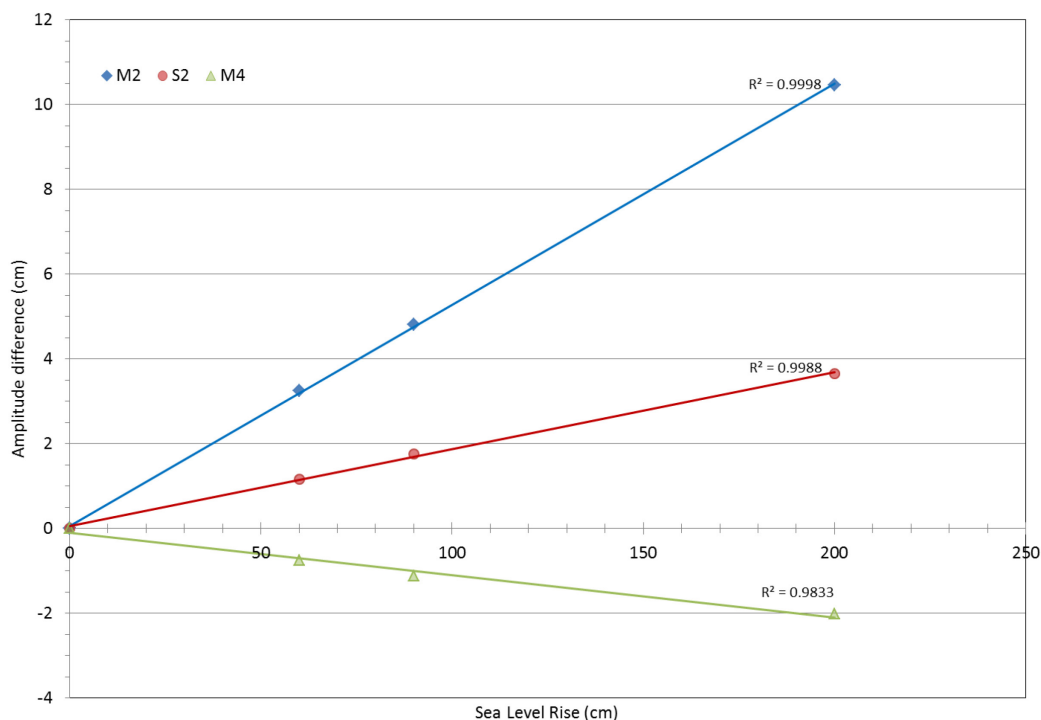




Figure 34: Averaged M2, S2, and M4 amplitude differences between each of the sea level rise scenarios and the Reference scenario versus sea level rise.



The phase of the M2, S2, M4 constituents, at the considered locations for all the investigated scenarios are shown respectively in Figure 35, Figure 36 and Figure 37. In general the phase of the considered constituents decreases with increasing sea level rise or in other words the phase shift increases with increasing sea level rise. Similarly to the amplitude analysis, the M2 and S2 phase shift (of each sea level rise scenario) increases more as the tidal wave reaches the mouth and the upstream locations of the Western Scheldt. For the M4 phase shift (of each sea level rise scenario), in contrast, there is a mild decreasing trend as we go upstream.

In Figure 38, the averaged (over all locations) M2, S2 and M4 phase shift between each of the sea level rise scenarios and the Reference scenario are plotted against the considered sea level rises. The best fit lines (linear regression) and the corresponding R-squared values are also depicted. It is also found that the averaged phases increase linearly with the sea level rise.

Figure 35: Phase of the M2 tidal constituent at the considered locations for all the investigated scenarios.

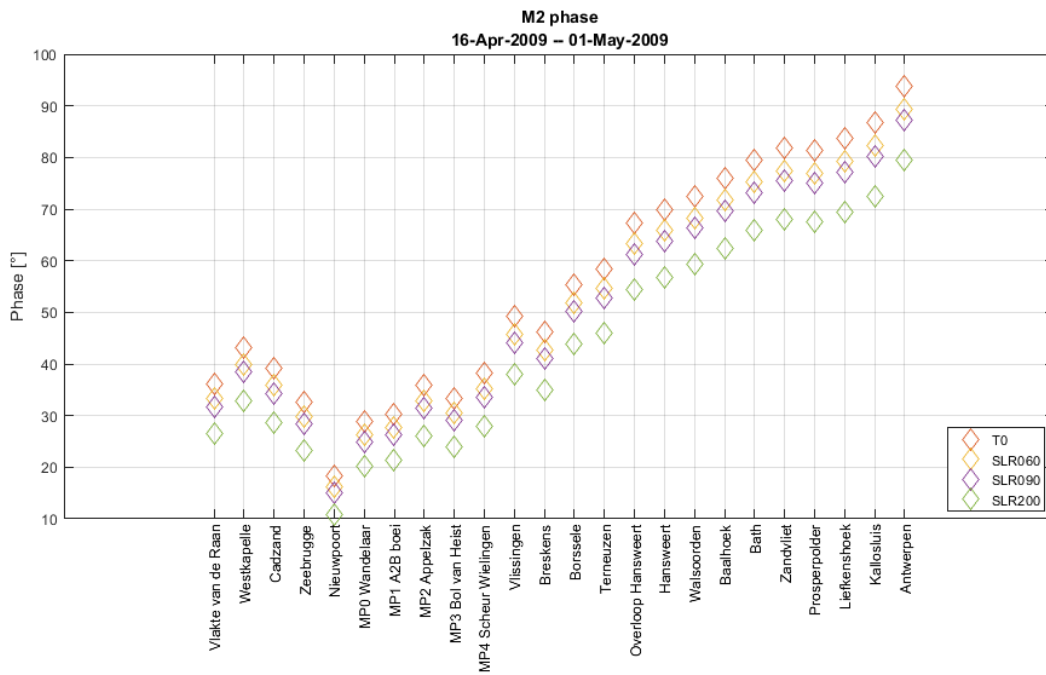


Figure 36: Phase of the S2 tidal constituent at the considered locations for all the investigated scenarios.

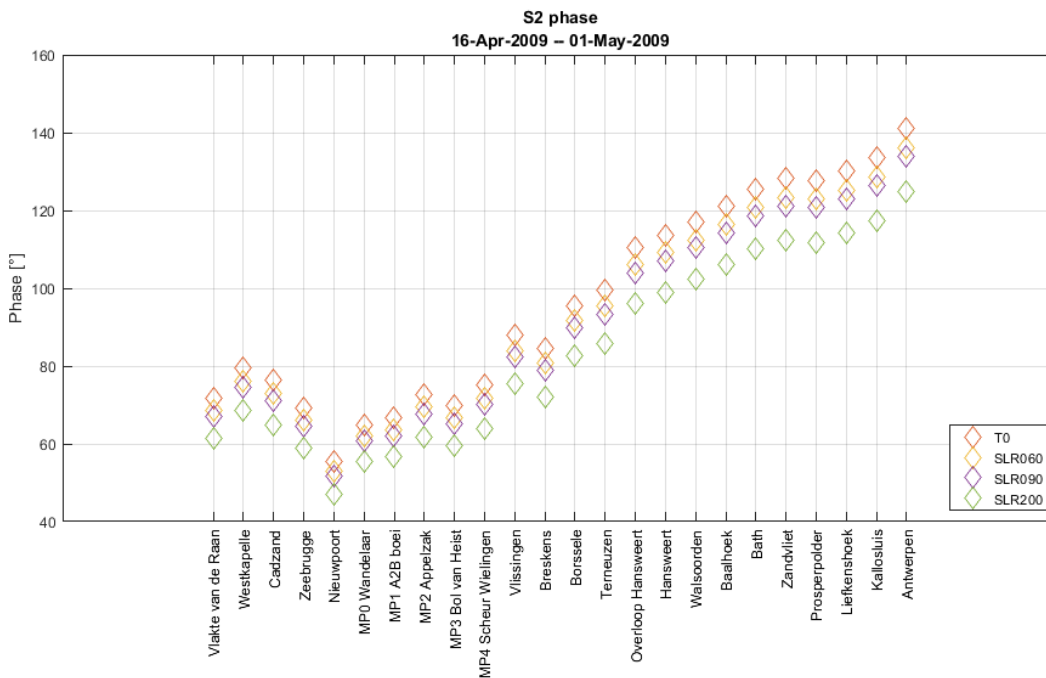


Figure 37: Phase of the M4 tidal constituent at the considered locations for all the investigated scenarios.

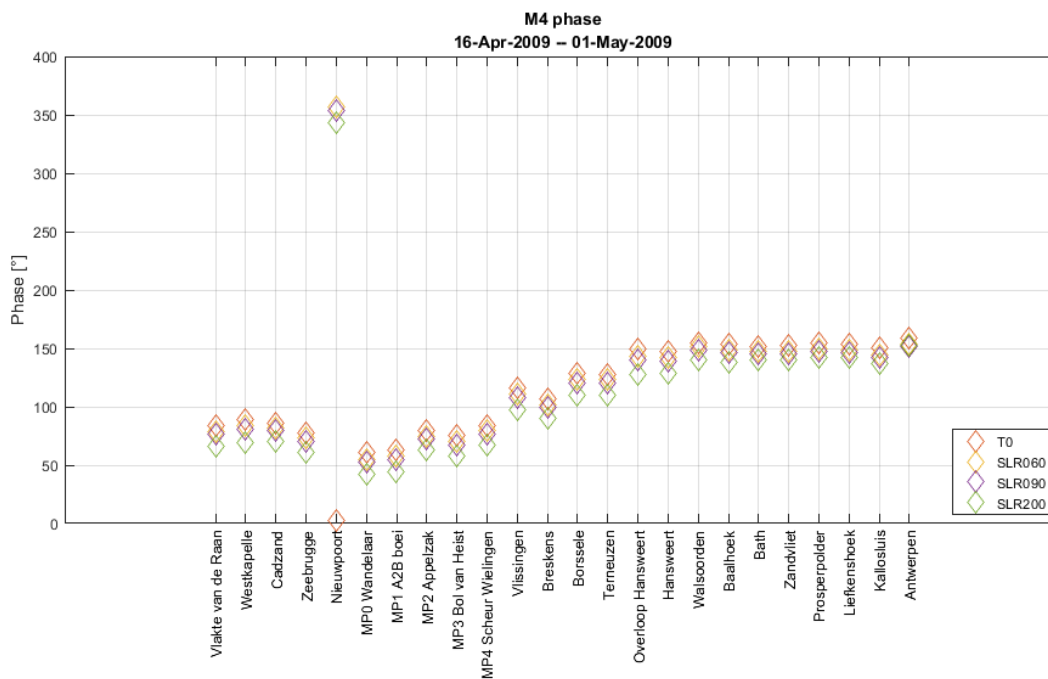
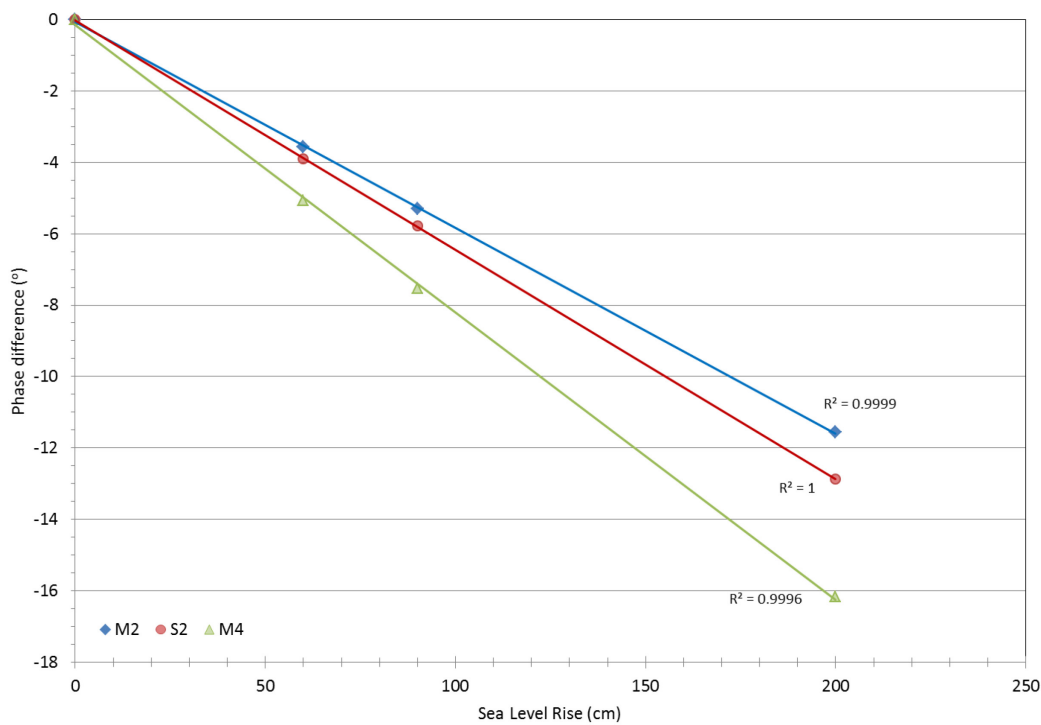


Figure 38: Averaged M2, S2, and M4 phase differences between each of the sea level rise scenarios and the Reference scenario versus sea level rise.

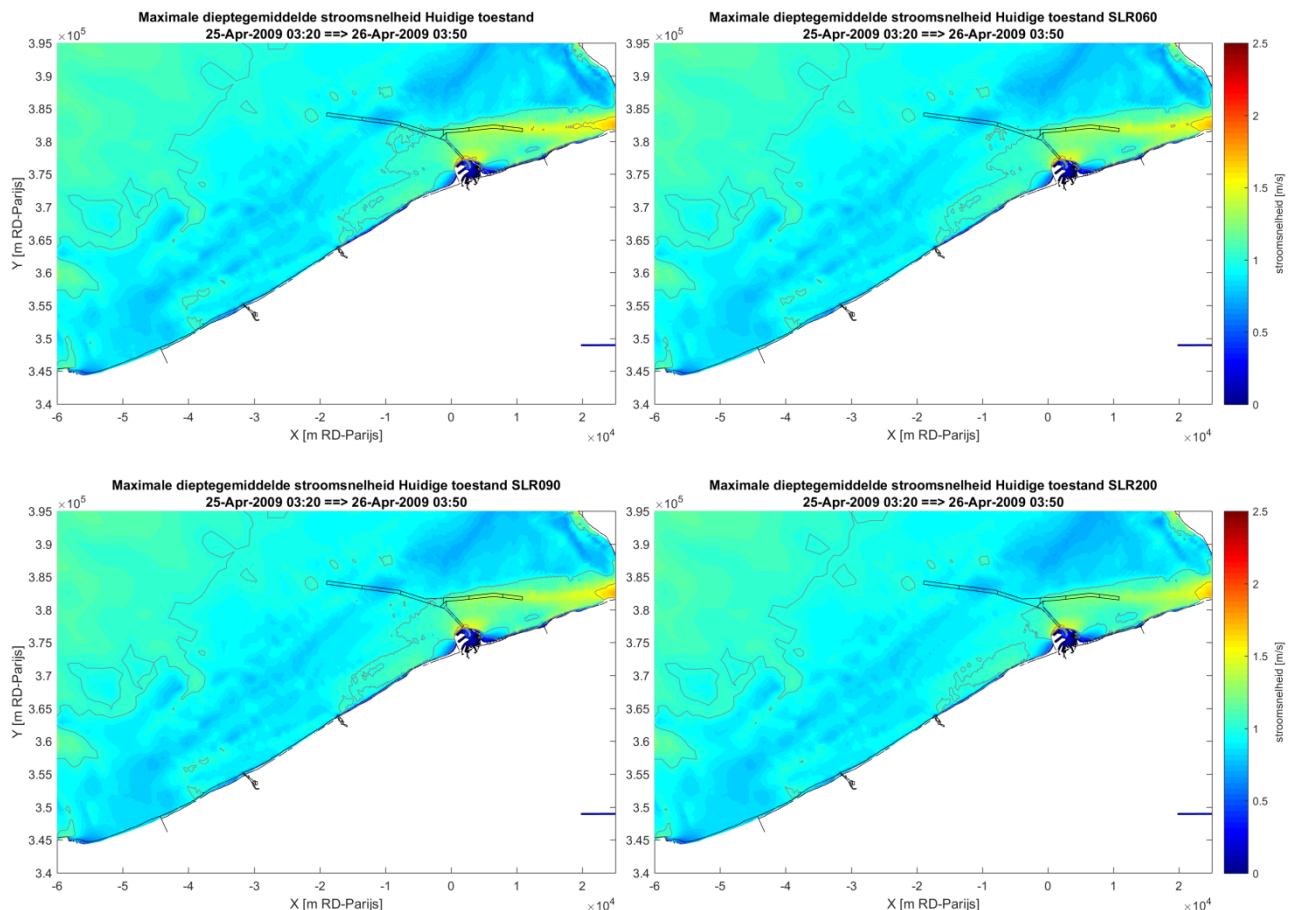


### 3.2.2 Sea level rise impact on coastal and estuarine hydrodynamics

The maximum depth-averaged flow during spring tide for the Reference and the sea level rise scenarios, and the difference of each of the sea level rise scenarios with the Reference scenario, are shown in Figure 39 and Figure 40, respectively. Observing the maps of Figure 39, differences between them are hardly noticeable. Nevertheless there are some differences in the maximum flow field located mainly between the mouth of Western Scheldt and the Zeebrugge harbor and, as expected, these are enhanced with increasing seal level (see Figure 40). It is found that, in general, sea level rise leads to reduction of the maximum flow magnitude in the area around the navigation channels of Scheur and Wielingen, which in the case of Worst-case scenario (SLR200) is spread to Wandelaar and Vlakte van de Raan, and to increase of maximum velocities at the mouth of Western Scheldt and specifically at the area between Vlissingen and Westkapelle. The differences seem to be slight for the case of the Moderate scenario (SLR060), but they reach values from about -25 cm/s to about 30 cm/s in the Worst-case scenario.

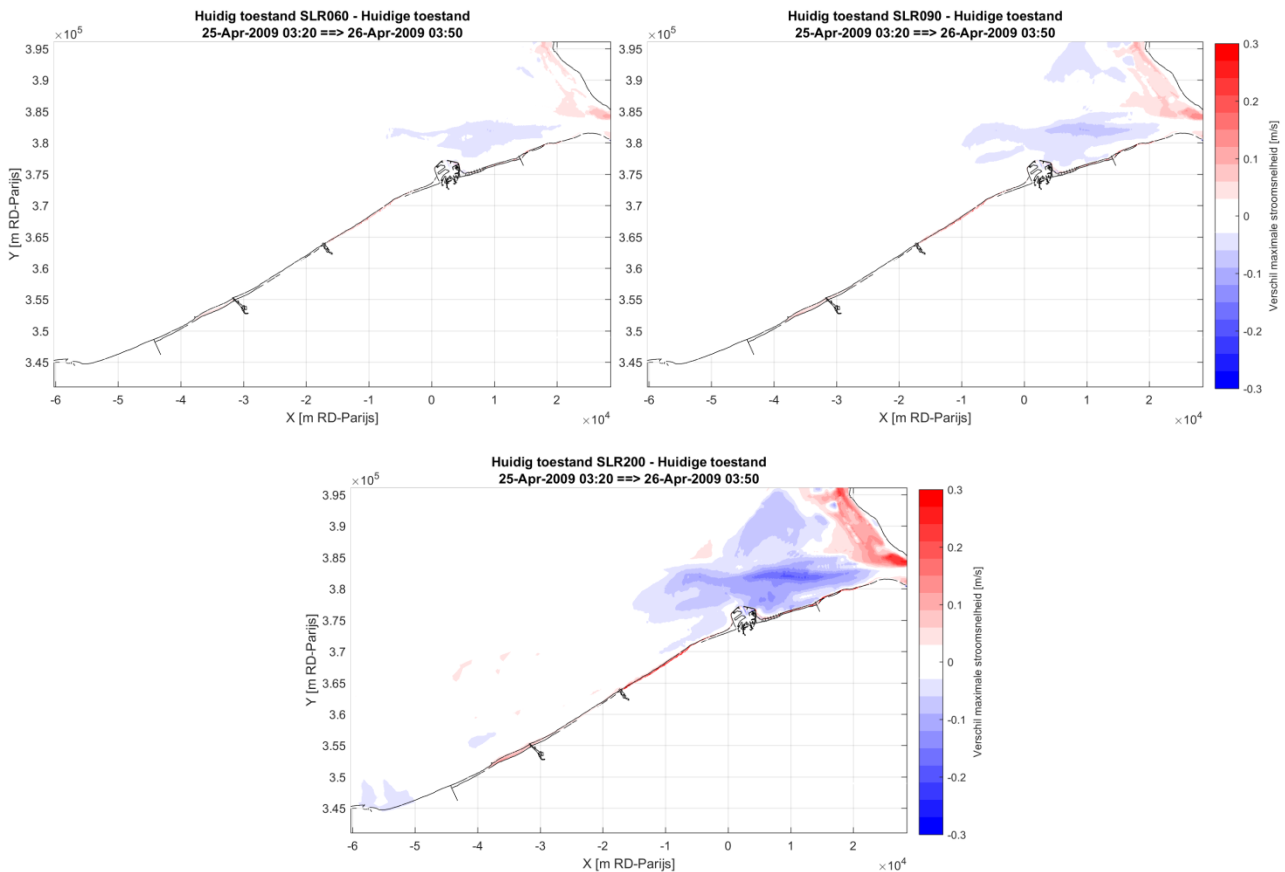
This behavior of the flow velocities can be explained by the relation between the increase of the flow discharge per tidal cycle,  $Q$ , and the increase of the cross-sectional area of the flow,  $A$ , due to the sea level rise. It seems that in the area of Scheur and Wielingen the increase of  $A$ , or in other words the increase of the mean sea level, prevails against the increase of the discharge  $Q$ , and therefore velocity  $U (= Q/A)$  decreases. The opposite occurs at the east side of the mouth where the increase of flow discharge prevails against the increase of  $A$  and so velocity increases. Especially during ebb phase the increase of the tidal amplitude will lead to decreased low water levels, fact that may also contribute in the increased flow velocities in the ebb-dominant east side of the mouth.

Figure 39: Maximum depth-averaged flow velocity (magnitude, m/s) during spring tide for the Reference and the sea level rise scenarios.



In Figure 62 and Figure 63 of Appendix D, the maximum depth-averaged flow during the flood phase and the ebb phase of the simulated spring tide for all the investigated scenarios, are shown respectively, while Figure 64 and Figure 65 depict the difference of each of the sea level rise scenarios with the Reference scenario for the flood and the ebb phase, respectively.

Figure 40: Difference in maximum depth-averaged flow velocity (magnitude, m/s) during spring tide between the sea level rise scenarios and the Reference scenario.



The maps included in Figure 41, which are details of the corresponding ones of Figure 40, are focusing on the coastal area of Zeebrugge port. In Figure 42 and Figure 43 similar maps for the flood and the ebb phase for all the sea level rise scenarios are, respectively, presented. As previously mentioned, the difference patterns are enhanced with increasing sea level. Observing Figure 41 and Figure 42, the main differences are located at the entrance, the central part of the outer port (CDNB), at the internal area of the eastern breakwater and at Baai van Heist. The differences at the two first locations (mainly reduction of the velocities), can be related to the modification of the existing flow recirculation patterns, while the differences at the two last locations are related to the wetting and drying which depends on the local water level of each scenario. Note that after inspection of the instantaneous velocity maps, it was found that the impact of the sea level rise (even for the worst-case scenario) on the structure of the eddies in the port is not substantial, and therefore it is not expected to play important role in port accessibility investigation.

The difference maps in Figure 41 and Figure 42 are quite similar, since the local maximum velocities, on which these maps are based on, occur mainly during the flood phase. Therefore, the corresponding maps during the ebb phase, shown in Figure 43, are also of great interest in search for hidden information. The main finding of these maps is the local increase of the maximum velocities in front of the port, i.e. along the western and the eastern breakwater especially enhanced in the worst case scenario. The maximum increase of the velocity, located at the corner of the east breakwater is about 30 cm/s.

Figure 41: Difference in maximum depth-averaged flow velocity (magnitude, m/s) during spring tide between the sea level rise scenarios and the Reference scenario at the area around Zeebrugge port.

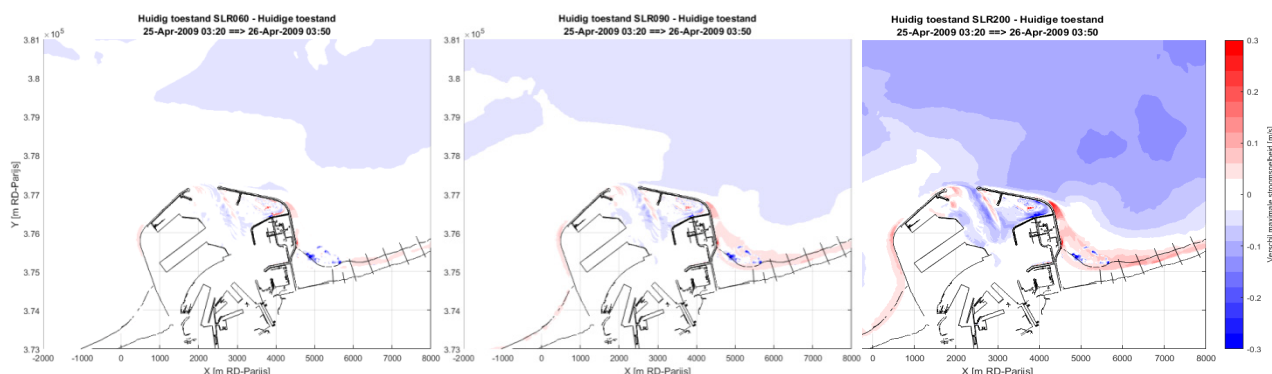


Figure 42: Difference in maximum depth-averaged flow velocity (magnitude) during **flood phase** of the spring tide between the sea level rise scenarios and the Reference scenario at the area around Zeebrugge port.

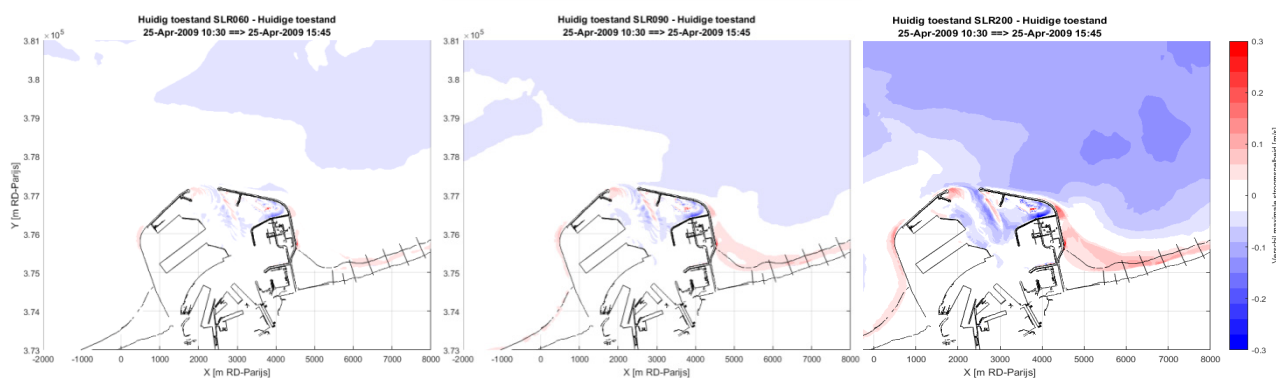
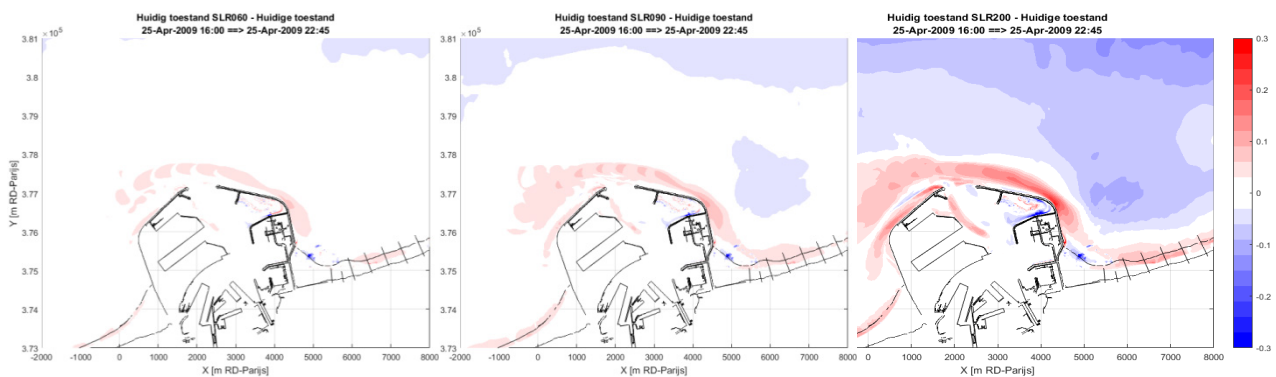


Figure 43: Difference in maximum depth-averaged flow velocity (magnitude) during **ebb phase** of the spring tide between the sea level rise scenarios and the Reference scenario at the area around Zeebrugge port.



Along with the results presented for the coastal area, the maximum depth-averaged flow during spring tide and the difference of each of the sea level rise scenarios with the Reference scenario for the area of the Western Scheldt are shown in Figure 44 and Figure 45, respectively. Observing the maps of Figure 44, differences between them can be noticed mainly at the intertidal areas and in a lesser extent at the

navigational channels and the mouth of the estuary. As expected these differences are enhanced with increasing sea level (see Figure 45). It is found that, in general, sea level rise leads to significant increase of maximum velocity in the intertidal areas and reduction of its magnitude in the navigation channels. The differences at the channels seem to be slight for the case of the Moderate scenario, but they reach values about 30 cm/s in the Worst-case scenario.

The maximum velocity differences are substantial at the intertidal areas which are completely dry in the Reference scenario (zero velocity) but they are flooded in the SLR scenarios. As expected the maximum velocity differences are greater for the Worst-case scenario. An idea of how the intertidal zones will change after a sea level rise of 200 cm is given in Figure 46, where the bathymetry of Western Scheldt is given with respect to the mean sea level (MSL) of the Reference and the Worst-case scenario.

In Figure 69 and Figure 70 of Appendix D, the maximum depth-averaged flow during the flood phase and the ebb phase of the simulated spring tide for all the investigated scenarios, are shown respectively, while Figure 71 and Figure 72 depict the difference of each of the sea level rise scenarios with the Reference scenario for the flood and the ebb phase, respectively. It is worth to mention that the reduction of the maximum velocity it is observed only during the flood phase (see Figure 71 and Figure 72).

Figure 44: Maximum depth-averaged flow velocity (magnitude, m/s) during spring tide for the Reference and the sea level rise scenarios at the area of Western Scheldt.

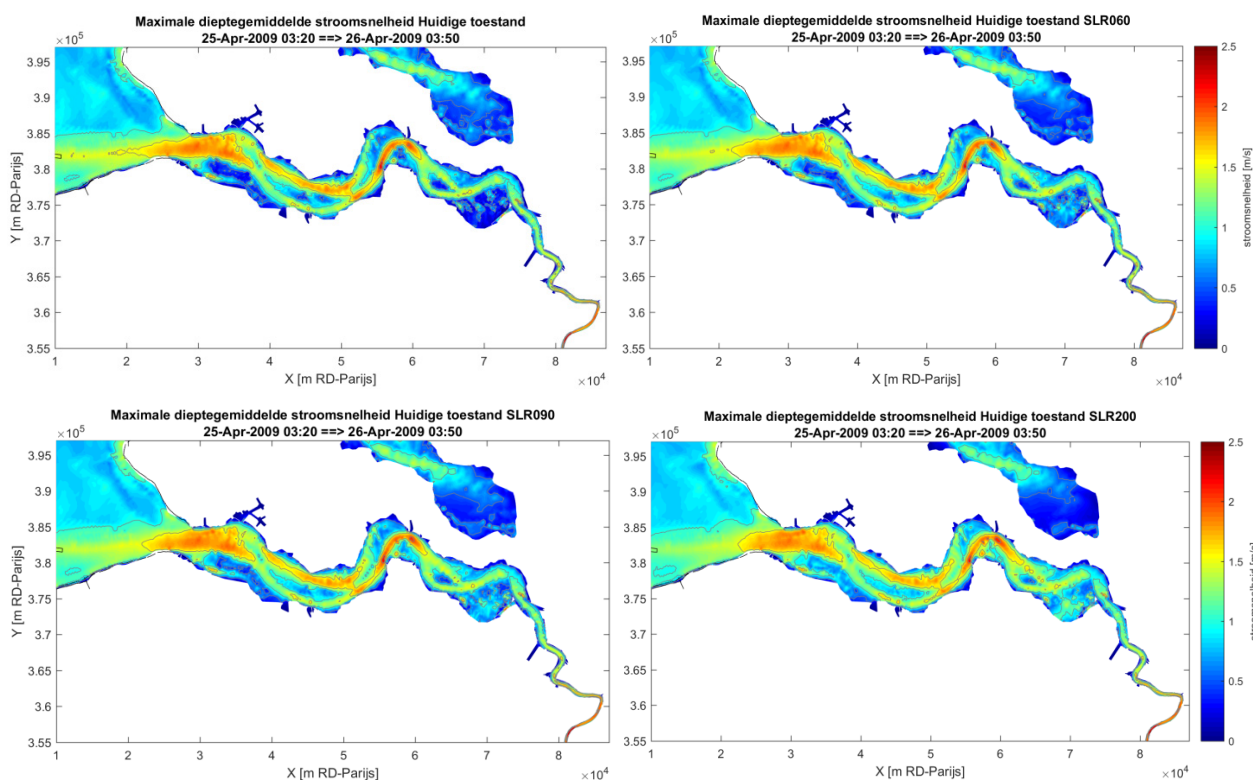


Figure 45: Difference in maximum depth-averaged flow velocity (magnitude, m/s) during spring tide between the sea level rise scenarios and the Reference scenario at the area of Western Scheldt.

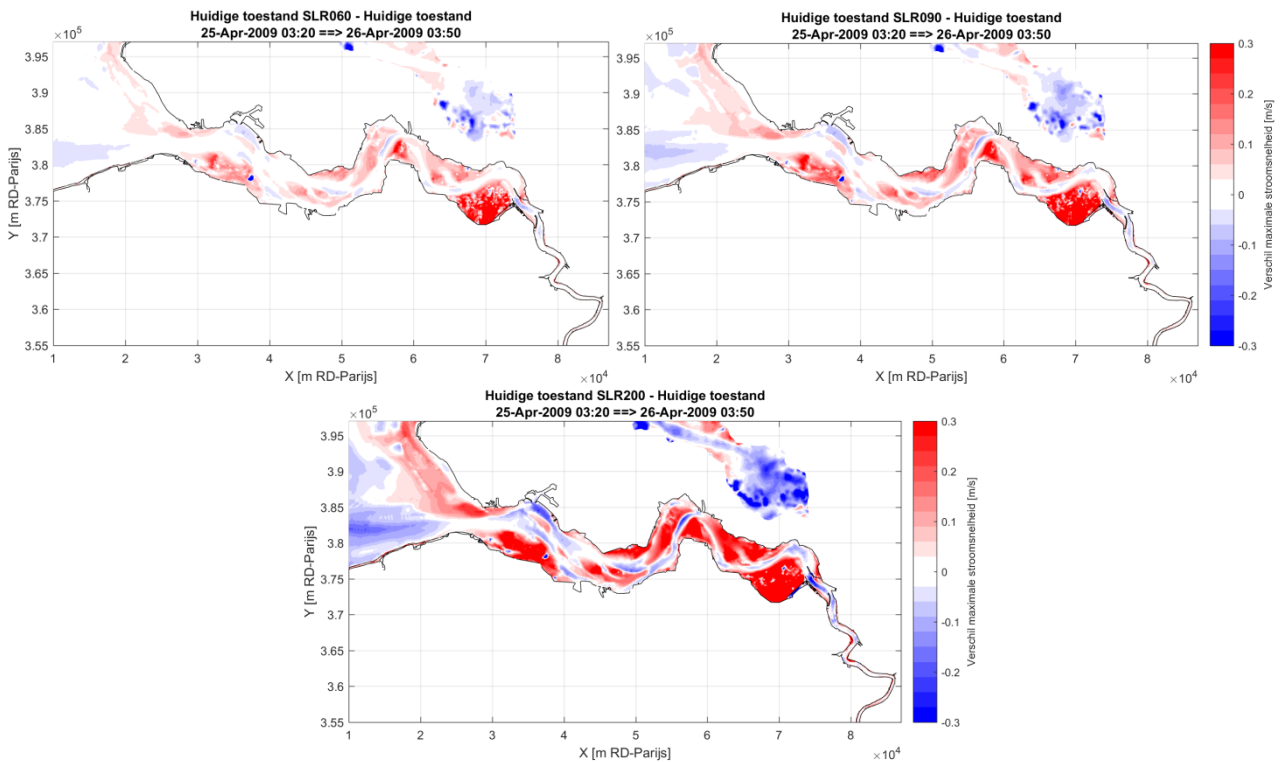
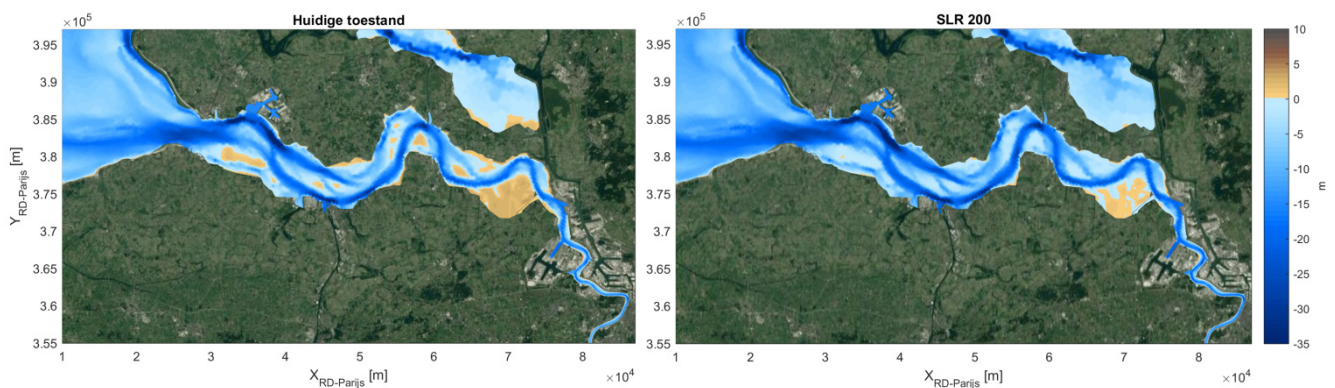


Figure 46: Bathymetry with respect to the mean sea level (MSL) at the area of Western Scheldt for the Reference (left) and the Worst-case sea level rise scenario (right).



### 3.2.3 Sea level rise impact on port accessibility

As shown in the previous section, high flow velocities are observed in the area in front of the Zeebrugge harbor (see Figure 39) for all the investigated scenarios. These local (depth-averaged) flow velocities can reach values greater than 1.5 m/s during spring tide. Due to these strong currents, which are mainly directed transversely to the Pas van het Zand navigation gully, there are time windows during which, the access of large container and LNG carriers is limited. For container carriers, the maximum velocities along the navigation gully during arrival and departure is limited to 2 knots (1.03 m/s). For LNG carriers, the maximum accepted velocity is 1.5 knots (0.77 m/s) during arrival and 2 knots during departure.



**Reference scenario**

Figure 47 shows the spatiotemporal evolution of the depth-averaged transverse current along the shipping route Pas van het Zand – CDNB during spring tide (25/04/2009 03:20 26/04/2009 03:50) for the reference scenario. Next, the time windows of transverse currents greater than 1.5 knots and 2 knots are shown in Figure 48. Note that these time barriers have resulted from the maximum depth-averaged transverse velocities along the Pas van he Zand trajectory. It is found that the limit of 2 knots is exceeded for about 2 hours during each flood phase, while the limit of 1.5 knots is exceeded for 2 hours and 40 minutes during each flood phase and for about 1 hour during each ebb phase. However, note that the time barrier is calculated here on the basis of the depth-averaged flow, therefore the velocity close to the free surface will be even higher (see figure 12 in De Maerschalc *et al.*, 2016). Finally, the temporal evolution of the transverse current magnitude at a location (on the navigation channel) close to the port entrance (Aa), and a second one in CDNB (Ad), are shown in Figure 49. The red lines showing the maximum accepted velocities for the navigation of container and LNG carriers are also denoted. As expected, the results of are in agreement with the corresponding ones of Figure 48.

Figure 47: Spatiotemporal evolution of the depth-averaged transverse current along the Pas van het Zand trajectory during the spring tide for the Reference scenario.

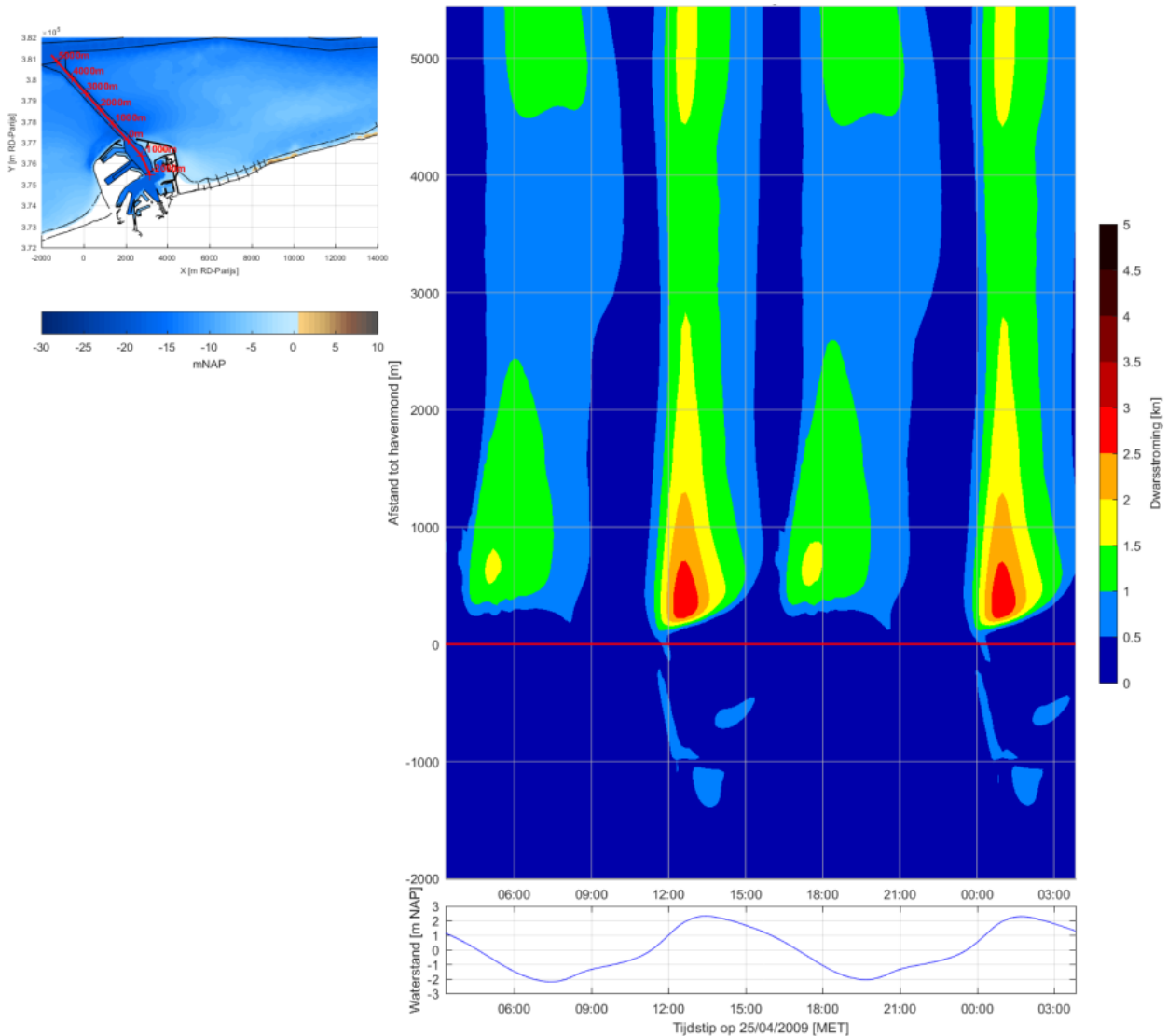


Figure 48: Time barriers for the transverse to the Pas van het Zand trajectory, depth-averaged current greater than 2kn (above) and 1.5kn (below) calculated for the Reference scenario during spring tide.

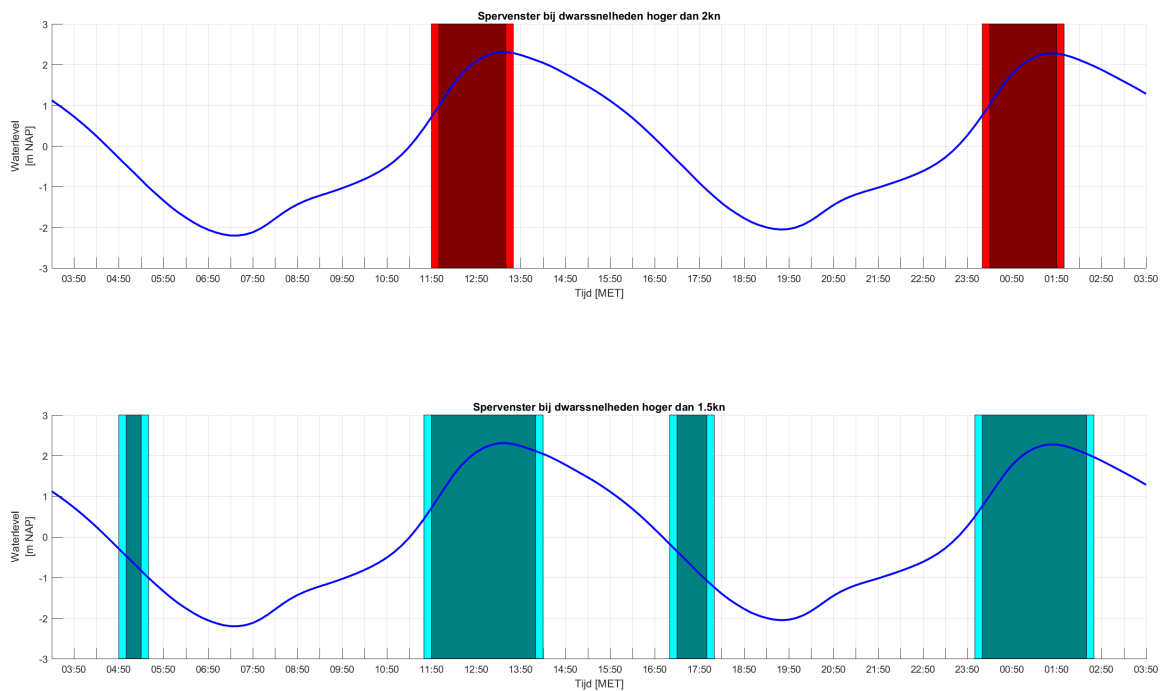
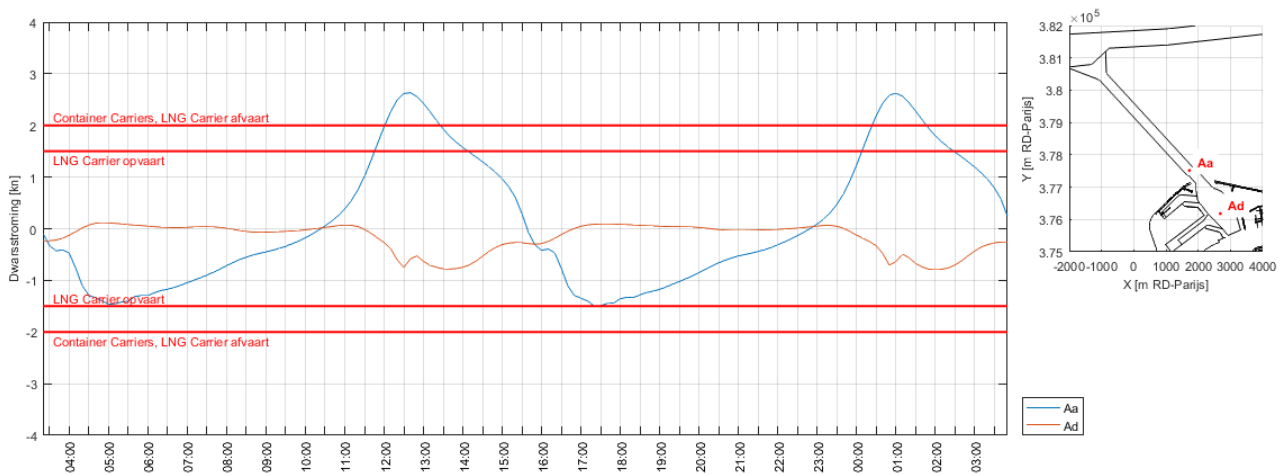


Figure 49: Depth-averaged transverse current at the Pas van het Zand trajectory (close to the port entrance, Aa) and in CDNB (Ad) during spring tide for the Reference scenario.



The red lines show the maximum accepted velocities for the navigation of container and LNG ships.

### Moderate sea level rise scenario

The spatiotemporal variation of the depth-averaged transverse flow velocity along the Pas van het Zand trajectory for the Moderate scenario (SLR60) is shown in the middle graph of Figure 50. The leftmost graph of Figure 50 corresponds to the difference plot of the velocity variation versus the Reference scenario. The latter plot indicates, in general, a slight increase (5-10 cm/s) of the transverse velocity along the trajectory. The maximum increase in the flow magnitude is observed close to the entrance of the harbor during the flood phase (about one hour before the high water).

Figure 50: Spatiotemporal evolution of the depth-averaged transverse current along the Pas van het Zand trajectory during the spring tide for the Moderate SLR scenario (left). Difference plot versus Reference scenario (right).

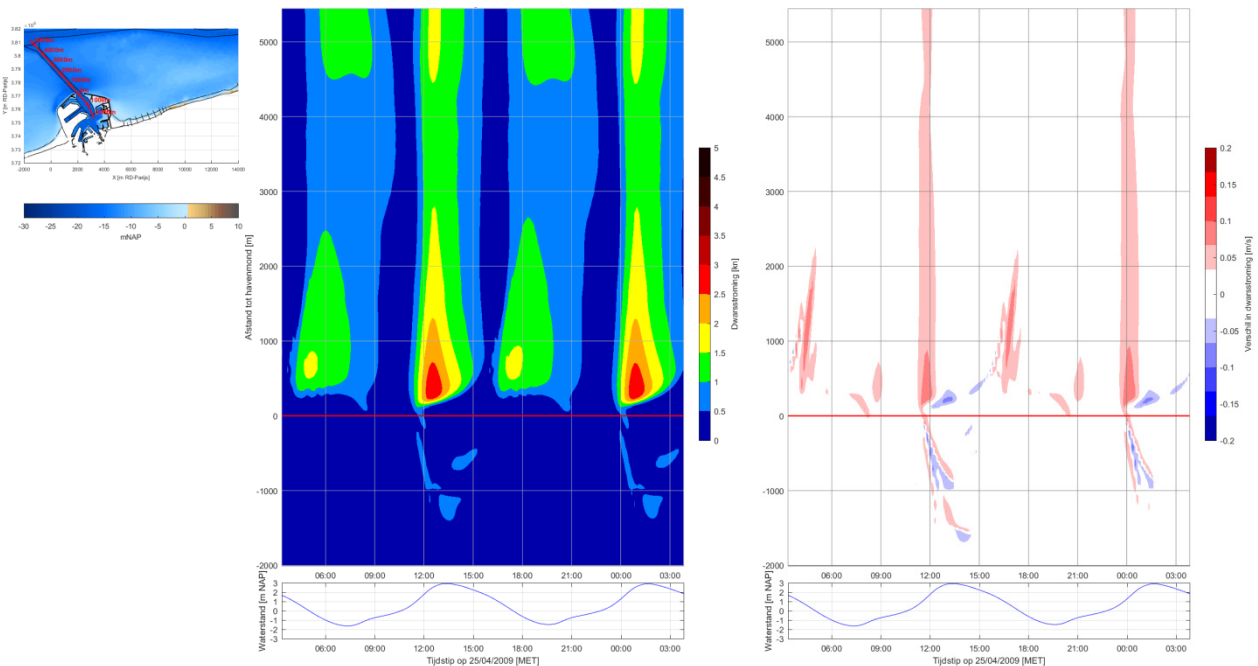
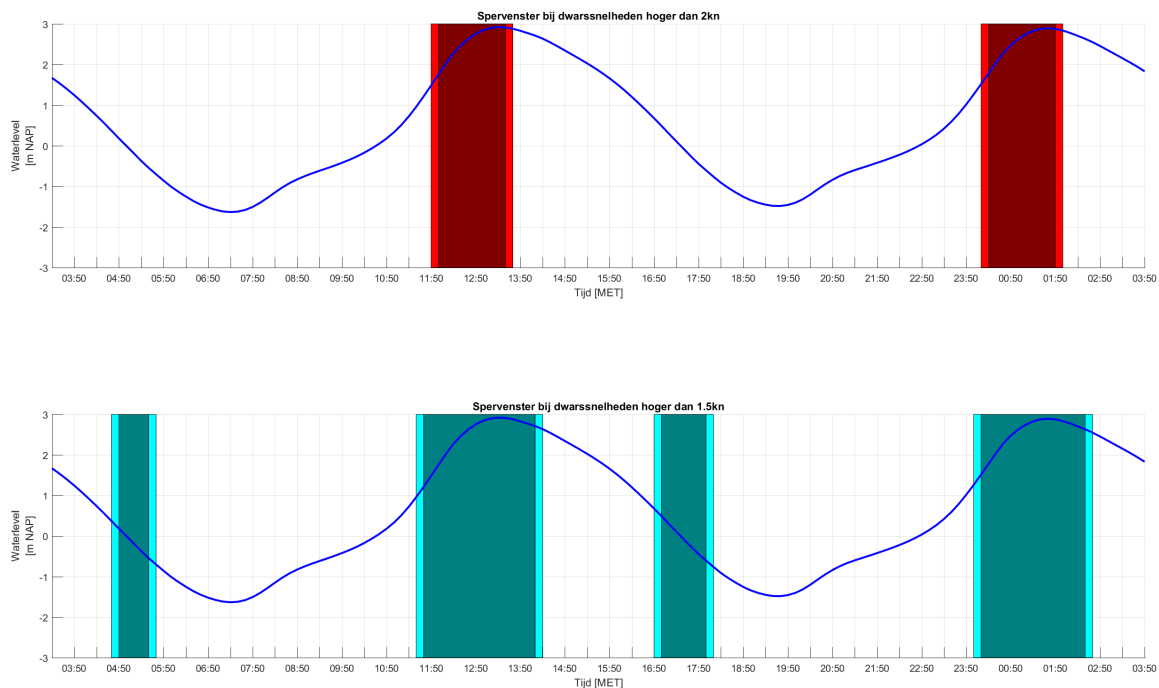


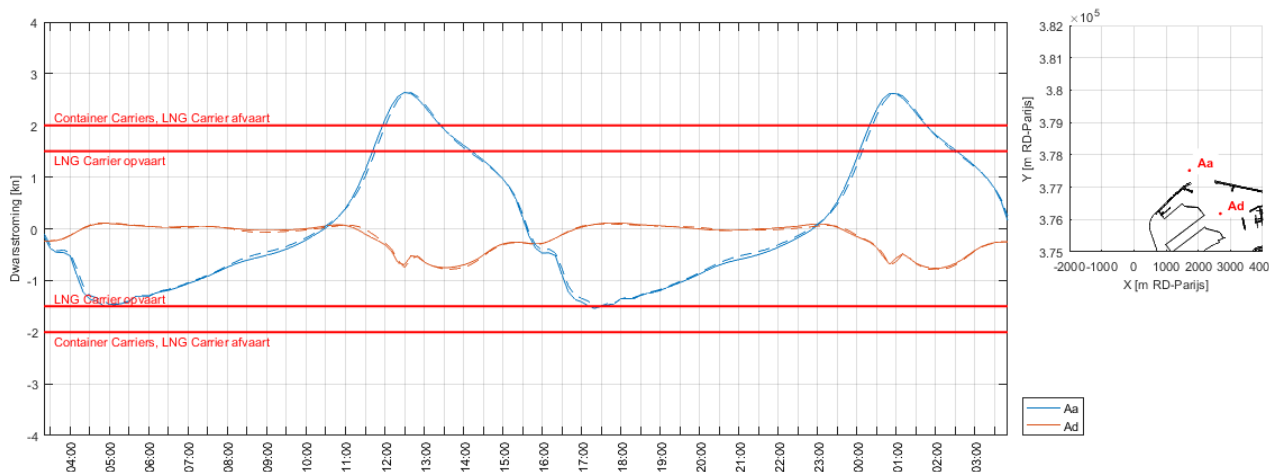
Figure 51: Time barriers for the transverse to the Pas van Zand trajectory, depth-averaged current greater than 2kn (above) and 1.5kn (below) calculated for the Moderate scenario (SLR060) during spring tide.



The time windows of the transverse currents greater than 1.5 knots and 2 knots are shown in Figure 51. It is found that the plot of the 2 knots limit (above) is identical to the one of the Reference scenario (Figure 48), while the plot of the 1.5 knots limit (below) presents slightly increased time barrier during the ebb phase (now is something more than 1 hour).

The temporal evolution of transverse current magnitude at the location close to the port entrance (Aa), and the one in CDN B (Ad), are shown in Figure 52, where the dashed lines correspond to the Reference scenario. Obviously, the curves of the two scenarios almost coincide presenting though a slight phase difference. Notice that the magnitude of the cross currents is hardly influenced. The differences in Figure 51 can be mainly attributed to the small phase differences.

Figure 52: Depth-averaged transverse current at the Pas van het Zand trajectory (close to the port entrance, Aa) and in CDN B (Ad) during spring tide for the Moderate scenario (SLR060).



The dashed lines correspond to the Reference scenario.

The red lines show the maximum accepted transverse velocities for the navigation of container and LNG ships.

### Warm sea level rise scenario

The spatiotemporal variation of the depth-averaged transverse flow velocity along the Pas van het Zand trajectory for the Warm scenario (SLR90) and the corresponding difference plot of the velocity variation versus the Reference scenario, are shown in Figure 53. In this case the increase of the transverse velocity along the trajectory is enhanced compared to the corresponding one of the Moderate scenario (SLR60) (see Figure 50). Specifically, the increase reaches values up to  $\approx 15$  cm/s, which, in addition, now appear more frequently in the tidal cycle. The maximum increase in the flow magnitude is observed close the entrance of the harbor during the flood phase (about one hour before the high water) and at about 1000 m away at the beginning of the ebb phase. The differences observed in the CDN B are also more pronounced now compared to those of the Moderate scenario.

The time windows of the transverse currents greater than 1.5 knots and 2 knots are shown in Figure 54. In this case, the plot of the 2 knots limit (above) is almost identical to the one of the Reference scenario (Figure 48), while the plot of the 1.5 knots limit (below) presents increased time barrier during each ebb phase (it is about 1.5 hours).

The temporal evolution of transverse current magnitude at the location close to the port entrance (Aa), and the one in CDN B (Ad), are shown in Figure 55, where the dashed lines correspond to the Reference scenario. Obviously, the curves of the two scenarios present almost the same amplitude but also a slight phase difference. The differences in Figure 53 during flood phase, are mainly attributed to this small phase shift.

Figure 53: Spatiotemporal evolution of the depth-averaged transverse current along the Pas van het Zand trajectory during the spring tide for the Warm sea level rise scenario (left). Difference plot versus Reference scenario (right).

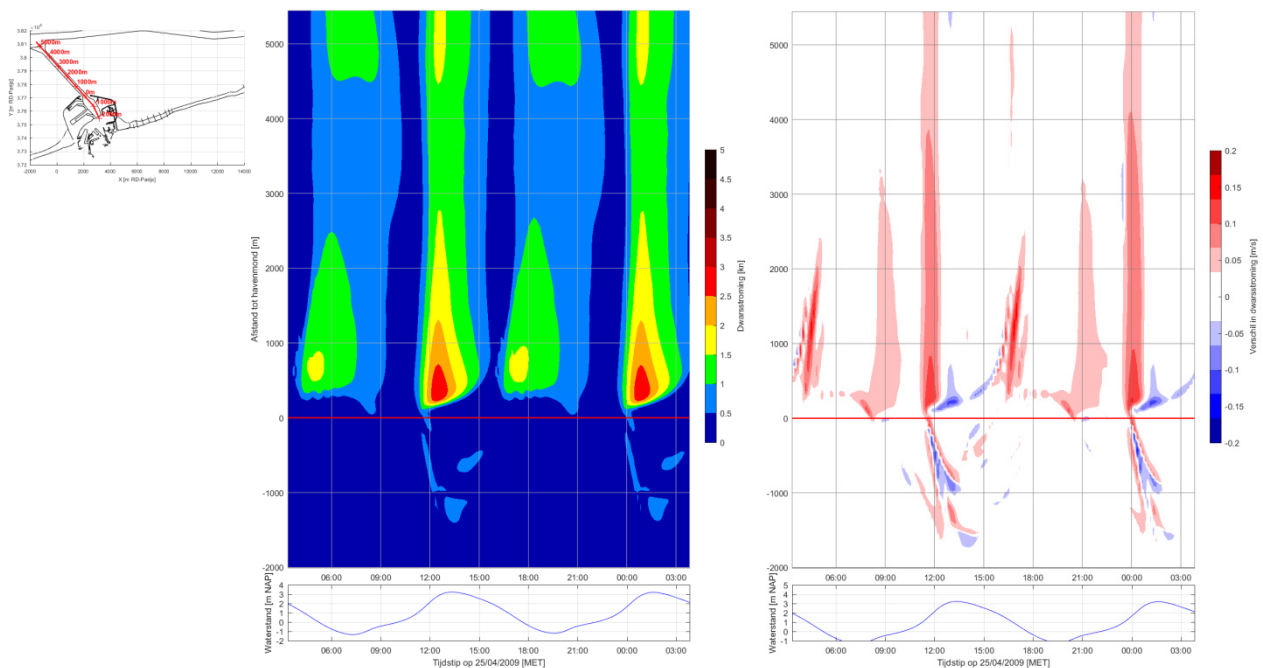


Figure 54: Time barriers for the transverse to the Pas van Zand trajectory, depth-averaged current greater than 2kn (above) and 1.5kn (below) calculated for the Warm scenario (SLR090) during spring tide.

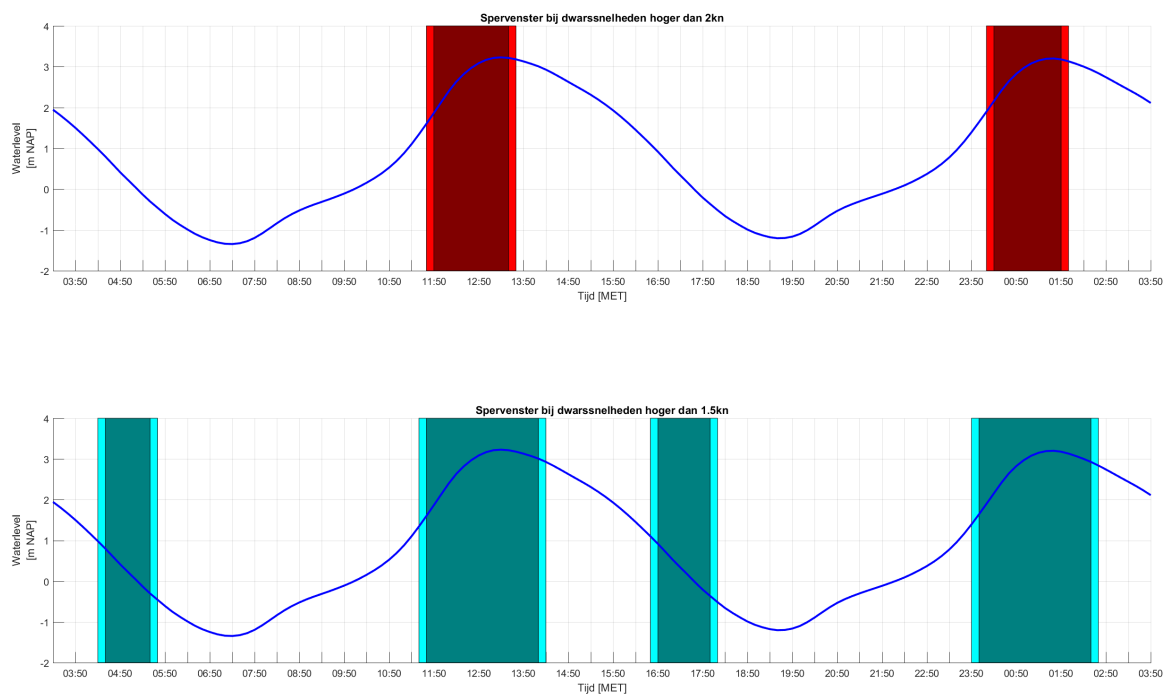
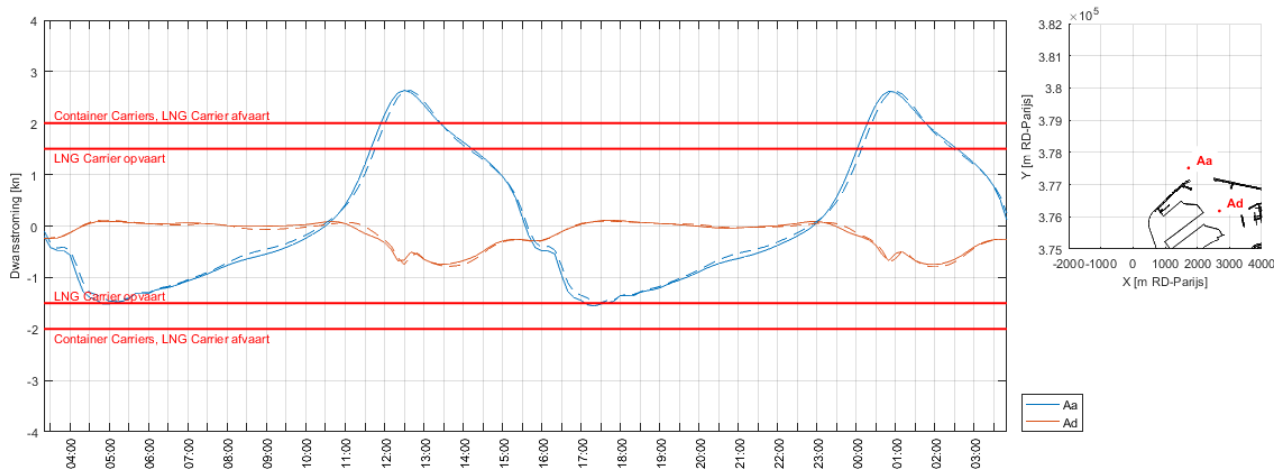


Figure 55: Depth-averaged transverse current at the Pas van het Zand trajectory (close to the port entrance, Aa) and in CDNB (Ad) during spring tide for the Warm scenario (SLR090).



The dashed lines correspond to the Reference scenario.

The red lines show the maximum accepted velocities for the navigation of container and LNG ships.

### Worst-case sea level rise scenario

The spatiotemporal variation of the depth-averaged transverse flow velocity along the Pas van het Zand trajectory for the Worst-case scenario (SLR200) and the corresponding difference plot of the velocity variation versus the Reference scenario, are shown in Figure 56. As expected, in this case the increase of the transverse velocity along the trajectory is enhanced compared to what was found for the Moderate and the Warm scenarios (shown in Figure 50 and Figure 53), respectively. Specifically, the increase reaches values up to  $\approx 20$  cm/s, which, in addition, now appear even more frequently in the tidal cycle. The maximum increase in the flow magnitude is observed close to the entrance of the harbor (but it is more stretched to the offshore direction) during a longer time period of the flood phase. It is also worth to mention that the differences observed in the CDNB do not seem to be substantially enhanced by the large sea level rise.

The time windows of the transverse currents greater than 1.5 knots and 2 knots are shown in Figure 57. For the plot of the 2 knots limit, each time barrier of the flood phase is larger by 10 minutes compared to those of the Reference scenario (Figure 48). In addition, the plot of the 1.5 knots limit presents 30 minutes increase in the each of the time barriers of the flood and the ebb phase of one tidal cycle. For clarity of the sea level rise effect on the time that the port remains accessible, the total duration of the time barriers per 24 hr on the basis of the 1.5 and 2 knots limits for all the investigated scenarios, are shown in Table 4.

The temporal evolution of the transverse current magnitude at the location close to the port entrance (Aa), and the one in CDNB (Ad), are shown in Figure 58, where the dashed lines correspond to the Reference scenario. One more time the curves of the two scenarios present almost the same amplitude but now the phase difference seems to be substantially larger than in the two milder scenarios. For this reason, this phase shift has been taken into account in the preparation of the difference plot of Figure 56, i.e. the time-series of the Worst-case scenario has been shifted forward in time by 10 minutes (one time-step). Figure 58 shows that although the maximum currents during flood are not affected in the vicinity of the port entrance, and the maximum flood currents are (according to Figure 42) even lowered by sea level rise along parts of the trajectory, still the time-barrier during flood does slightly increases due to the change in tidal asymmetry.

Figure 56: Spatiotemporal evolution of the depth-averaged transverse current along the Pas van het Zand trajectory during the spring tide for the Worst-case sea level rise scenario (left). Difference plot versus Reference scenario (right).

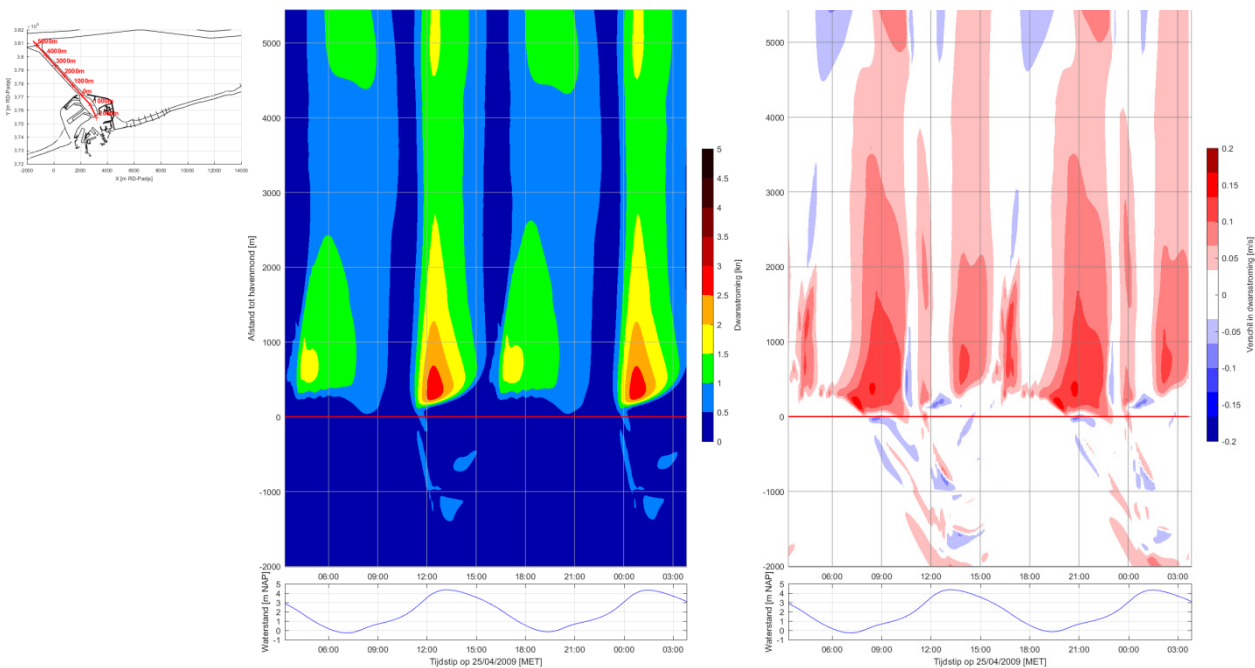


Figure 57: Time barriers for the transverse to the Pas van Zand trajectory, depth-averaged current greater than 2kn (above) and 1.5kn (below) calculated for the Worst-case scenario (SLR200) during spring tide.

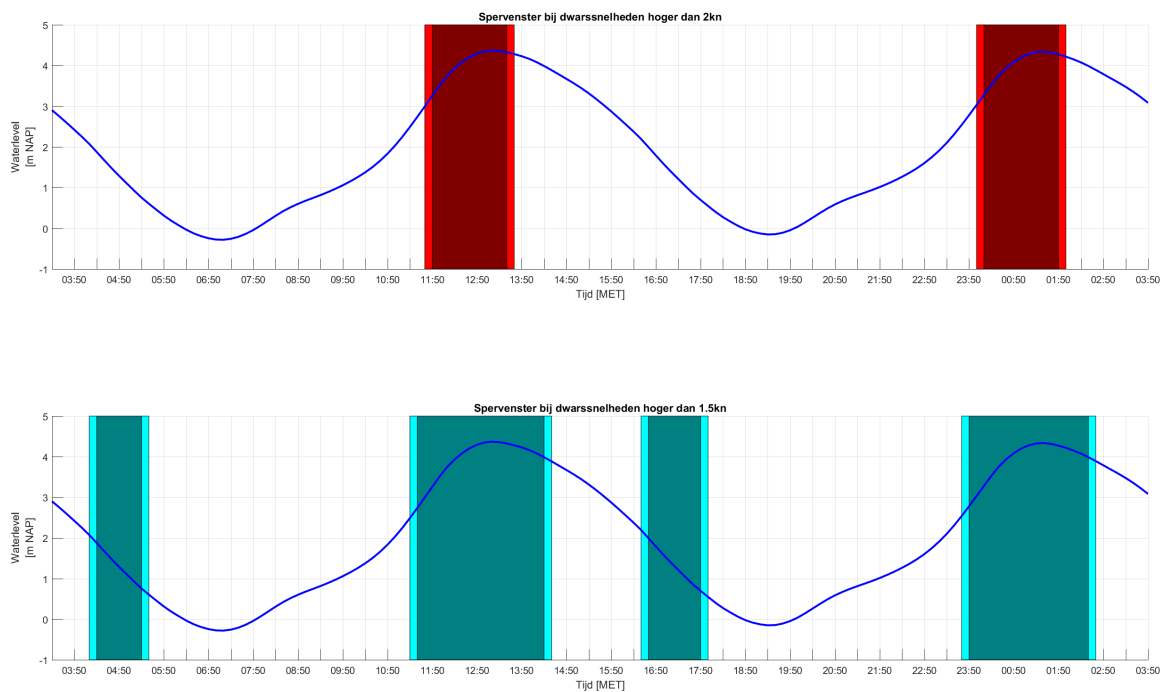
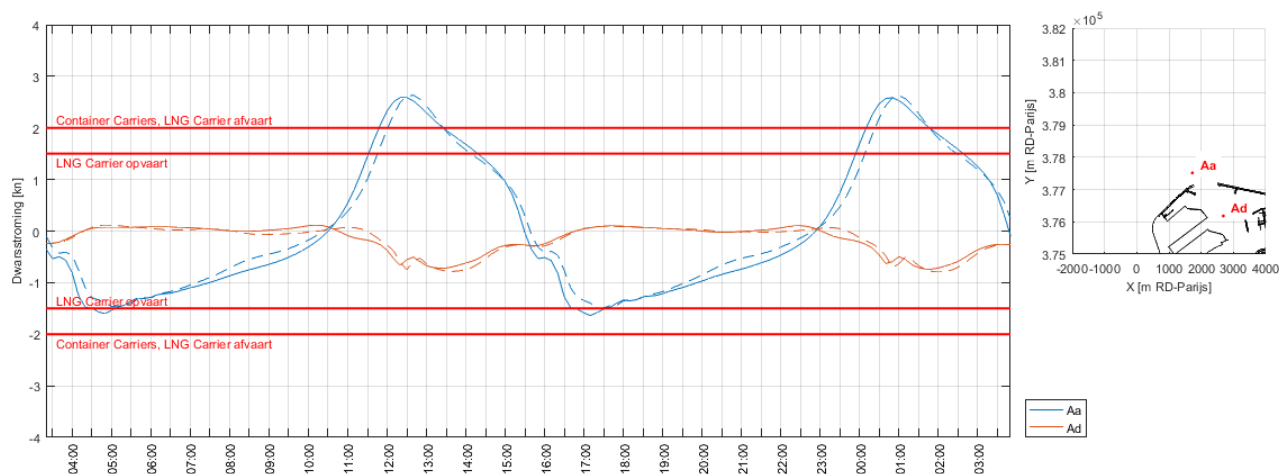


Figure 58: Depth-averaged transverse current at the Pas van het Zand trajectory (close to the port entrance, Aa) and in CDNB (Ad) during spring tide for the Worst-case scenario (SLR200).



The dashed lines correspond to the Reference scenario.

The red lines show the maximum accepted transverse velocities for the navigation of container and LNG ships.

Table 4: Maximum depth-averaged transverse velocities along the Pas van het Zand trajectory during spring tide and total duration of the time barriers per 24 hr on the basis of the maximum allowed velocities (1.5 and 2 kn) for all the investigated scenarios.

Scenario	Max. transverse current (kn)	Difference transverse current (%)	Duration 2kn time barrier (hh:mm)	Difference 2kn time barrier (%)	Duration 1.5kn time-barrier (hh:mm)	Difference 1.5kn time-barrier (%)
Reference	2.92	-	03:20	-	06:20	-
Moderate	2.92	0.0%	03:20	0.0%	07:10	+13.3%
Warm	2.90	-0.7%	03:30	+5.1%	07:50	+23.7%
Worst-case	2.84	-2.7%	03:40	+10.2%	08:20	+31.6%



## Summary

In the present report, the work that has been done by the authors in the first six months of the three-year contract of the position **'Modelleur in het kader van project 15\_068: Modelleren getij, sedimenttransport en morfologie voor de Belgische kustzone volgens gekend projectplan'**, was presented.

First, results from the Telemac3D hydrodynamic simulations by use of the so-called Zeebrugge (ZB) model were presented, considering two scenarios of a dunebelt (scenario 13: completely closed; scenario 14: opening at Zeebrugge), spanning along the entire Belgian coast from Dunkirk to Cadzand. Regarding with the impact of the dunebelt on the coastal currents, a general increase of the maximum flow magnitude of order 10 to 20 cm/s, along the western part of the Belgian coast and near Wielingen gully was found. On the contrary, reduction (20-30 cm/s) of the flow strength was observed in the area around the Pas van het Zand navigation channel. As for the port accessibility, it was indicated that the shape of the dunebelt has a positive effect on the accessibility, as transverse velocities along the Pas van Zand trajectory are always less than 2 kn, while they exceed 1.5 kn only for one hour during flood phase (spring tide).

Next, another Telemac3D hydrodynamic model, Scaldis, was utilized in order to ensure that the flow results at the area close to the southwestern end of the dunebelt (French borders) are not, or minimally affected by the boundary of the (ZB model) domain. It was found that the impact of the southwestern boundary in the area nearby is limited and therefore the ZB model is still proper for the investigation of the dunebelt scenarios provided that the seawall extends up to the French borders.

Next, the impact of sea level rise (SLR) on the nautical accessibility of the port of Zeebrugge has been investigated throughout the Telemac3D Zeebrugge model. Three scenarios have been investigated: a moderate sea level rise of 60 cm, a warm scenario of 90 cm sea level rise and a worst case scenario of 200 cm sea level rise. The model runs show that with increased sea level rise, not only the mean sea level increases, but also the tidal amplitude increases at the Belgian and Dutch coast and upstream the Scheldt estuary. Changes in the tidal amplitude, are expected to be accompanied by some changes in the tidal phase. Although the scenarios show an increase in maximum depth-averaged velocities near the mouth area and the coast of Walcheren, mainly during ebb phase, in general the currents in the vicinity of the port of Zeebrugge (Scheur, Wielingen and Pas van het Zand) are lower in case of sea level rise. However during ebb phase, a local increase along the eastern breakwater and in front of the port can be noticed (up to 30 cm/s in the worst case scenario). As for the currents in the Western Scheldt, it is found that sea level rise leads to significant increase of maximum velocity in the intertidal areas, where dry areas become wet, and reduction of its magnitude in the navigation channels (about 30 cm/s in the worst case scenario).

The impact of sea level rise on the port accessibility is rather small. Sea level rise has hardly any impact on the time window with respect to the 2 knots cross current limit, i.e. the limit during arrival and departure of container carriers and departure of LNG carriers. On the other hand, the total duration of the window of 1.5 knots limit (arrival of LNG carriers) is reasonably affected by the sea level rise, which is translated to a maximum increase of about 30% in the worst case scenario.

## References

- ANSYS inc.** (2015). Introduction to ANSYS Meshing: Mesh quality & advanced topics, Lecture7. <https://www.academia.edu>.
- Chu, K.** (2017). CSM and ZUNO run of 2009 including 60, 90, 200 cm sea level rise. WL Memo, WL2017M15\_068\_19. Flanders Hydraulics research: Antwerp, Belgium
- De Maerschallck, B.; Renders, D.; Vanlede, J.; Gourgue, O.; Willems, M.; Verwaest, T.; Mostaert, F.** (2016). Modelling Vlaamse Baaien: deelrapport 1. Hydrodynamische modellering scenario's Oostkust. Versie 5.0. *WL Rapporten*, 15\_068\_1. Waterbouwkundig Laboratorium/Afdeling Maritieme Toegang: Antwerpen
- Geuzaine, C. and Remacle, J.-F.** (2009). Gmsh: A 3-D finite element mesh generator with built-in pre- and post-processing facilities. *Int. J. Numer. Meth. Engng.*, 79: 1309–1331. doi:10.1002/nme.2579
- IMDC** (2013). Analyse impact havenuitbreiding Zeebrugge op onderhoudsbaggerwerken vaargeulen Noordzee en voorhaven Zeebrugge – Leveren van ondersteunend numeriek scenario-onderzoek, Telemac model – Model set-up. I/RA/11401/12.202/ABR.
- IMDC** (2015). Analyse impact havenuitbreiding Zeebrugge op onderhoudsbaggerwerken vaargeulen Noordzee en voorhaven Zeebrugge – Leveren van ondersteunend numeriek scenario-onderzoek, Telemac Zeebrugge model – Set-up, calibration and validation I/RA/11401/13.072/JUD.
- De Maerschallck, B.; Dijkstra, J.; Nnafie, A.; Vroom, J.; van Oyen, T.; Röbbke, B.R.; van der Werf, J.; Van der Wegen, M.; van Maren, B.; Taal, M.; Vanlede, J.; Verwaest, T.; Mostaert, F.** (2017). Modelling Belgische kustzone en Scheldemonding: deelrapport 3. Modelling van de morfologische effecten na aanleg nieuwe Geul van de Walvischstaart. Versie 3.0. *WL Rapporten*, 15\_068\_3. Deltares: Antwerpen
- De Maerschallck, B.; Renders, D.; Vanlede, J.; Gourgue, O.; Willems, M.; Verwaest, T.; Mostaert, F.** (2016). Modelling Vlaamse Baaien: deelrapport 1. Hydrodynamische modellering scenario's Oostkust. Versie 5.0. *WL Rapporten*, 15\_068\_1. Waterbouwkundig Laboratorium/Afdeling Maritieme Toegang: Antwerpen
- Dujardin, A.; Vanlede, J.; De Maerschallck, B.; Mostaert, F.** (2011). Verbetering numeriek instrumentarium Zeebrugge: deelrapport 3 stromingsmodel met verfijnde rekenrooster voor Zeebrugge en de Pas van het ZandID: 208473; M3: BibLevel: MSER -. *WL Rapporten*, 753\_08. Waterbouwkundig Laboratorium: Antwerpen
- Hassan, W.; Suzuki, T.; De Maerschallck, B.; Verwaest, T.; Mostaert, F.** (2016). Modelling Belgische kustzone en Scheldemonding: rekennota - berekeningen golfklimaat Vlaamse Baaien scenario's E4 en F1. Versie 3.0. *WL Rapporten*, 15\_068\_4. Waterbouwkundig Laboratorium: Antwerpen. VII, 10 + 2 bijlagen pp.
- Leyssen, G.; Vanlede, J.; Decrop, B.** (2012). Modellentrein CSM-ZUNO: deelrapport 2. Validatie 2009. *WL Rapporten*, 753\_12. Waterbouwkundig Laboratorium: Antwerpen
- Suzuki, T.; Hassan, W.; Kolokythas, G.K.; Verwaest, T.; Mostaert, F.** (2016). Wave climate for inland vessels between Zeebrugge and the mouth of the Western Scheldt: estimation by the Belgian coast model in SWAN. *FHR reports*, 15\_026. Flanders Hydraulics Research: Antwerp
- Van den Eynde, D.; De Smet, L.; De Sutter, R.; Francken, F.; Maes, F.; Ozer, J.; Polet, H.; Ponsar, S.; Van der Biest, K.; Vanderperren, E.; Verwaest, T.; Volckaert, A.; Willekens, M.; De Smet, L.; Francken, F.; Haelters, J.; Maes, F.; Malfait, E.; Ozer, J.; Polet, H.; Reyns, J.; Van der Biest, K.; Vanderperren, E.; Verwaest, T.; Volckaert, A.; Willekens, M.** (2009). Evaluation of climate change impacts and adaptation responses for marine activities CLIMAR: final report phase 1 (S. Ponsar, Ed.). Belgian Science Policy Office: Brussel. 81 pp.



## Appendix A: Summary of model settings

A detailed description of the model the reader is referred to De Maerschalck *et al.* (2016) or for the full model setup and calibration reports of IMDC (2013, 2015).

### Boundary conditions

Space-varying water level time-series as well as the velocity time-series (timestep equal to 10 min) were prescribed at each computational node of the semi-circular offshore boundary of the computational domain. Additionally, discharges (hourly time-series) were defined at 7 different locations in the model, i.e. Zeebrugge harbor, the lock at Bath, the channel from Gent to Terneuzen at Terneuzen, and 4 schematized tributaries of the Scheldt River (Scheldt at Melle, Dijle/Zenne (combined), Nete at Lier, and Dender at Dendermonde).

### Bottom roughness

A space varying Manning coefficient map was utilized for the bottom roughness, where values equal to  $0.02 \text{ m}^{1/3}/\text{s}$  at the sea and in the Western Scheldt and Eastern Scheldt,  $0.01 \text{ m}^{1/3}/\text{s}$  in the Lower Sea Scheldt and  $0.04 \text{ m}^{1/3}/\text{s}$  in the straight channel section, were considered. Increased roughness at the harbor breakwaters was applied (IMDC, 2015).

### Software version

The Telemac3D version 7p0r0 (Linux) was utilized for the simulations of the 'dunebelt' scenarios I3 and I4, while version 7p2r0 (Linux) was utilized for the simulations of the sea level rise scenarios. The duration of a simulation was around 18 hours using 32 cores (Bernoulli) in parallel.

### Other major settings

Parameter	Value
Time-step	20 s
Layer distribution (bottom up; %)	0,5,10,20,40,60,80,90,95,100
Horizontal viscosity	Smagorinsky model
Vertical viscosity	Mixing length
Wind forcing	Off
Salinity transport	Off
Coriolis	Yes

## Appendix B: Maximum flow velocities during ebb and flood – scenarios I3 and I4

Figure 59: Maximum depth-averaged flow velocity (magnitude [m/s]) during flood phase [25-Apr-2009 11:00 → 15:00] (left) and ebb phase [25-Apr-2009 16:00 → 19:00] (right) for dunebelt scenario I3.

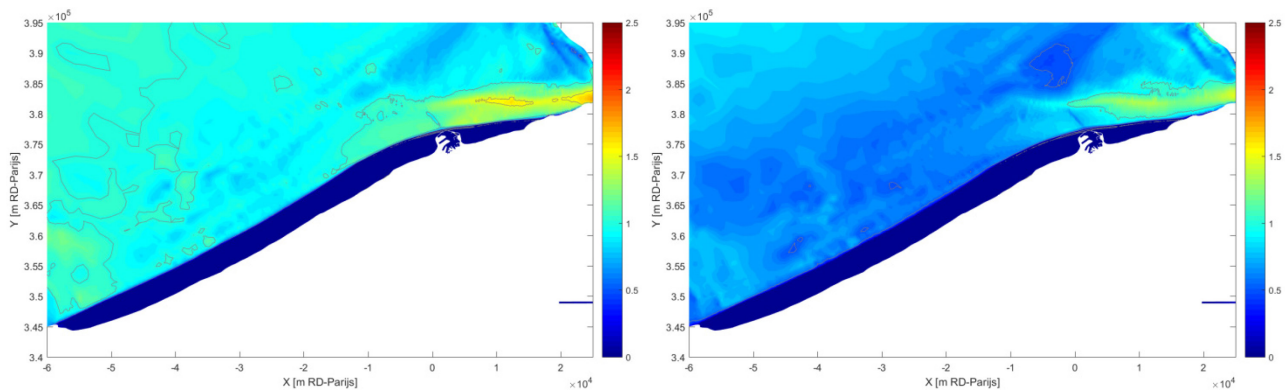
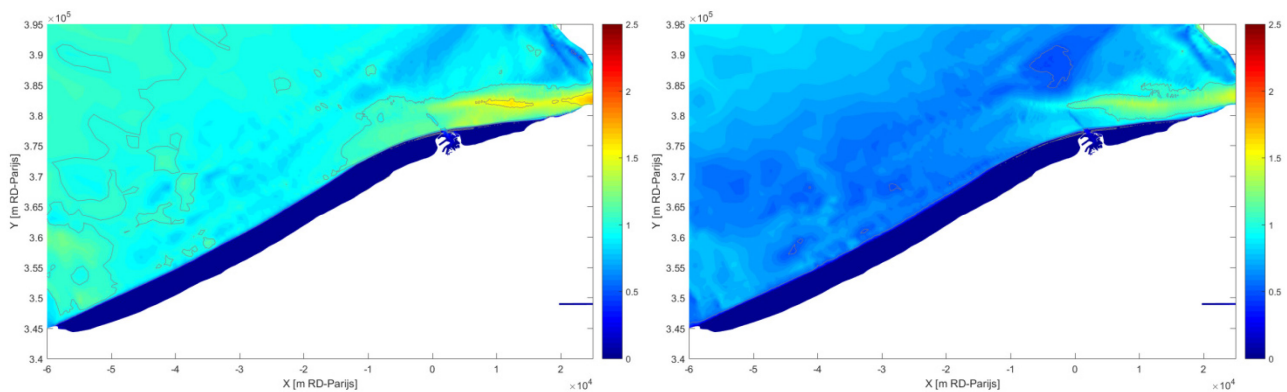


Figure 60: Maximum depth-averaged flow velocity (magnitude [m/s]) during flood phase [25-Apr-2009 11:00 → 15:00] (left) and ebb phase [25-Apr-2009 16:00 → 19:00] (right) for dunebelt scenario I4.



## Appendix C: Dunebelt scenarios I1 and I2

These scenarios have been discussed in detail in De Maerschalck *et al.* (2016). For comparison the results are adopted in this appendix. Note: for these scenarios the grid was not refined at the location of the belt.

Figure 61: Bathymetry of the dunebelt scenarios I1 and I2.

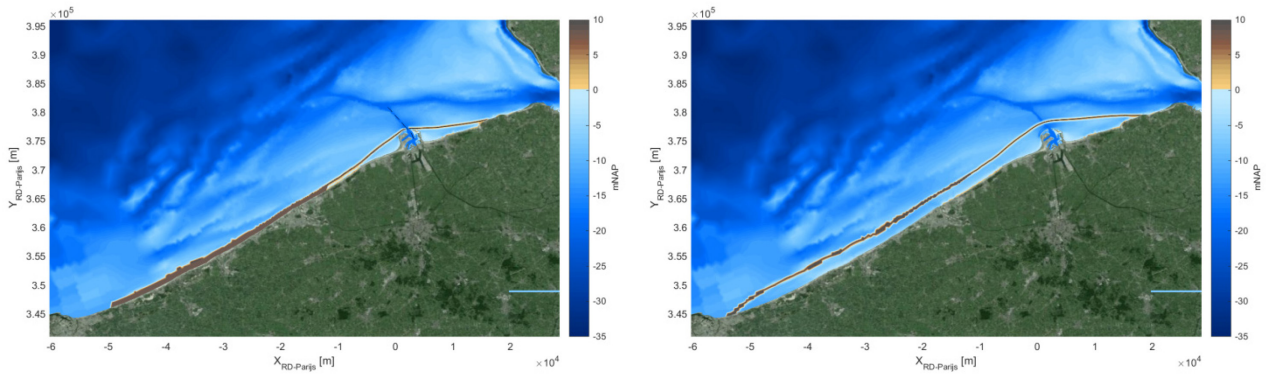


Figure 62: Maximum depth-averaged flow velocity (magnitude) for dunebelt scenario I1 (left) and I2 (right) during spring tide.

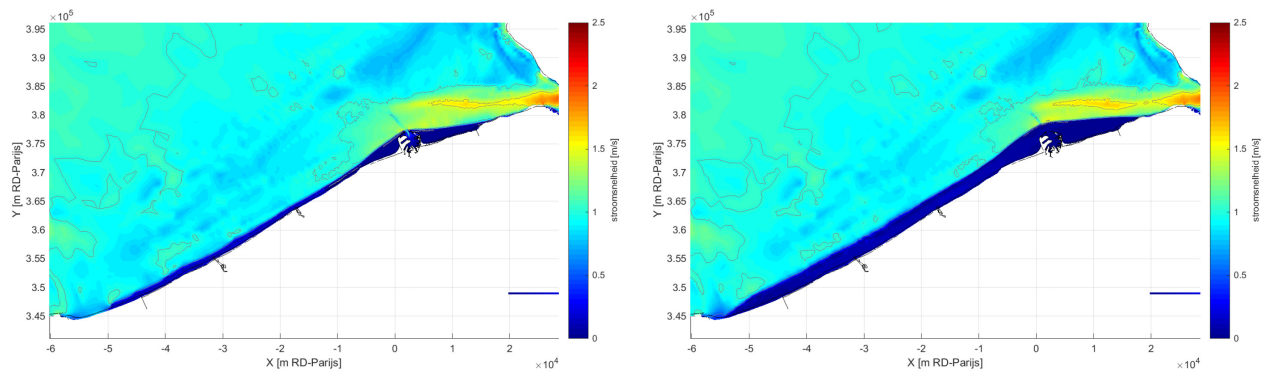


Figure 63: Difference in maximum depth-averaged flow velocity between dunebelt scenario I1 and Reference scenario (left) and I2 and Reference scenario (right) during spring tide.

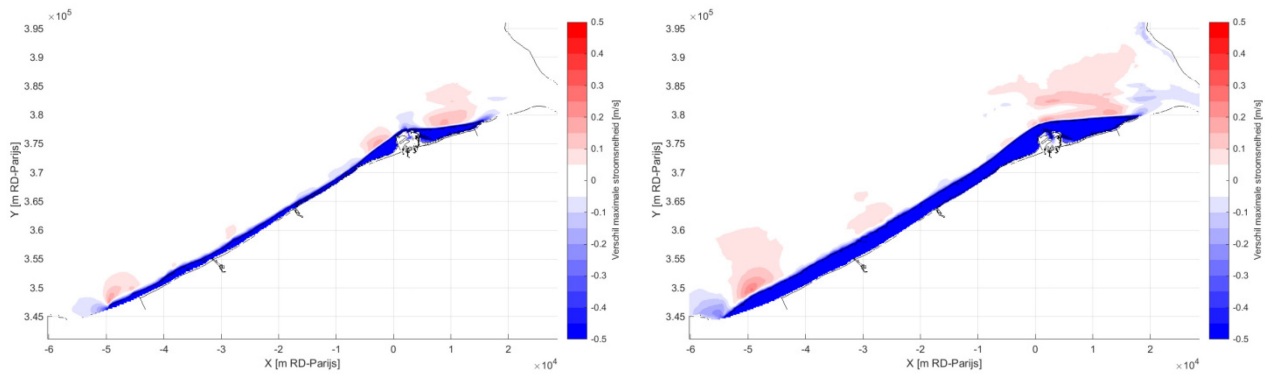
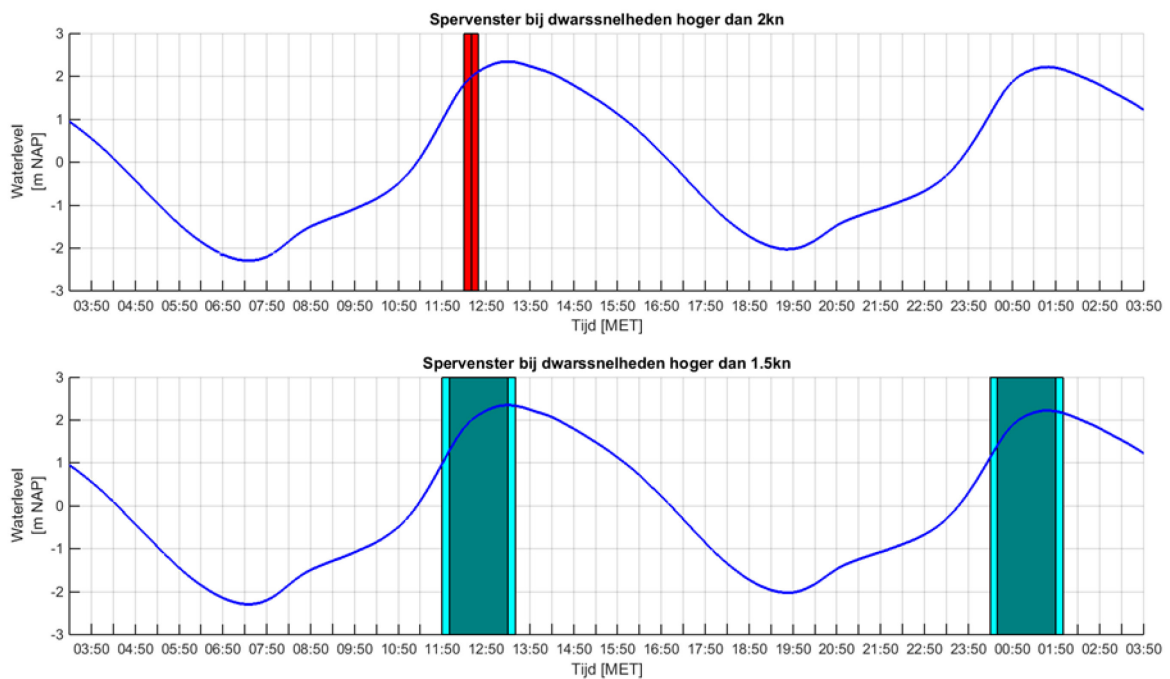


Figure 64: Window barriers for the, transverse to the Pas van Zand trajectory, depth-averaged velocities greater than 2kn (above) and 1.5kn (below) calculated for scenario I1 during spring tide.



# Appendix D: Maximum flow velocities during ebb and flood – SLR scenarios

Figure 65: Maximum depth-averaged flow velocity (magnitude) during flood phase of the spring tide for the Reference and the sea level rise scenarios.

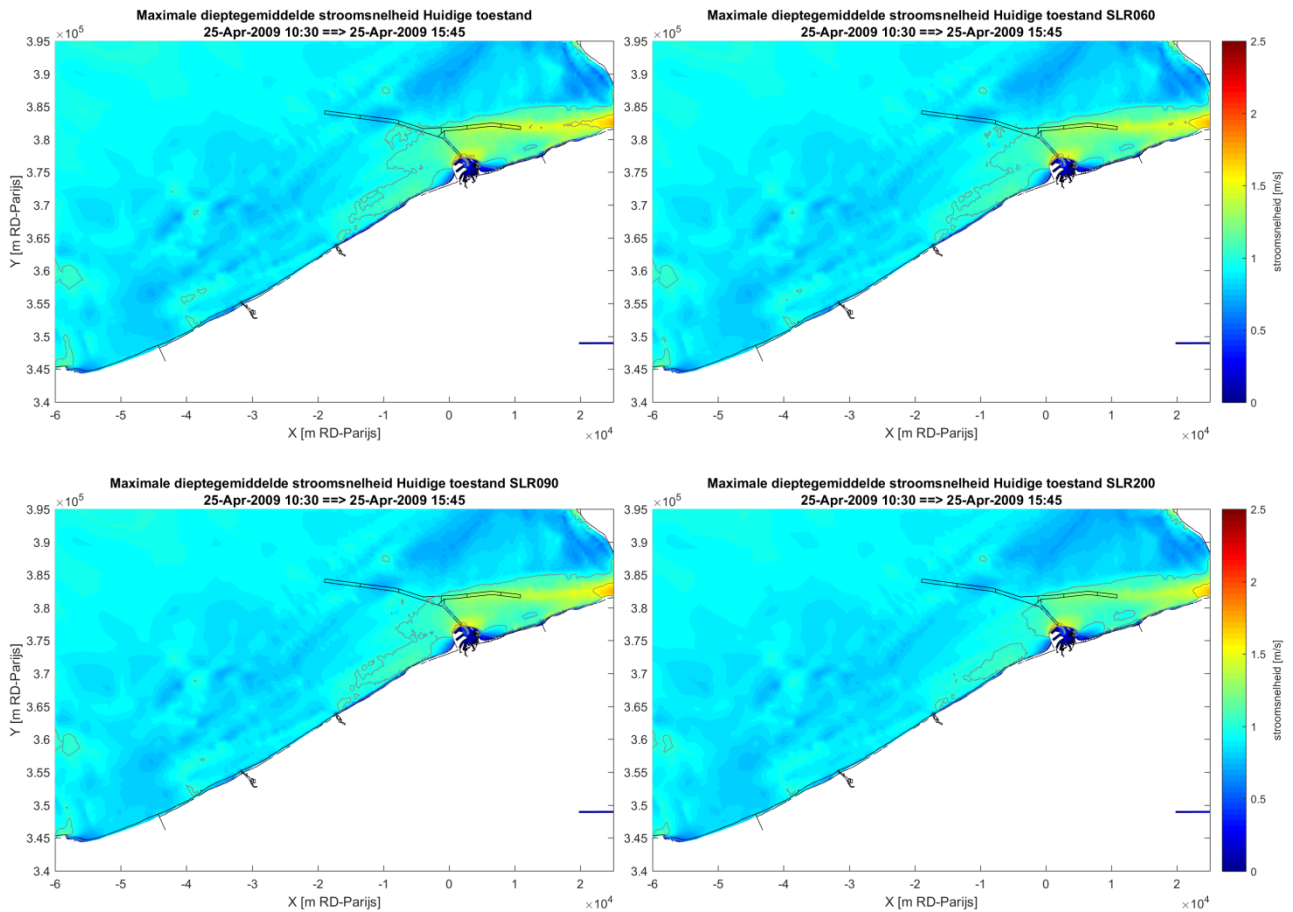




Figure 66: Maximum depth-averaged flow velocity (magnitude) during ebb phase of the spring tide for the Reference and the sea level rise scenarios.

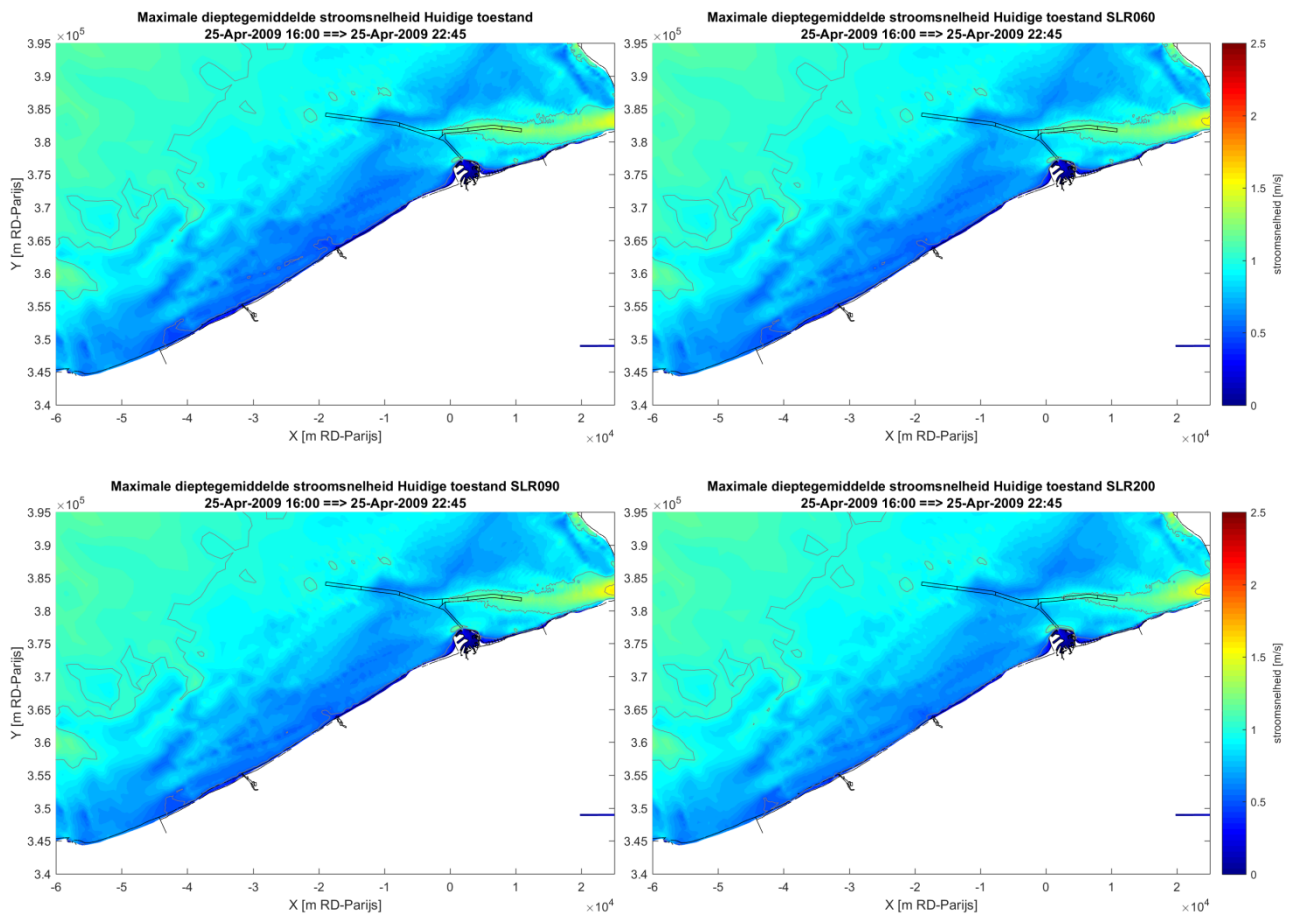


Figure 67: Difference in maximum depth-averaged flow velocity (magnitude) during flood phase of the spring tide between the sea level rise scenarios and the Reference scenario.

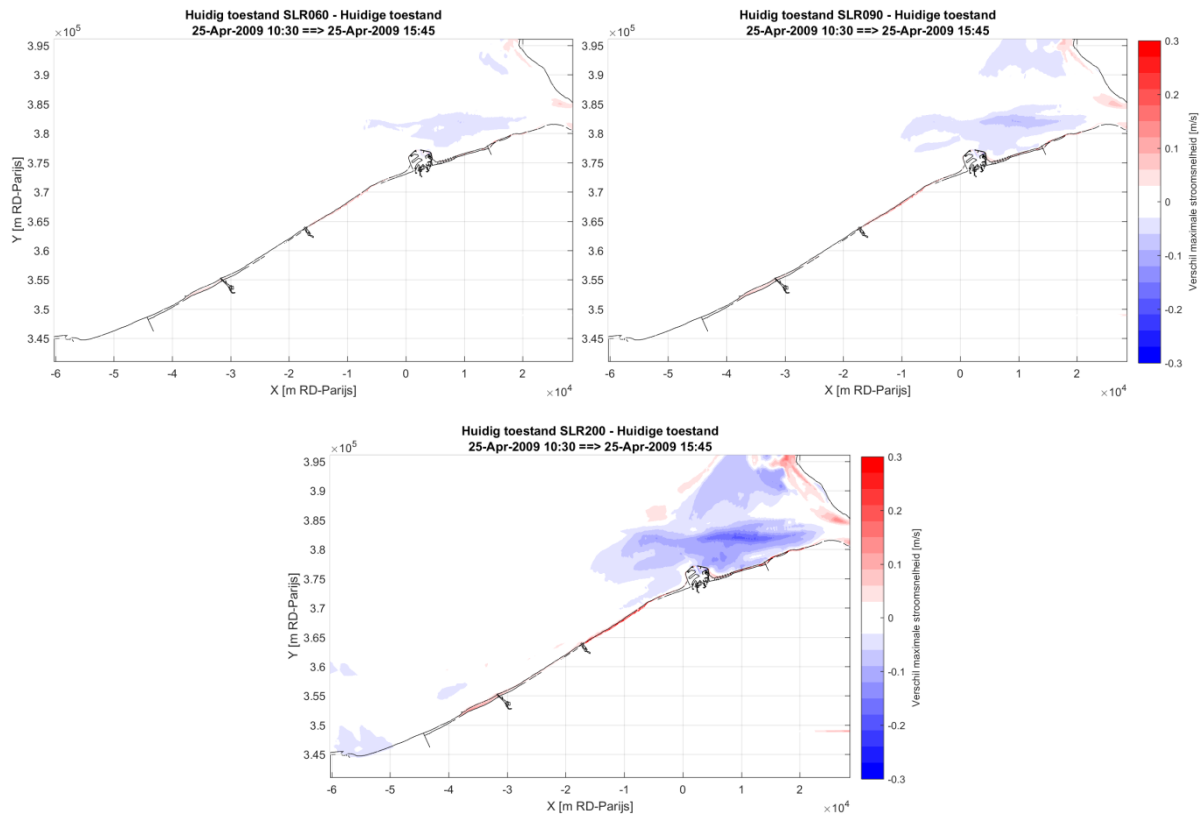


Figure 68: Difference in maximum depth-averaged flow velocity (magnitude) during ebb phase of the spring tide between the sea level rise scenarios and the Reference scenario.

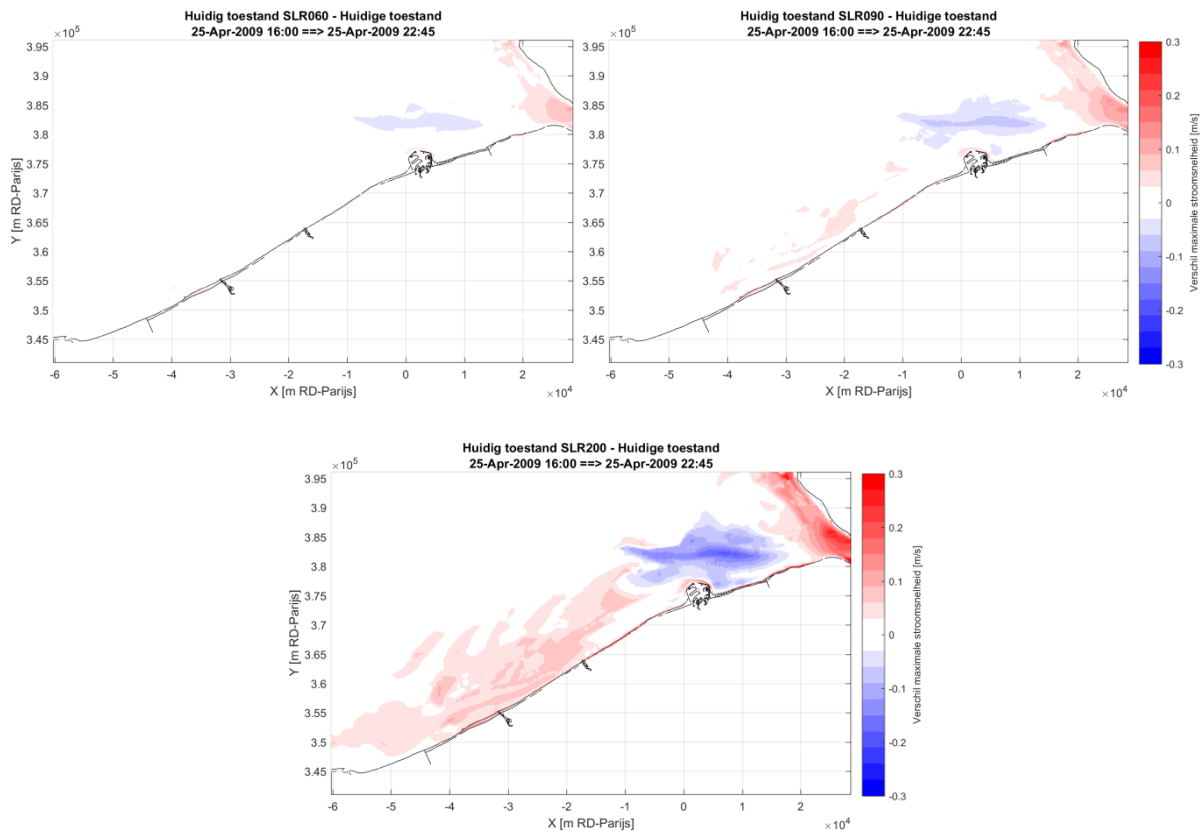


Figure 69: Maximum depth-averaged flow velocity (magnitude) during flood phase of the spring tide for the Reference and the sea level rise scenarios at the area of Western Scheldt.

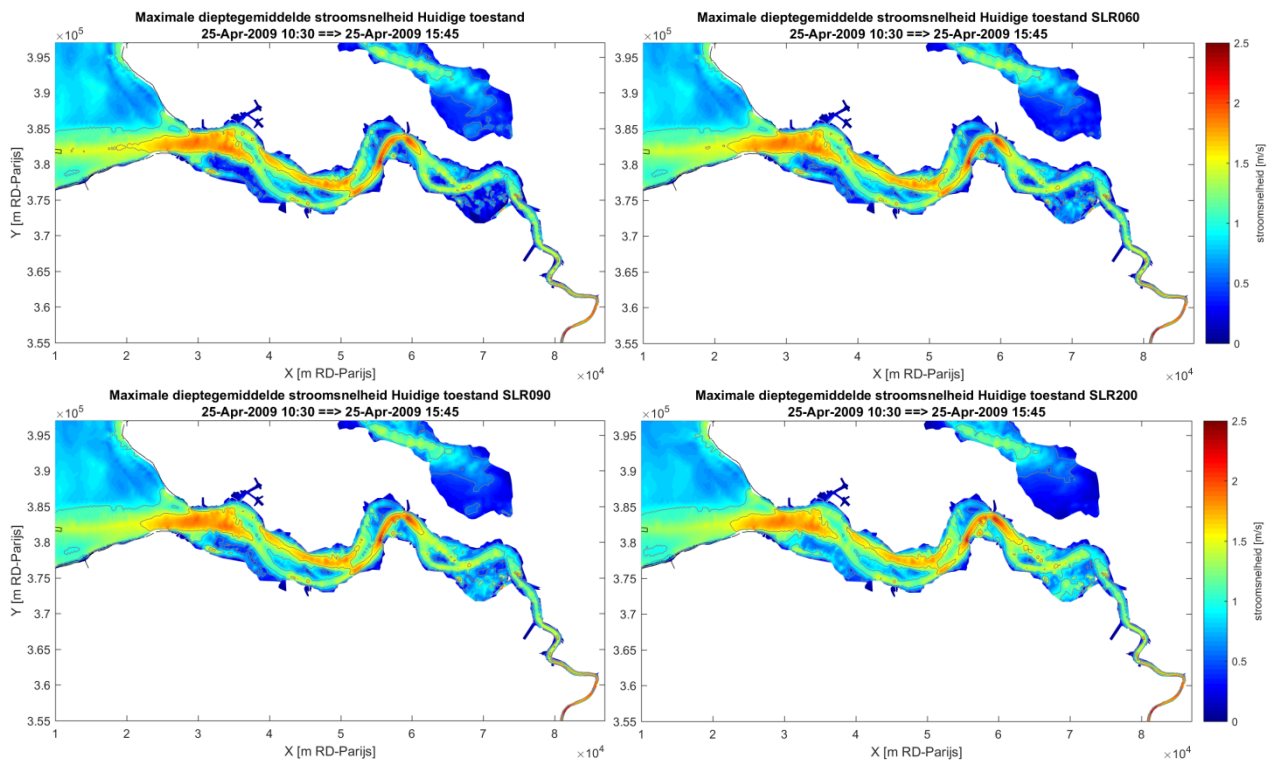


Figure 70: Maximum depth-averaged flow velocity (magnitude) during ebb phase of the spring tide for the Reference and the sea level rise scenarios at the area of Western Scheldt.

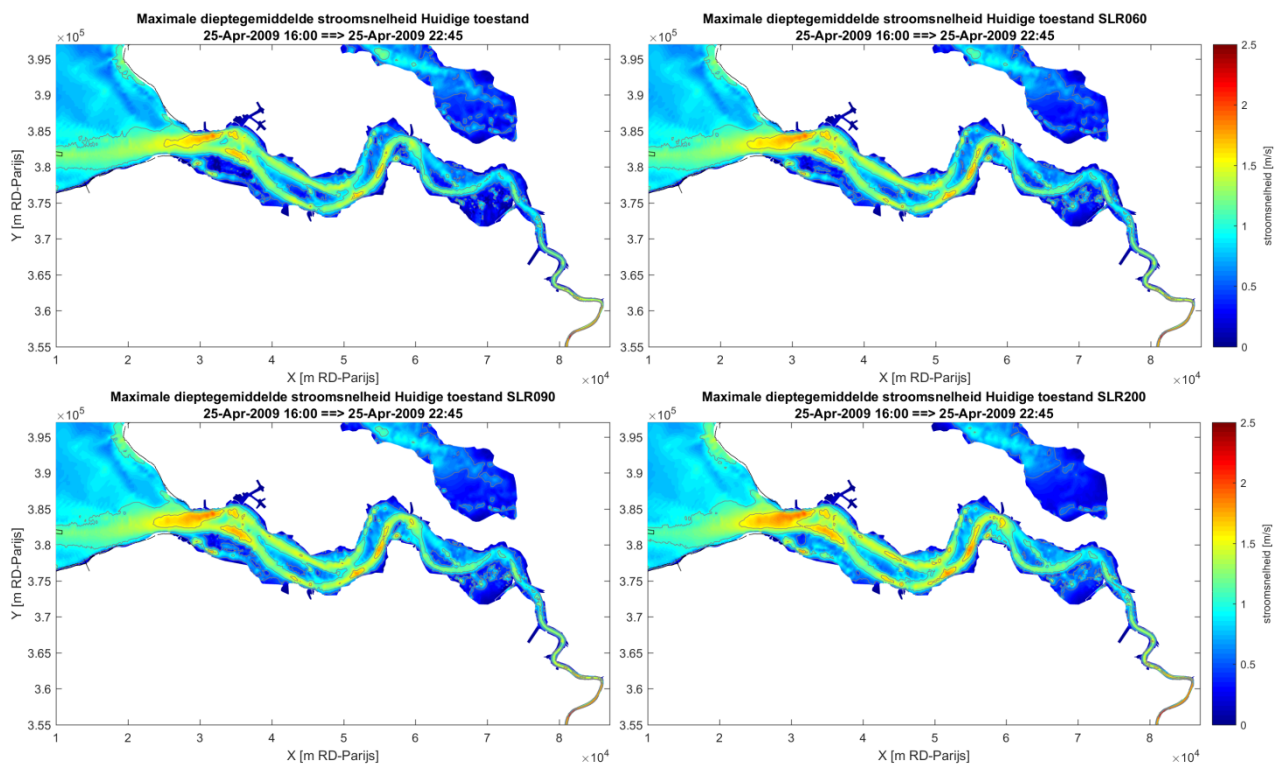


Figure 71: Difference in maximum depth-averaged flow velocity (magnitude) during flood phase of the spring tide between the sea level rise scenarios and the Reference scenario at the area of Western Scheldt.

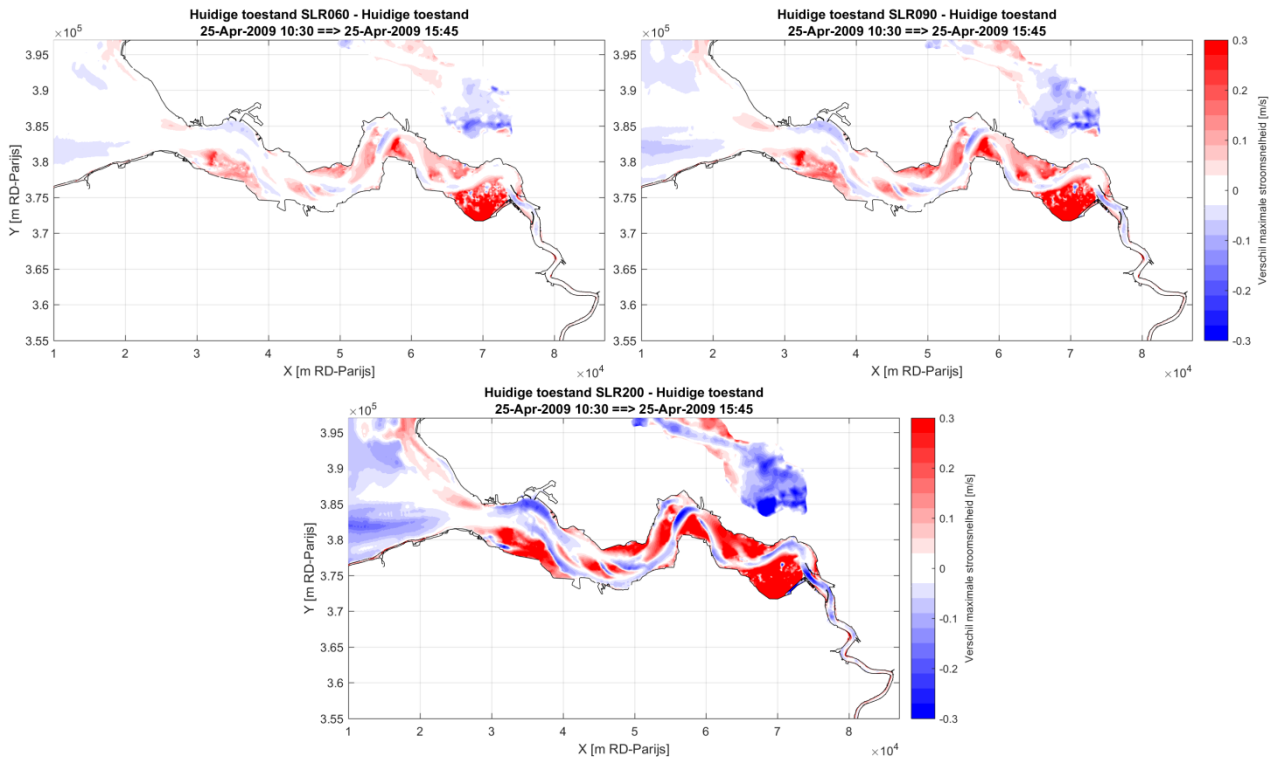
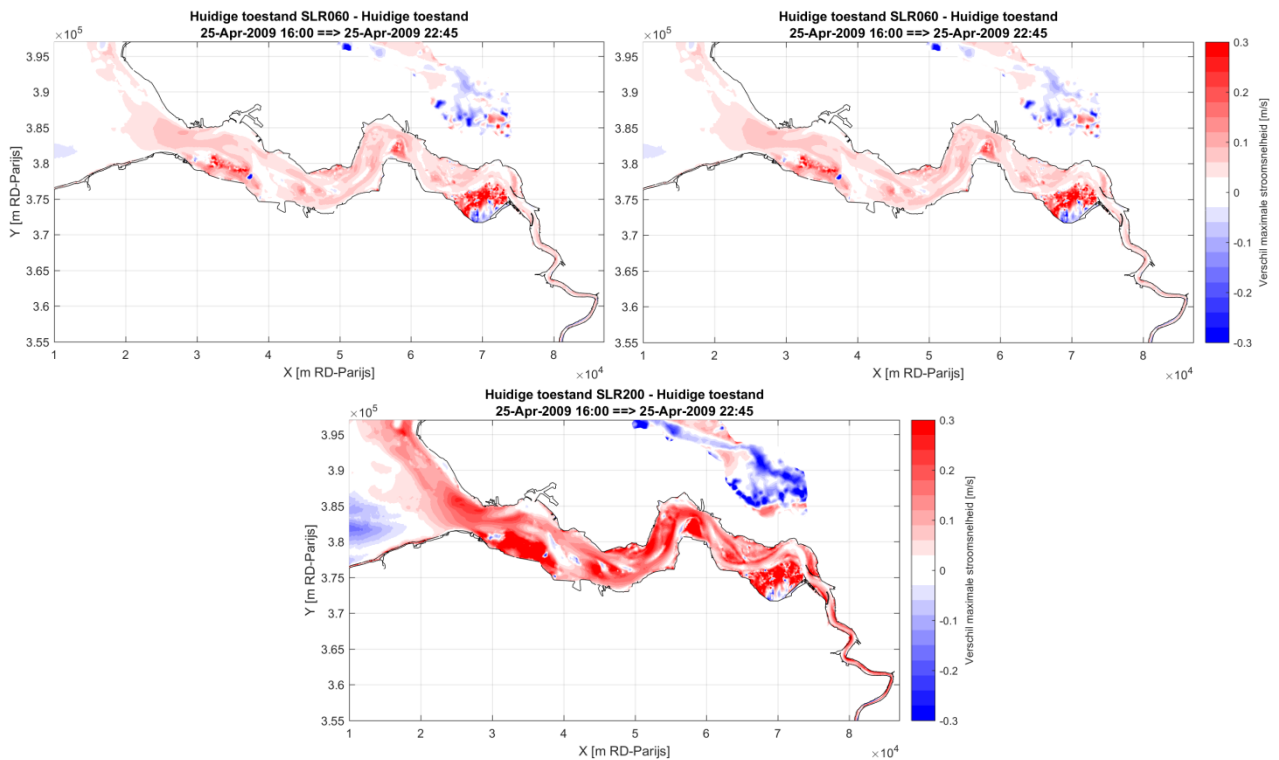


Figure 72: Difference in maximum depth-averaged flow velocity (magnitude) during ebb phase of the spring tide between the sea level rise scenarios and the Reference scenario at the area of Western Scheldt.



# Appendix E: Memo: CSM and ZUNO run of 2009 including 60, 90 and 200 cm sea level rise

////////////////////////////////////  
Titel: CSM and ZUNO run of 2009 including 60, 90 and 200 cm sea level rise  
Datum: 6/07/2017  
Auteurs: Chu, Kai  
Ref.: WL2017M15\_68\_19  
////////////////////////////////////

## 1 Introduction

In the framework of project 15\_068, the impact of future sea level rise (SLR) on the accessibility of harbor Zeebrugge will be evaluated with a Telemac model. In the preparation for the Temelac model setups, two large scale models of CSM and ZUNO are needed to provide boundary conditions through nesting. This memo describes the setups of CSM and ZUNO model. The CSM and ZUNO model are validated against measurments. After all the sea boundary condtions of water level and velocity for the ZeeBrugge Telemac model are provided by ZUNO model via nesting.

## 2 Model settings

### 2.1 Modelling software

SIMONA (Simulatie Modellen Natte waterstaat) is a program developed by Rijkswaterstaat, for 2D (WAQUA module) and 3D (TRIWAQ module) modelling of water movement, particle dispersion and fluid mud transport and consists of a number of programs for preprocessing (preparation of simulations) and post processing (visualisation of the model results). The **2015** version of SIMONA is used in this study.

### 2.2 CSM MODEL

The Continental Shelf Model (CSM) has an orthogonal grid constructed from sphere coordinates in the spherical coordinate system ED50. It includes the continental shelf from 48° to 62.25° northern latitude and from 12° western longitude to 13° eastern longitude. The model includes the North sea, the Wadden sea, Eems, Dollard, the Channel, the Keltic sea, the Irish sea, Skagerrak and Kattegat (Figure 2-1). The grid has resolution of 9.3 to 6.5 km in the west-east direction and 9.25 km in the south-north direction (*Leysen et al.*, 2012).

The selected version of the CSM model is driven at the ocean boundaries by the astronomical water levels defined by 11 tidal components: M2, S2, N2, K2, O1, K1, Q1, P1, NU2, L2 and SA. The primary model settings are presented in Table 2-1.

The harmonic run of CSM2009 is used for this study, wind is neglected since at this phase of the 15\_068 project it is unknown what windfield should be implemented in the climate change scenario's. It is archived on the WL subversioning system at the locaton below:

[https://wl-subversion.vlaanderen.be/svn/repoSpNumMod/SIMONA/CSM/004\\_CSM\\_2009](https://wl-subversion.vlaanderen.be/svn/repoSpNumMod/SIMONA/CSM/004_CSM_2009)

Figure 2-1: CSM model grid.



Table 2-1: Model parameters of CSM model.

Model parameter	Value
Time step	10 min
Smoothing Time	720 min
Eddy viscosity	0.00 m <sup>2</sup> /s
Initial water level	0 m to NAP
Chézy (varying in space)	55-100m <sup>1/2</sup> /s
Wind	off
Water density	1023.0 kg/m <sup>3</sup>
Air density	1.205 kg/m <sup>3</sup>
Salinity	Off
Dimensions	2D
Simulation period	01/04/2009 00:00 – 01/05/2009 00:00

## 2.3 ZUNO MODEL

The Southern North sea (Zuidelijke Noordzee) model is a curvilinear model in RD Parijs coordinate system. It includes the southern North sea and the Channel, bounded by the lines Aberdeen (Great Britain) - Hanstholm (Denmark) in North and Bournemouth (Great Britain) - Cherbourg (France) in South-West (Figure 2-2). The model resolution is about 4.5 to 6 km along the English coast, 2.5 to 4 km in the Channel and the German Bight and 1 to 2 km along the Dutch coast (Leysen et al., 2012).

ZUNOV3 is nested in the CSM model (Figure 2-3) with the help of the **modnst** software (Rijkswaterstaat, 2015a). The primary model settings are presented in Table 2-2.

The harmonic run of ZUNO2009 is used for this study. The ZUNO model is archived in the WL subversioning repository here:

[https://wl-subversion.vlaanderen.be/svn/repoSpNumMod/SIMONA/ZUNO/003\\_ZUNO\\_v3\\_2009](https://wl-subversion.vlaanderen.be/svn/repoSpNumMod/SIMONA/ZUNO/003_ZUNO_v3_2009)

---

Figure 2-2: ZUNOV3 model grid.

---



Figure 2-3: CSM and ZUNOV3 grid with ZUNOV3 boundary points.

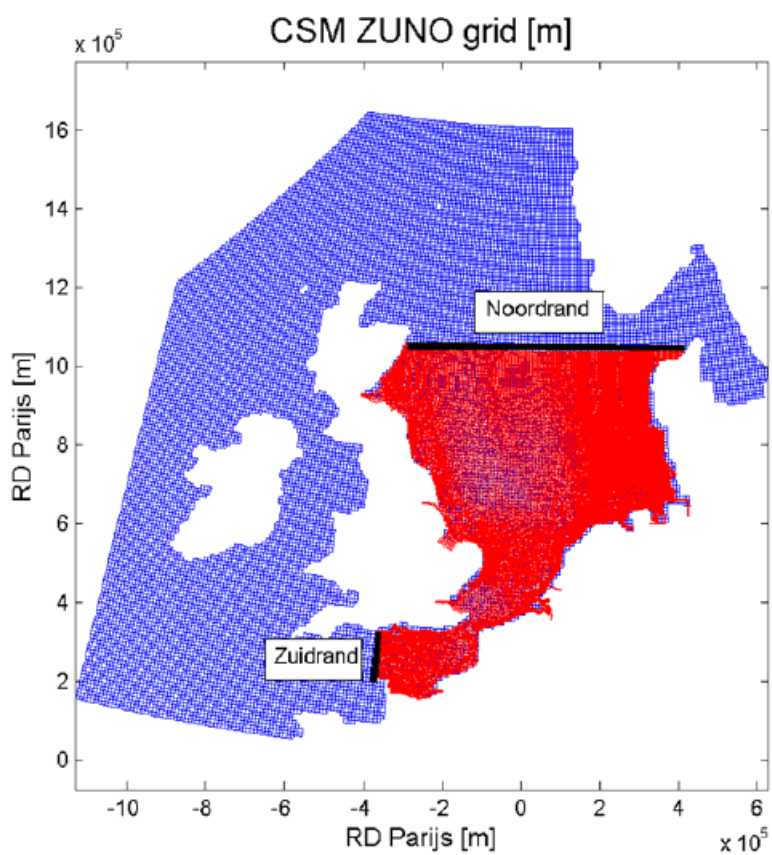


Table 2-2: Model parameters of ZUNO model.

Model parameter	Value
Time step	2.5 min
Smoothing Time	720 min
Eddy viscosity	10 m <sup>2</sup> /s
Chézy (varying in space)	Depth dependent (53-78 m <sup>1/2</sup> /s)
Wind conversion coefficient	Off
Water density	1023.0 kg/m <sup>3</sup>
Air density	1.205 kg/m <sup>3</sup>
Salinity	Off
Dimensions	2D
Simulation period	01/04/2009 00:00 – 01/05/2009 00:00



### 3 Validation

First of all the quality of nesting between CSM and ZUNO model is inspected by Figure 3-1. There is no substantial discrepancies found between water levels predicted by CSM and ZUNO model. The nesting holds satisfactory accuracy.

The water levels predicted by the CSM and ZUNO model are then systematically compared with measurements for the period 01/04/2009 00:00 – 01/05/2009 00:00. The statistical results on bias, RMSE and RMSE0 (the definitions can be found in §Annex1) are presented as below.

Figure 3-2 to Figure 3-4 present the bias, RMSE and RMSE0 of the complete time series of water level respectively. The model statistical results of CSM and ZUNO model are intercompared with the recent calibration results of CSM and ZUNO model for the year 2014 (Maximova et al., 2015). Table 3-1 and Table 3-2 show that the bias of water level for both CSM and ZUNO model for the 2009 run is typically within the range of 15 cm while the RMSE and RMSE0 of water level are typically between 20 and 30 cm. The model accuracy is slightly worse compared with the calibrated run for the year 2014. The discrepancies are mainly attributed to the absent forcing of wind for the 2009 simulations.

The complete set of VIMM analysis results can be found:

[p:\15\\_068-VlabaKustzone\3\\_Uitvoering\1\\_ScenarioAnalyses\1\\_HydrodynamischSimulatiesTelemac\Nesting\BCsWithS\\_LR\VIMM](p:\15_068-VlabaKustzone\3_Uitvoering\1_ScenarioAnalyses\1_HydrodynamischSimulatiesTelemac\Nesting\BCsWithS_LR\VIMM)

Figure 3-1: Bias of complete time series of water level (ZUNO - CSM).

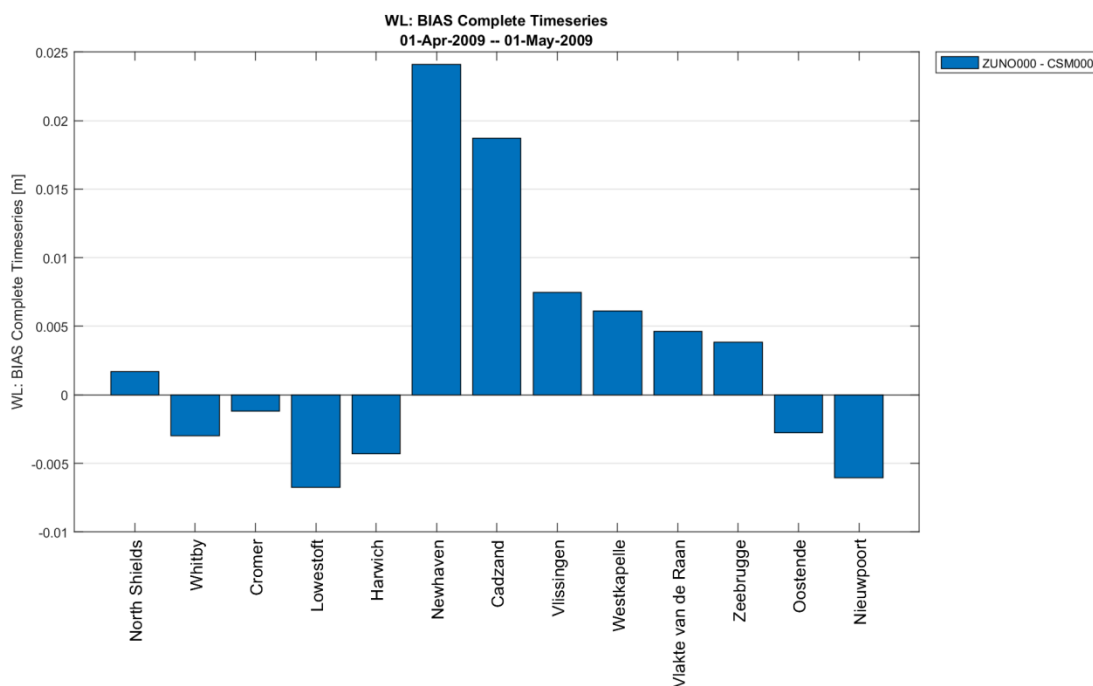


Figure 3-2: Bias of complete time series of water level.

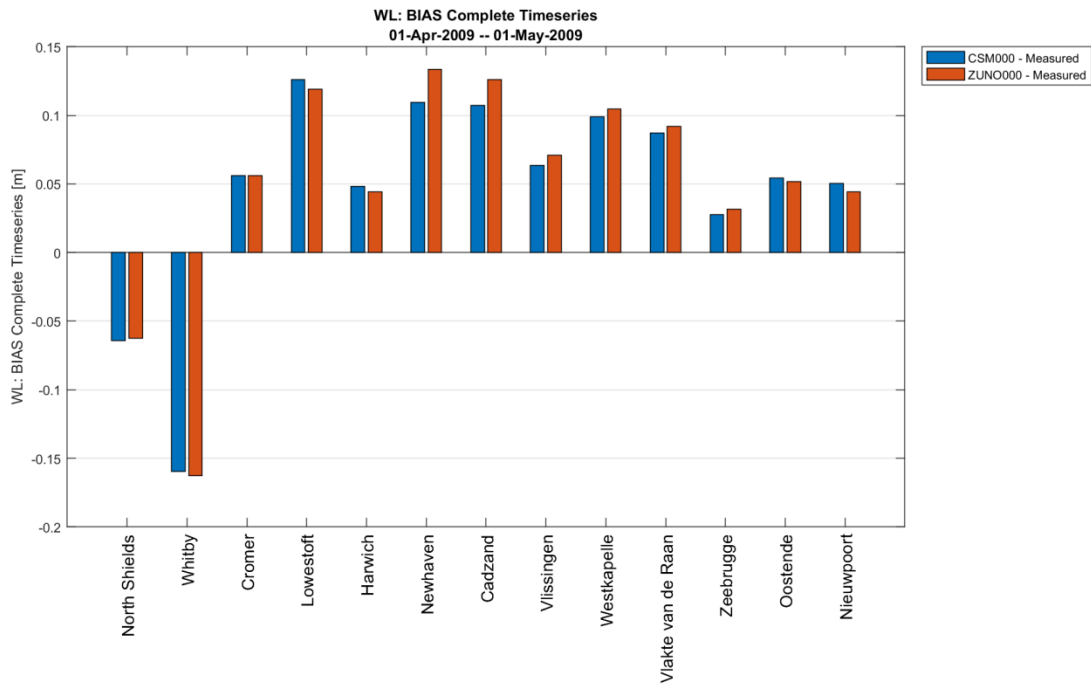


Figure 3-3: RMSE of complete time series of water level

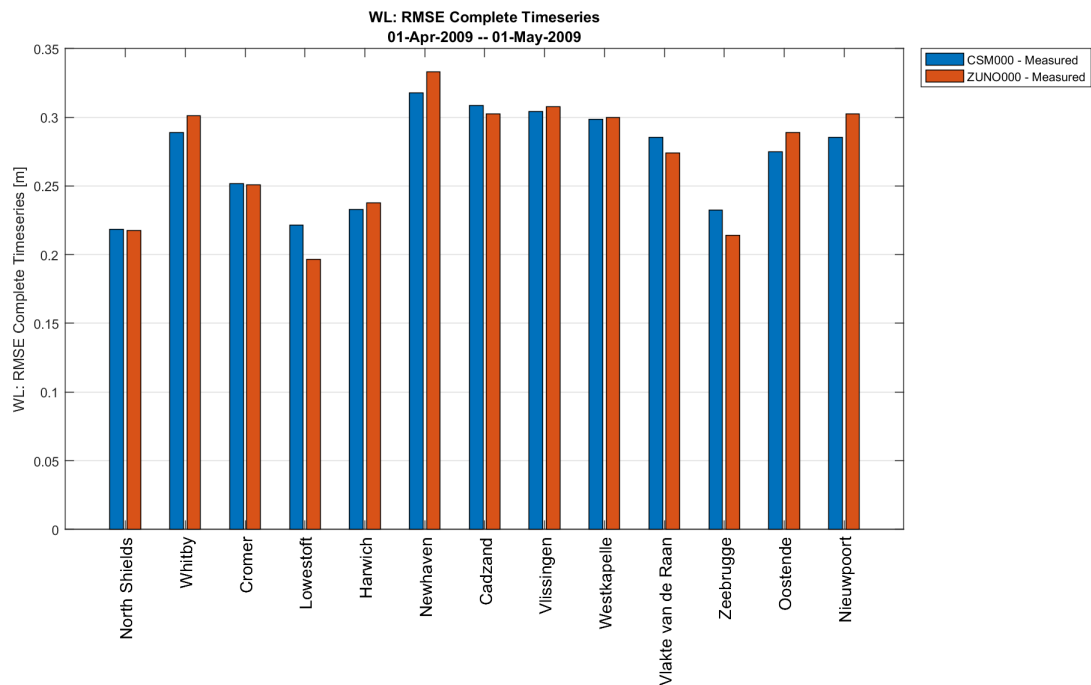


Figure 3-4: RMSE0 of complete time series of water level.

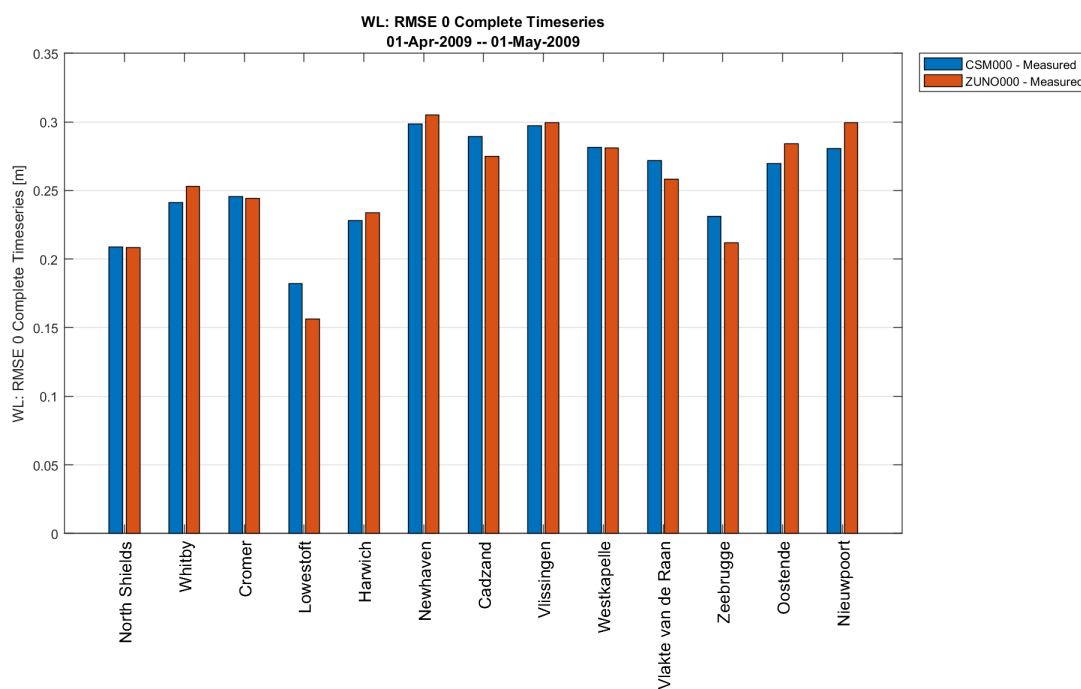


Table 3-1: Statistical parameters for the water level time series (CSM vs. measurements)

Station	Complete Time Series					
	BIAS TS [m]		RMSE TS [m]		RMSE_0 TS [m]	
	CSM2014	CSM2009	CSM2014	CSM2009	CSM2014	CSM2009
North Shields	-0.11	-0.06	0.16	0.22	0.12	0.21
Whitby	-0.23	-0.16	0.25	0.29	0.12	0.24
Immingham	0.02	-	0.83	-	0.83	-
Cromer	0	0.06	0.14	0.25	0.14	0.25
Lowestoft	0.05	0.13	0.14	0.22	0.13	0.18
Harwich	0	0.05	0.12	0.23	0.12	0.23
Dover	0.09	-	0.24	-	0.22	-
Newhaven	0.07	0.11	0.17	0.32	0.16	0.30
Cadzand	0.03	0.11	0.15	0.31	0.14	0.29
Vlissingen	0.01	0.06	0.25	0.30	0.25	0.30
Westkapelle	0.03	0.10	0.27	0.30	0.27	0.28
Vlakke van de Raan	0.02	0.09	0.13	0.29	0.13	0.27
Zeebrugge	-0.04	0.03	0.2	0.23	0.2	0.23
Oostende	-0.01	0.05	0.22	0.28	0.22	0.27
Nieuwpoort	0	0.05	0.22	0.29	0.22	0.28

Table 3-2: Statistical parameters for the water level time series (ZUNO vs. measurements).

Station	Complete Time Series					
	BIAS TS [m]		RMSE TS [m]		RMSE_0 TS [m]	
	ZUNO2014	ZUNO2009	ZUNO2014	ZUNO2009	ZUNO2014	ZUNO2009
North Shields	-0.11	-0.06	0.16	0.22	0.12	0.21
Whitby	-0.23	-0.16	0.26	0.30	0.13	0.25
Immingham	0.09	-	0.44	-	0.43	-
Cromer	0	0.06	0.12	0.25	0.12	0.24
Lowestoft	0.05	0.12	0.1	0.20	0.09	0.16
Harwich	-0.01	0.04	0.13	0.24	0.13	0.23
Dover	0.1	-	0.17	-	0.14	-
Newhaven	0.08	0.13	0.18	0.33	0.16	0.30
Cadzand	0.1	0.13	0.18	0.30	0.15	0.27
Vlissingen	0.08	0.07	0.17	0.31	0.16	0.30
Westkapelle	0.09	0.10	0.17	0.30	0.15	0.28
Vlakte van de Raan	0.06	0.09	0.17	0.27	0.16	0.26
Zeebrugge	0.02	0.03	0.17	0.21	0.16	0.21
Oostende	0.03	0.05	0.23	0.29	0.23	0.28
Nieuwpoort	0.03	0.04	0.24	0.30	0.24	0.30

## 4 Scenarios

The scheduled scenarios are presented in Table 4-1. The additional CSM and ZUNO runs for the scenarios are carried out. For the SLR scenario runs, 60, 90 and 200 cm is added respectively as a constant to the offshore CSM boundary layer. This is done by modifying the parameter AZero (Amplitude for zero frequency [m], see Rijkswaterstaat, 2015b) in the file ‘..\CSM\includes\harmonic’. All other harmonic components are kept constant. It is assumed that on the boundary of the continental shelf, the influence of the SLR on the harmonics has rather a limited impact due to the large depth. Inside the domain the harmonics will change (Pickering et al., 2012). Throughout the nesting the SLR but also the change in the harmonic components will be passed through the detailed Telemac model.

The model response to SLR are evaluated and shown in Figure 4-1 and Figure 4-2. Both of the CSM and ZUNO model simulated the sea level rise as expected.

From the harmonic point of view, Figure 4-3 to Figure 4-5 show the comparison of M2, M4 and S2 amplitude respectively with and without SLR. In the Belgian continental shelf the amplitude of both M2 and S2 tidal components increases as a response to the SLR, while the M4 amplitude drops slightly (< 1 cm).

The complete set of VIMM analysis results can be found:

[p:\15\\_068-VlabaKustzone\3\\_Uitvoering\1\\_ScenarioAnalyses\1\\_HydrodynamischSimulatiesTelemac\Nesting\BCsWithSLR\VIMM](p:\15_068-VlabaKustzone\3_Uitvoering\1_ScenarioAnalyses\1_HydrodynamischSimulatiesTelemac\Nesting\BCsWithSLR\VIMM)

After all, the sea boundary conditions for the ZeeBrugge Telemac model are extracted from the ZUNO runs through nesting.

Table 4-1: Description of scenarios.

Scenarios	Sea Level Rise [cm]
Reference	0
SLR060	60
SLR090	90
SLR200	200

In order to check the influence of SLR on the generated water level and velocity boundary conditions for the ZeeBrugge model, 3 points are selected at the open sea boundary of the ZeeBrugge model (Figure 4-6). The water level and velocities used as boundary conditions for the ZeeBrugge model are analyzed at those 3 locations. Figure 4-7 to Figure 4-9 show the comparison of water level and velocities. Table 4-2 and Table 4-3 present the statistical analysis results.

For water level, the SLR increases the M2 and S2 magnitude at all 3 locations while the M4 amplitude hardly change. As a response to SLR, the phase of M2, S2 and M4 tide are decreased respectively at all 3 locations.

For velocity, The SLR increases the velocity at the northern point and decreases the velocity at the southern point. The velocity at the middle point hardly change. Compared with the reference run, SLR leads to substantial RMSE values of velocity magnitude at all locations (in the order of 1-4 cm/s). The velocity directions are also modified by SLR at all locations, the changes of circular standard deviation are in the range of (5-15 degree).

Figure 4-1: Bias of complete time series of water level (CSM scenario runs – CSM reference run).

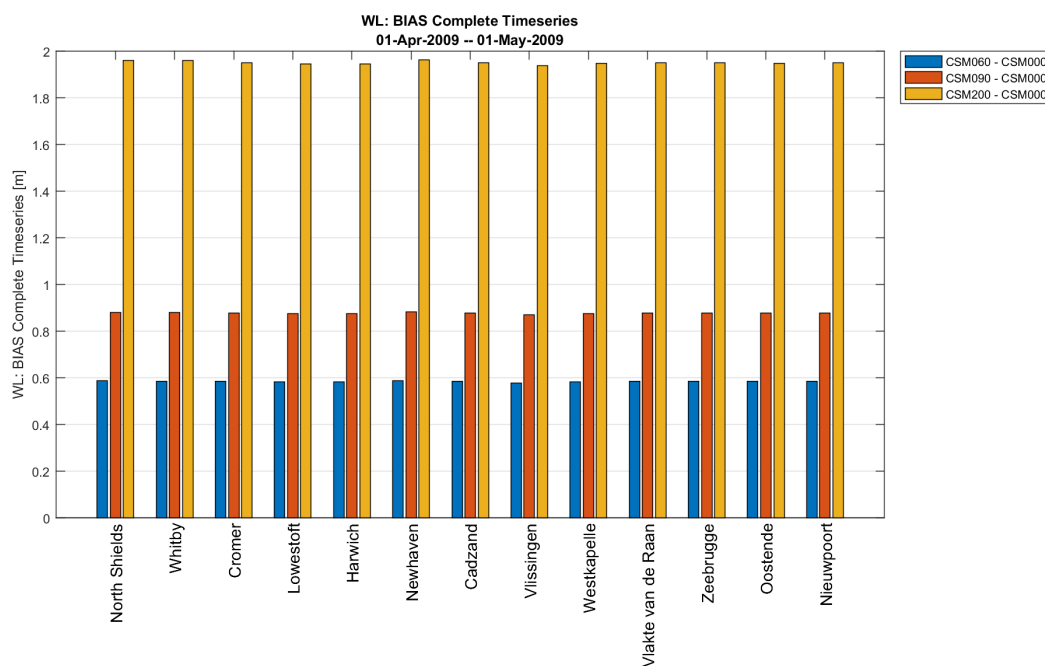


Figure 4-2: Bias of complete time series of water level (ZUNO scenario runs – ZUNO reference run).

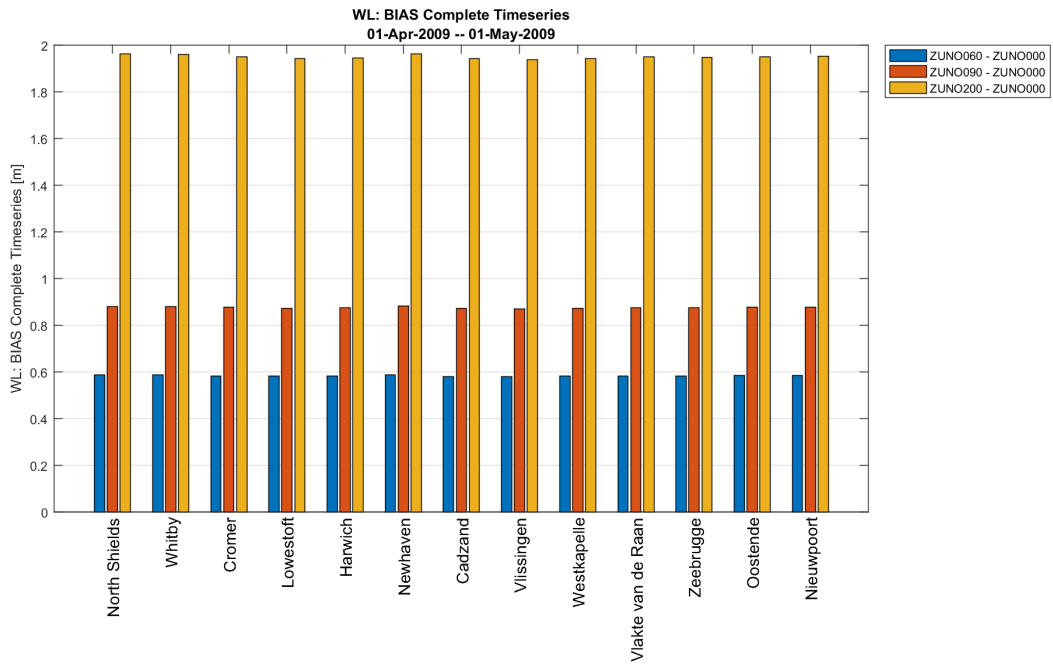


Figure 4-3: Comparison of M2 amplitude with and without SLR.

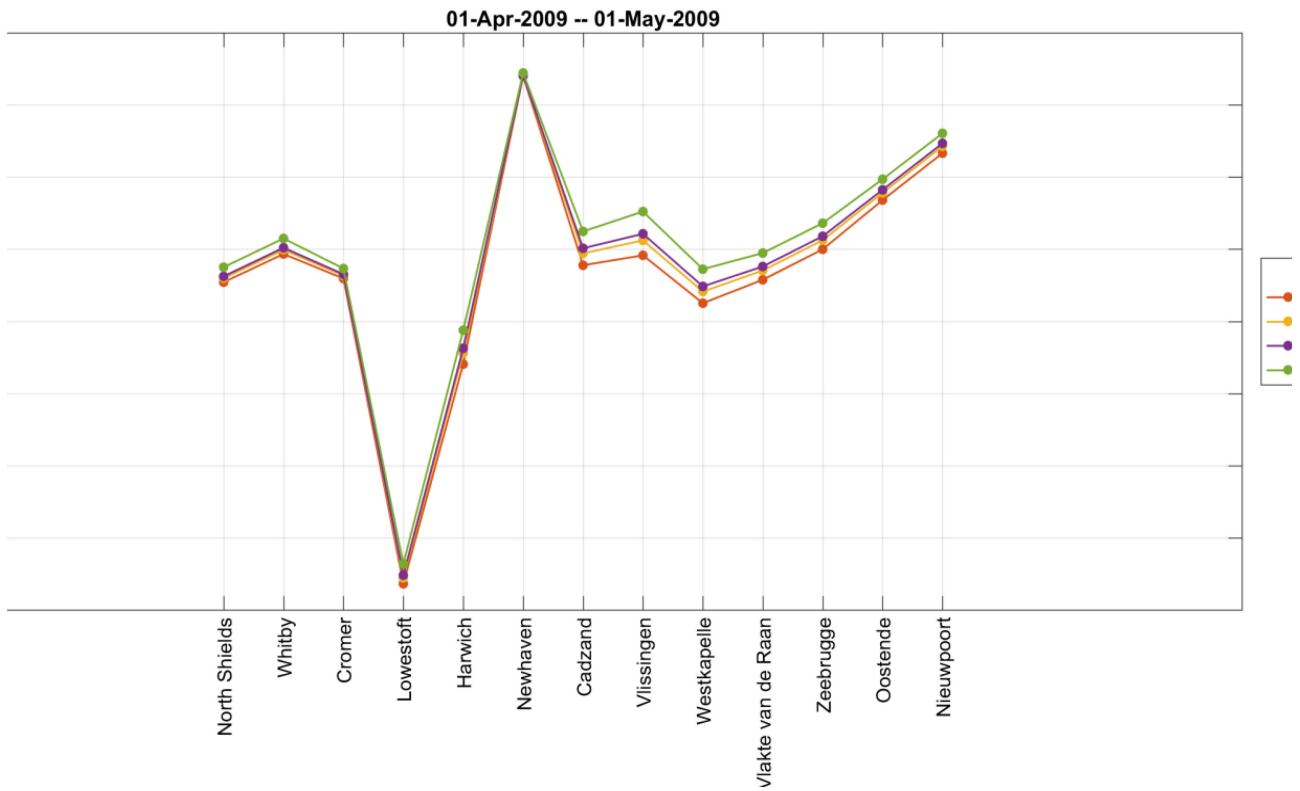


Figure 4-4: Comparison of M4 amplitude with and without SLR.

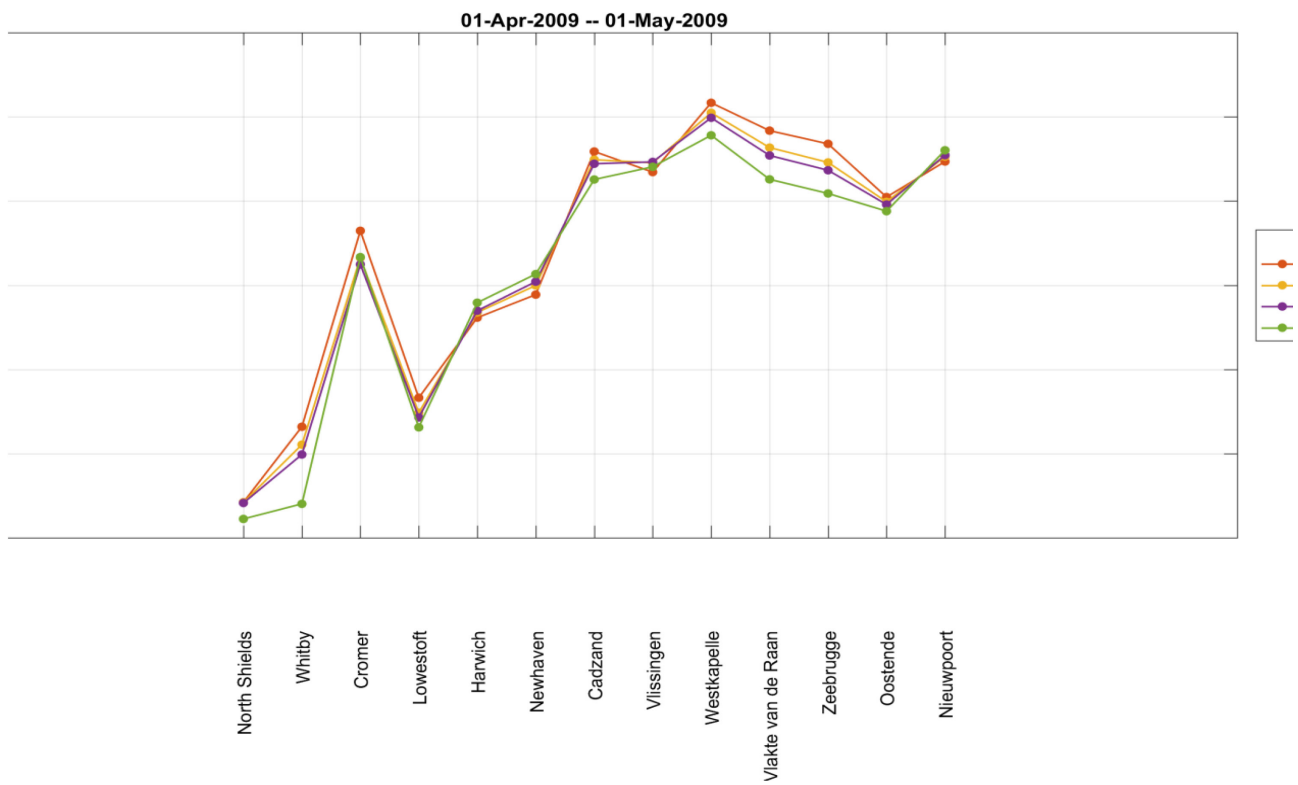


Figure 4-5: Comparison of S2 amplitude with and without SLR.

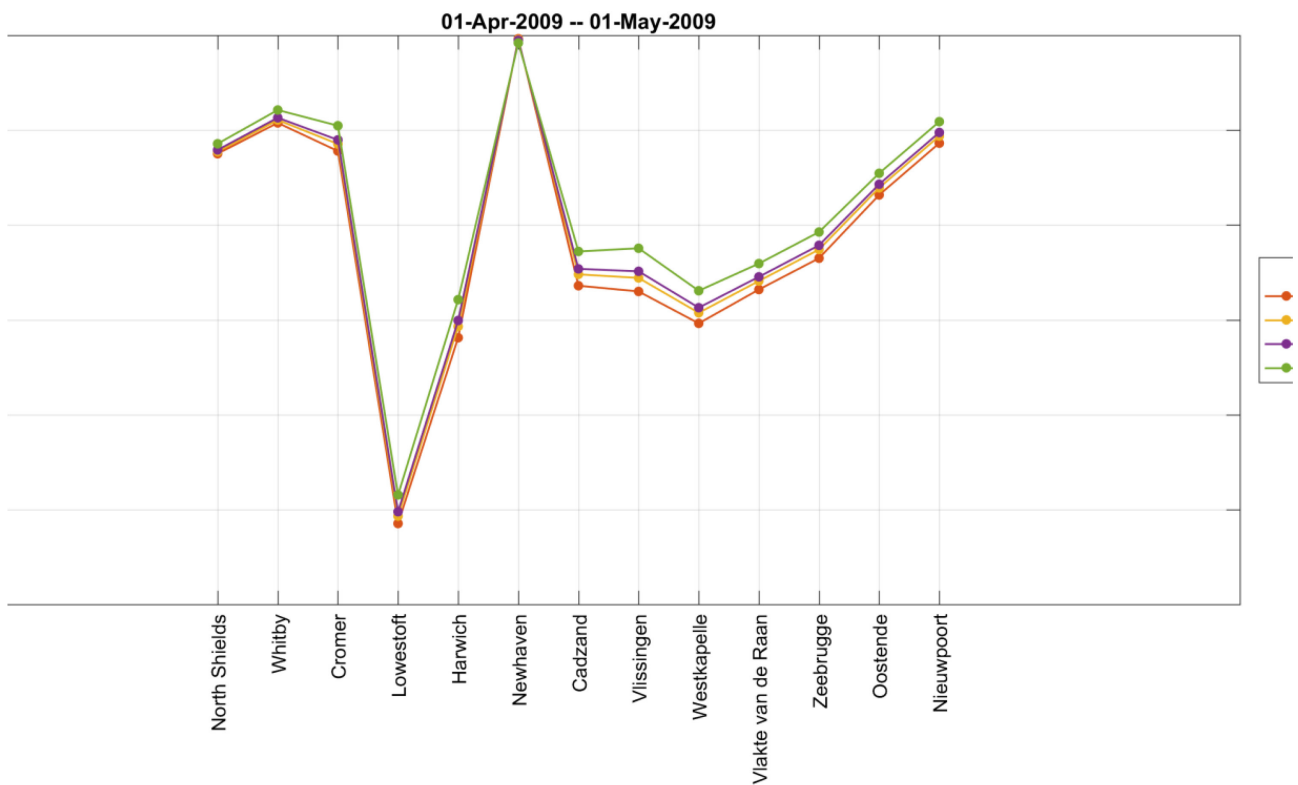


Figure 4-6: Three points are imposed at the open sea boundary of the ZeeBrugge model domain.

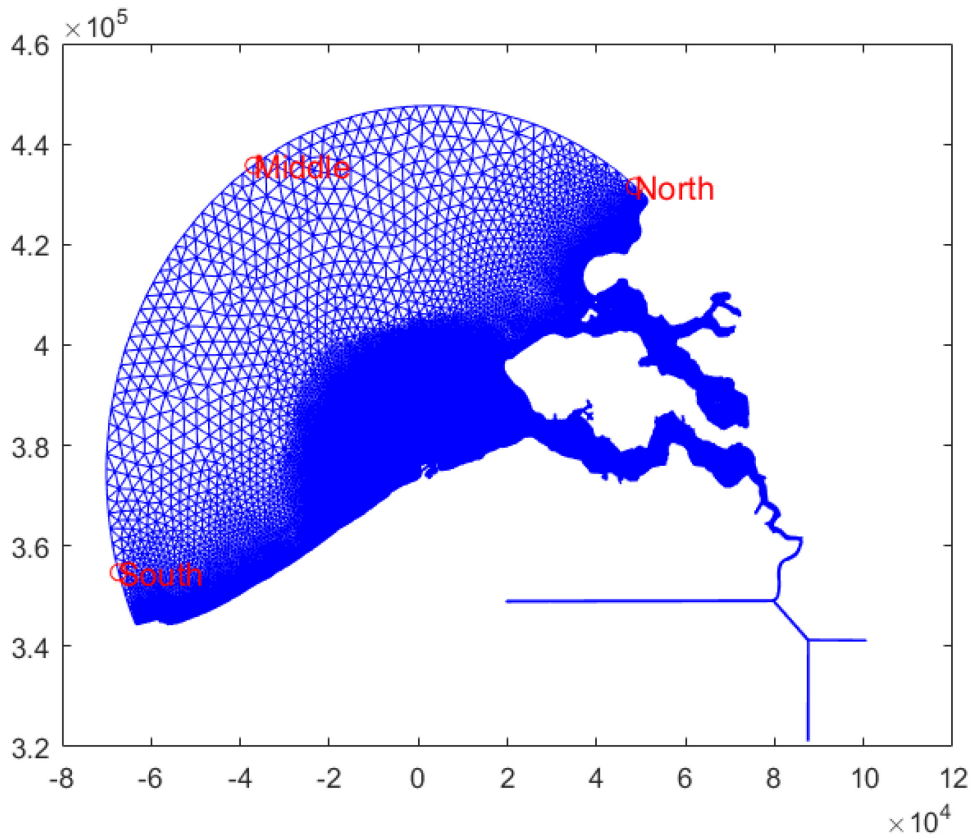


Figure 4-7: Comparison of water level and velocity at the Northern point between reference and SLR scenarios.

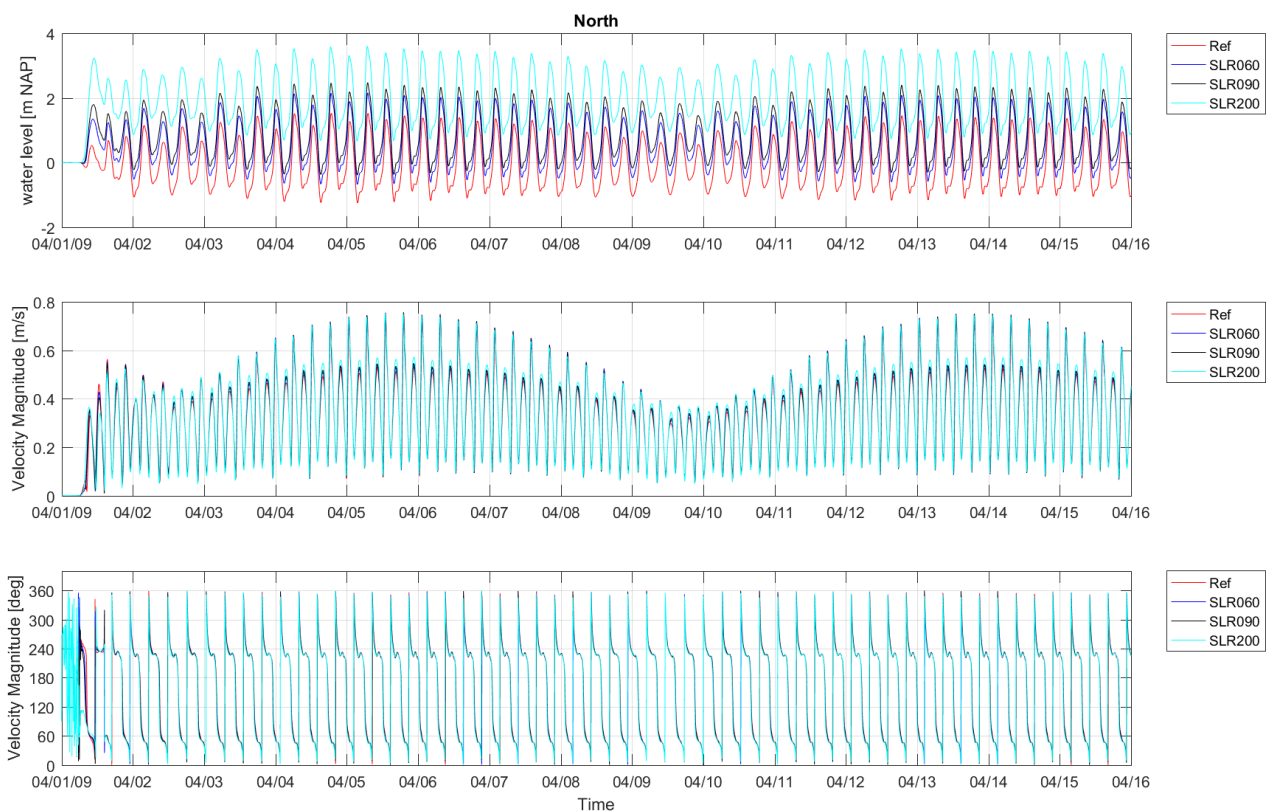




Figure 4-8: Comparison of water level and velocity at the **Middle** point between reference and SLR scenarios.

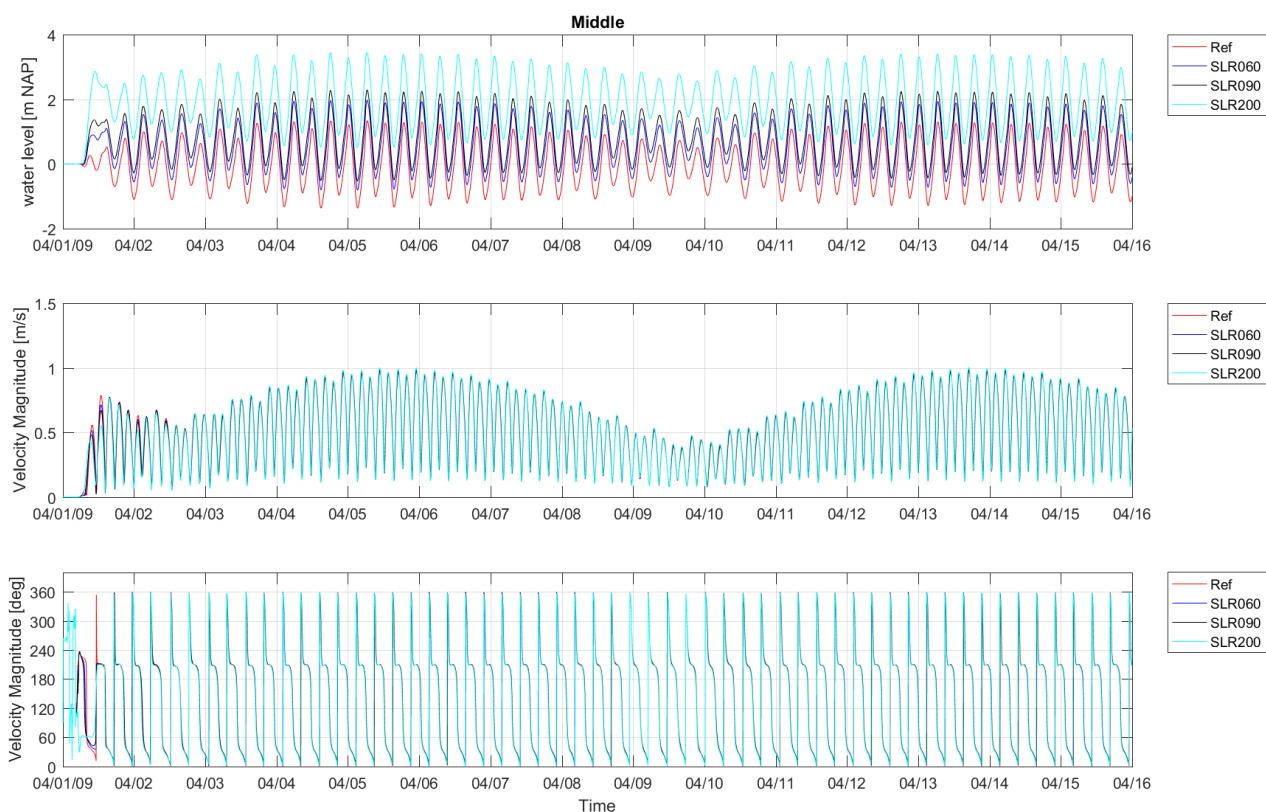


Figure 4-9: Comparison of water level and velocity at the **Southern** point between reference and SLR scenarios.

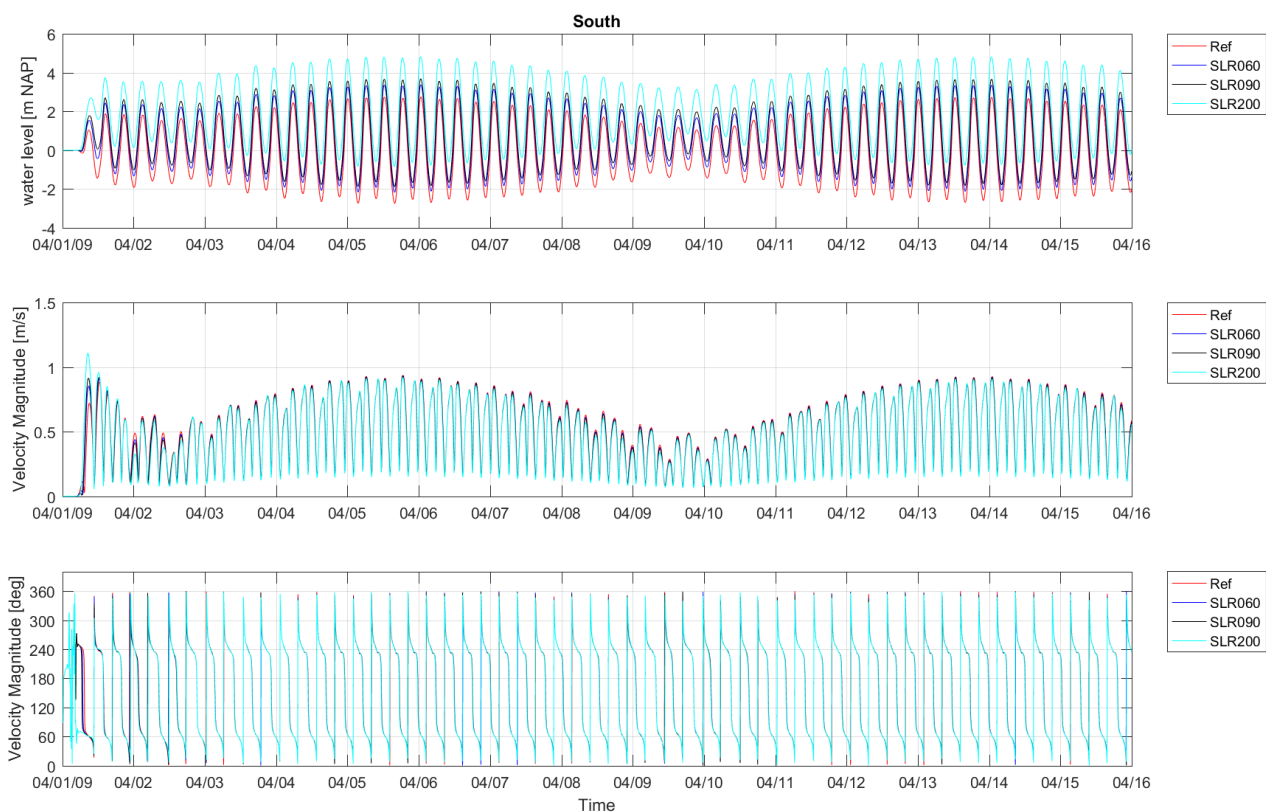


Table 4-2: Comparison of harmonic component M2, S2 and M4 with and without SLR.

		M2		S2		M4	
		Amp [m]	Phase [deg]	Amp [m]	Phase [deg]	Amp [m]	Phase [deg]
<b>North</b>	Ref	0.94	215.30	0.30	99.55	0.16	84.31
	SLR060	0.96	212.03	0.30	95.83	0.16	79.35
	SLR090	0.96	210.42	0.30	93.81	0.16	76.80
	SLR200	0.99	204.49	0.31	86.30	0.16	67.05
<b>Middle</b>	Ref	0.91	168.70	0.32	50.35	0.06	24.27
	SLR060	0.93	166.33	0.33	47.24	0.06	17.98
	SLR090	0.94	165.14	0.34	45.57	0.06	15.03
	SLR200	0.98	160.70	0.35	39.38	0.05	4.25
<b>South</b>	Ref	1.98	163.54	0.77	49.82	0.12	274.27
	SLR060	2.00	161.62	0.77	47.18	0.13	269.29
	SLR090	2.00	160.66	0.77	45.82	0.13	266.81
	SLR200	2.02	157.10	0.78	40.91	0.13	257.99

Table 4-3: Statistical analysis on velocities.

		<b>North</b>	<b>Middle</b>	<b>South</b>
Bias [m/s] (SLR - Ref)	SLR060 vs Ref	0.007	0.001	-0.006
	SLR090 vs Ref	0.011	0.001	-0.010
	SLR200 vs Ref	0.022	0.003	-0.022
RMSE velocity [m/s]	SLR060 vs Ref	0.015	0.018	0.022
	SLR090 vs Ref	0.022	0.026	0.032
	SLR200 vs Ref	0.046	0.056	0.064
Circular standard deviation of velocity direction [deg]	SLR060 vs Ref	4.92	5.22	5.10
	SLR090 vs Ref	7.05	7.24	6.91
	SLR200 vs Ref	14.47	14.36	13.36

## 5 List of References

**Leyssen, G.; Vanlede, J.; Decrop, B.; Van Holland, G.; Mostaert, F.** (2012). Modellentrein DCSMv5-ZUNOV3. Deelrapport 2: Validatie. WL Rapporten, 753\_12. Waterbouwkundig Laboratorium & IMDC: Antwerpen, België.

**Maximova, T.; Vanlede, J.; De Maerschallck, B.; Van Oyen, T.; Verwaest, T.; Mostaert, F.** (2015). Verbetering morfologisch instrumentarium: Subreport 2 – Modellentrein DCSMv5–ZUNOV3: validatie modelrun 2014. Version 3.0. WL Rapporten, 14\_094. Flanders Hydraulics Research: Antwerp, Belgium.

**Pickering, M.D.; Wells, N.C.; Horsburgh, K.J.; Green, J.A.M.** (2012). The impact of future sea-level rise on the European Shelf tides. *Cont. Shelf Res.* 35: 1–15. doi:10.1016/j.csr.2011.11.011

**Rijkswaterstaat**, 2015a. User's Guide MODNST. Nesting of models, create boundary conditions.

**Rijkswaterstaat**, 2015b. User's Guide WAQPRE. 2.9.1.5 HARMONIC.

## 6 Annex 1: Definition of Statistics

The **Bias** of water level represents the average deviation of the differences between model predicted water level and measurement.

The **RMSE** of water level represents the sample standard deviation of the differences between predicted water level and measurement.

The **RMSE0** is the bias corrected root mean square error which describes the forecast errors not associated with the bias.

The mathematical expressions are listed below.  $y$  and  $x$  represent modeled and measured values respectively and  $n$  is the number of samples.

$$\text{Bias} = \bar{y} - \bar{x}$$

$$\text{RMSE} = \sqrt{\frac{\sum_{i=1}^n (y_i - x_i)^2}{n}}$$

$$\text{RMSE0} = \sqrt{\frac{\sum_{i=1}^n ((y_i - x_i) - (\bar{y} - \bar{x}))^2}{n}}$$

DEPARTMENT **MOBILITY & PUBLIC WORKS**  
Flanders hydraulics Research

Berchemlei 115, 2140 Antwerp

**T** +32 (0)3 224 60 35

**F** +32 (0)3 224 60 36

[waterbouwkundiglabo@vlaanderen.be](mailto:waterbouwkundiglabo@vlaanderen.be)

[www.flandershydraulicsresearch.be](http://www.flandershydraulicsresearch.be)